IDWA Number B50011/Member Contract No. ZA0226
Report CRAD-9408-TR-3342

High Speed Research - Airframe Technology

Airframe Materials & Structures
4.2.6 - Aeroelasticity

Technical Milestone Report:

Parametric Flutter Analysis of the TCA Configuration and Recommendation for FFM Design and Scaling

Report Date: November 21, 1997

Prepared for
The Boeing Company
Seattle, Washington 98124-2207

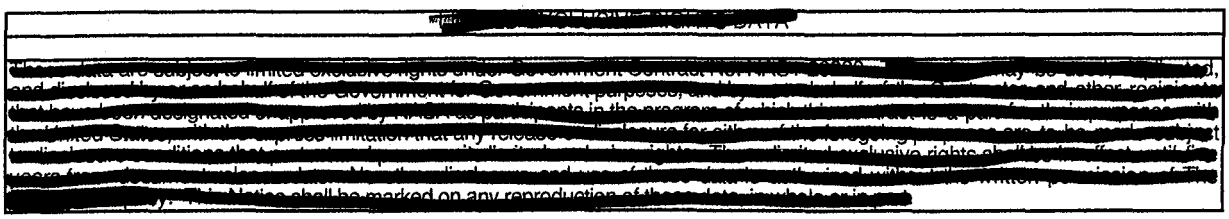

SIGNATURES

MDC HSR II Airframe Task 26 (WBS 4.2.6)
Aeroelasticity
Parametric Flutter Analysis of the TCA Configuration and Recommendation for FFM Design and Scaling
IDWA Number B50011/Member Contract No. ZA0226

MDC Report CRAD-9306-TR-3342

Report Date: 11/21/97

Report prepared by:

M. Baker, Ph.D.
Principal Investigator
HSR Aeroelasticity

Peter Lenkey
FFM Focal Point
HSR Aeroelasticity

Report approved by:

P. Goggin
Manager
Loads, Flutter, and Optimization

Report approved by:

S. J. Hatakayama
Program Manager
Airframe Materials & Structures

Report approved by:

K. Ludas
Senior Manager
Design & Technology

FOREWORD

This document is being submitted to satisfy the deliverable "Parametric Flutter Analysis of TCA Configuration" (WBS 4.2.6.2) of the High Speed Research II - Airframe Technologies Contract NAS1-20220.

The work reported here is part of the effort in Aeroelasticity, and was performed by a team of experts from Boeing Long Beach.

The NASA technical point of contact for this task is Rob Scott of NASA Langley Research Center.

The key personnel responsible for this effort were:

Name	Function
Dr. Myles Baker	Sub-Task PI, Aeroelasticity
Mr. Peter Lenkey	Flutter Analysis
Dr. Lei Fu	Flutter Analysis

Table of Contents

1. Introduction

The current HSR Aeroelasticity plan to design, build, and test a full span, free flying transonic flutter model in the TDT has many technical obstacles that must be overcome for a successful program. One technical obstacle is the determination of a suitable configuration and point in the sky to use in setting the scaling point for the ASE models program. Determining this configuration and point in the sky requires balancing several conflicting requirements, including model buildability, tunnel test safety, and the ability of the model to represent the flutter mechanisms of interest.

As will be discussed in detail in subsequent sections, the current TCA design exhibits several flutter mechanisms of interest. It has been decided that the ASE models program will focus on the low frequency symmetric flutter mechanism, and will make no attempt to investigate high frequency flutter mechanisms. There are several reasons for this choice. First, it is believed that the high frequency flutter mechanisms are similar in nature to classical wing bending/torsion flutter, and therefore there is more confidence that this mechanism can be predicted using current techniques. The low frequency mode, on the other hand, is a highly coupled mechanism involving wing, body, tail, and engine motion which may be very difficult to predict. Second, the high frequency flutter modes result in very small weight penalties (several hundred pounds), while suppression of the low frequency mechanism inside the flight envelope causes thousands of pounds to be added to the structure.

In order to successfully test the low frequency flutter mode of interest, a suitable starting configuration and point in the sky must be identified. The configuration and point in the sky must result in a wind tunnel model that (1) represents the low-frequency wing/body/engine/empennage flutter mechanisms that are unique to HSCT configurations, (2) flutters at an acceptably low frequency in the tunnel, (3) flutters at an acceptably low dynamic pressure in the tunnel, (4) allows sufficient weight for model buildability without inordinately high cost, and (5) has significant separation between the target flutter mechanism and other, potentially catastrophic, flutter mechanisms.

The approach taken to identify the design configuration was to start with the Long Beach DITS TCA design, and investigate the flutter behavior of this "baseline" airplane in detail. This included analysis of all mass conditions at Mach numbers between 0.6 and 1.2. Most of this effort was performed under the DITS subtask, but some additional conditions were analyzed in order to cover the full Mach range of the TDT. Once the flutter behavior of the "baseline" TCA was understood, a series of variations to the TCA were constructed and analyzed. For each variation, all mass conditions were again analyzed in a Mach range between 0.6 and 1.2 so that no relevant information would be missed. This required a total of 200 flutter analyses for each parametric variation (20 mass conditions, 5 Mach numbers, and two symmetry conditions) for a total of approximately 6,000 flutter analyses. The variations considered are listed in Table 1-1.

Once the flutter analyses had been performed, the V-G and V-F plots were printed, and the impact of each variation on the FFM design (with secondary attention to the TCA vehicle) was assessed, and a candidate design configuration was identified.

Condition	Symmetric	Antisymm.
Flutter Sized Model (Baseline -- Performed Under DITS)	* Yes	Yes
Strength Sized Model	Yes	Yes
Double Fuselage Mass	Yes	Yes
No Tail Aerodynamics	Yes	No
Double Tail Aerodynamics	Yes	No
Stiffen Pylon by +20%	Yes	Yes
Stiffen Pylon by +10%	Yes	Yes
Stiffen Pylon by -20%	Yes	Yes
No Engine Aerodynamics	Yes	Yes
Double Engine Aerodynamics	Yes	Yes
Move Engine xcg forward 20% of nacelle length	Yes	Yes
Move Engine xcg forward 10% of nacelle length	Yes	Yes
Move Engine xcg aft 10% of nacelle length	Yes	Yes
Move Engine xcg aft 20% of nacelle length	Yes	Yes
Change Engine Mass Properties by +20%	Yes	Yes
Change Engine Mass Properties by +50%	Yes	Yes
Change Engine Mass Properties by -50%	Yes	Yes
Change Engine Mass Properties by -20%	Yes	Yes
Stiffen Outboard Wing Skins by +20%	Yes	Yes
Stiffen Outboard Wing Skins by +10%	Yes	Yes
Tip Weight: 100 lb on Front Spar	Yes	Yes
Tip Weight 200 lb on Front Spar	Yes	Yes
Tip Weight: 500 lb on Front Spar	Yes	Yes
Tip Weight: 1000 lb on Front Spar	Yes	Yes
Reduced Stiffness (20% Frequency Reduction)	Yes	Yes
Recommended Flutter Model Design Configuration Strength Sized Model, Double Fuselage Mass, Reduced Stiffness, Outboard Wing Skins Stiffened by +40%	Yes	Yes
Recommended Design Configuration in Freon Scaled TDT Properties up to Airplane Scale	Yes	Yes

Table 1-1: Summary of Parameter Variations Analyzed.

2. Baseline Flutter Analysis

The starting point for the parametric variations considered in this report is the Long Beach DITS-released TCA model, internally known as TCA9UUD, which is a strength/flutter sized configuration. The first 10 flexible symmetric and antisymmetric vibration modes are shown in Figures 2-1(a-j) and 2-2(a-j).

There are six flutter mechanisms of primary interest in this configuration for mass case MT-1. Three of these mechanisms are symmetric, and include a low frequency mode with a relatively mild crossing, a high frequency mode with a very sharp crossing, and a high frequency hump mode. The three antisymmetric mechanisms fall into similar categories, containing a single low frequency mode, a high frequency "hard" mode, and a high frequency hump mode. The flutter boundaries for these mechanisms are shown in Figure 2-3, and animation frames for each of the flutter modes are shown in Figures 2-4 through 2-9.

This configuration has several shortcomings with respect to a tunnel test configuration, and the parametric variations were designed to alleviate these problems. Easily the most severe problem with designing a wind tunnel model based on TCA9UUD is the shape of the flutter boundaries of the different mechanisms, and the lack of a significant flight regime where the low frequency symmetric target mode is clearly critical. As can be clearly seen in Figure 2-3, the mechanism that is critical over most of the Mach regime is the antisymmetric high frequency hard flutter mode, which is essentially an outboard wing flutter mode (Figure 2-8).

This is undesireable for three reasons. First, the high frequency flutter mechanisms do not appear to cause a large weight penalty in the TCA, while the low frequency mechanisms cause large weight penalties. Second, the high frequency mechanisms are dominated by outboard wing motion, and we have a fairly high degree of confidence in analytical predictions. The low frequency mechanism, on the other hand, is a highly coupled wing/body/engine/tail mode which is dramatically different from the flutter encountered in traditional subsonic transports, so we have a low degree of confidence in analytical predictions of this mechanism. Finally, testing for the high frequency flutter mechanisms would almost certainly result in loss of the model. Due to the high frequency and steep crossing of this mode, encountering the high frequency mechanism during flutter testing would result in a very violent oscillations that would likely destroy the model before the test could be halted. It is therefore critical that the FFM be designed such that the low frequency flutter mechanism is the first mechanism encountered, and that there be a significant separation between this "target" mode and the potentially catastrophic high frequency modes.

The flutter behavior (V-G and V-F plots) of the TCA9UUD configuration with mass condition MT-1 (Maximum takeoff weight, forward CG, dumbelled payload) is shown in Figures 2-10(a-e) and 2-11(a-e). A full set of V-G and V-F plots for all 20 DITS-defined mass cases is attached as Appendix A, but since MT-1 was eventually selected for the recommended flutter model design point, all results presented in the body of the report will relate to the MT-1 mass condition.

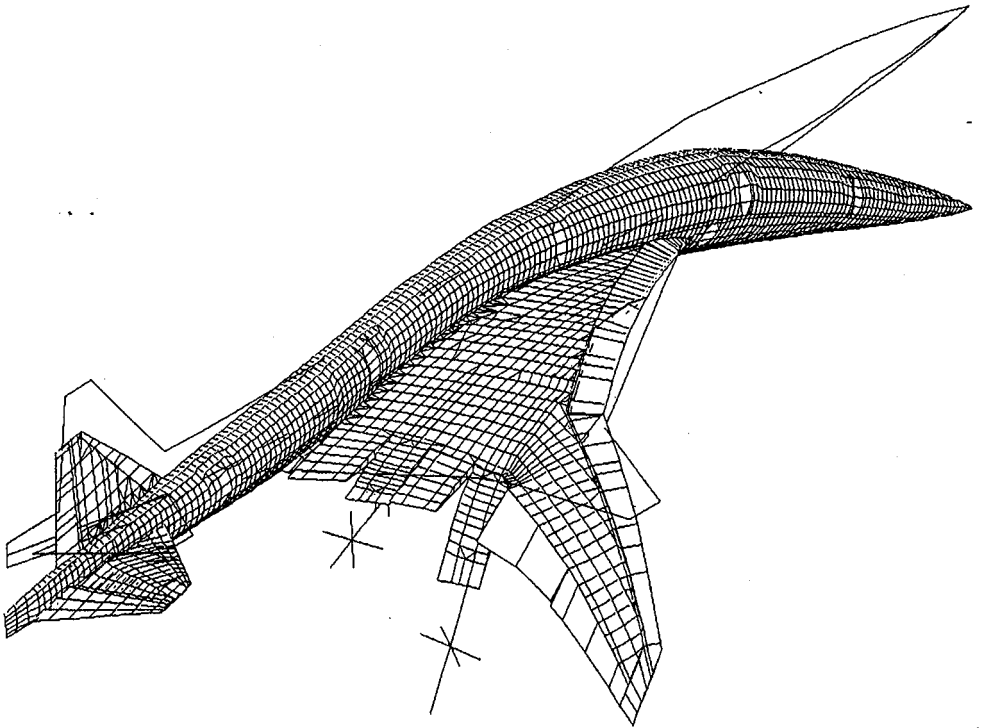

Figure 2-1(a): TCA9UUD Flexible Mode #1. Symmetric, MT-1 Mass Case, Frequency = 1.33 Hz.

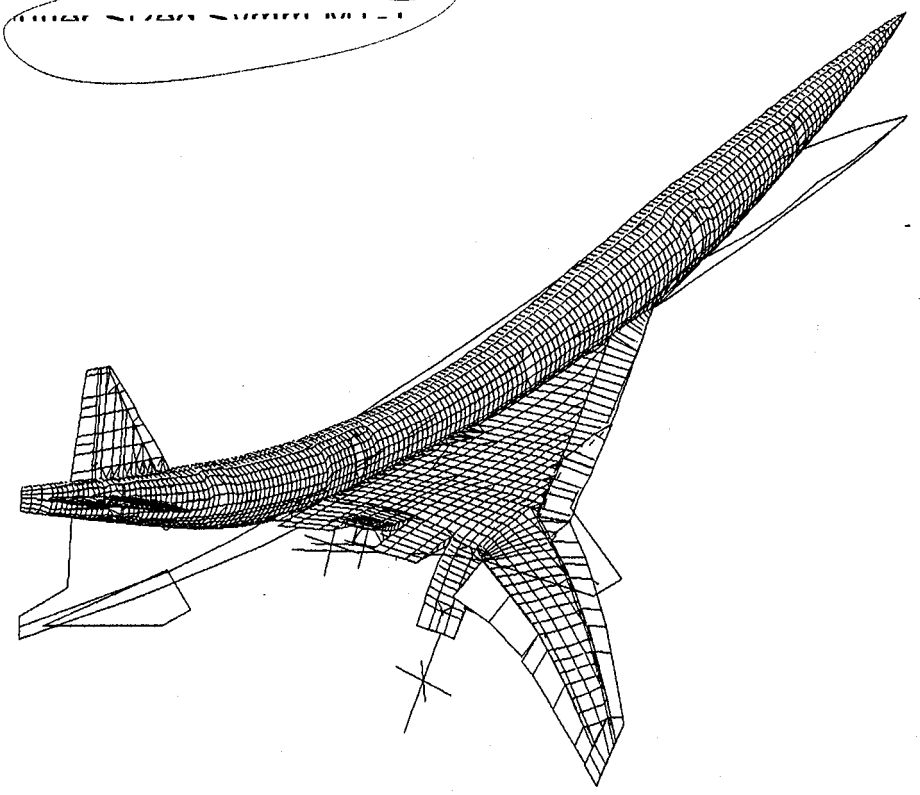

Figure 2-1(b): TCA9UUD Flexible Mode #2. Symmetric, MT-1 Mass Case, Frequency = 1.49 Hz.

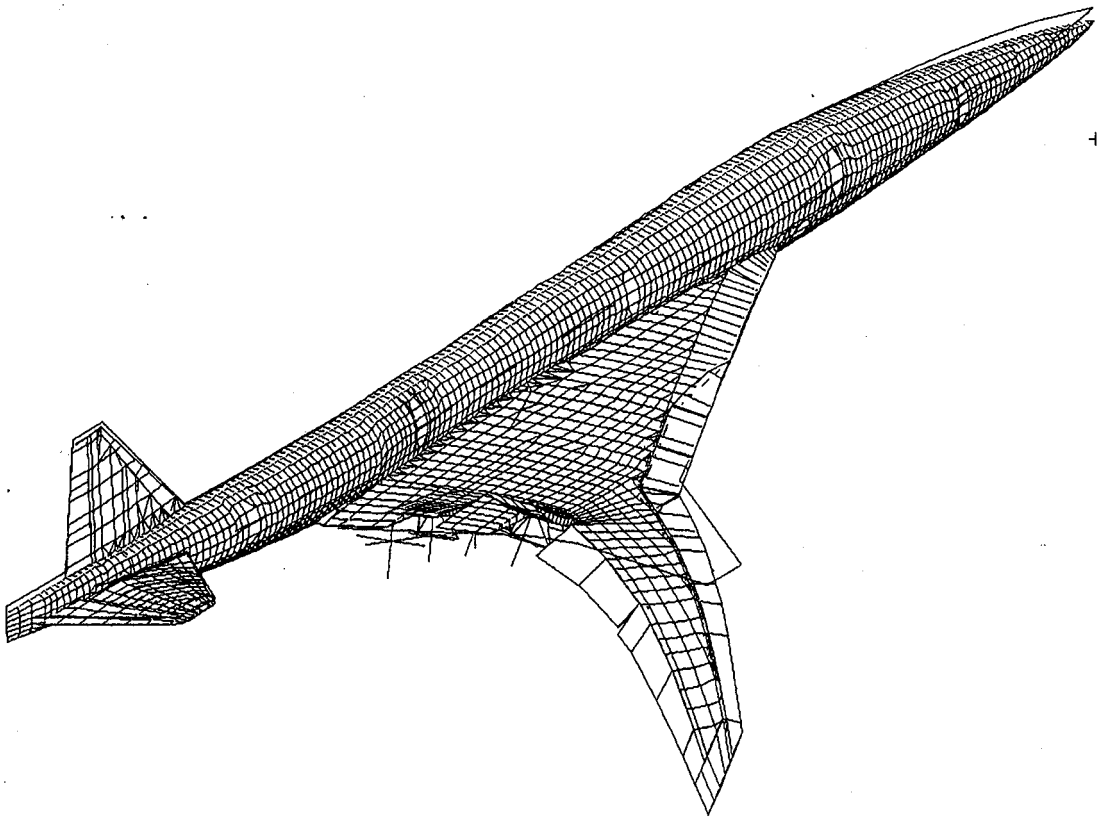

Figure 2-1(c): TCA9UUD Flexible Mode #3. Symmetric, MT-1 Mass Case, Frequency = 1.89 Hz.

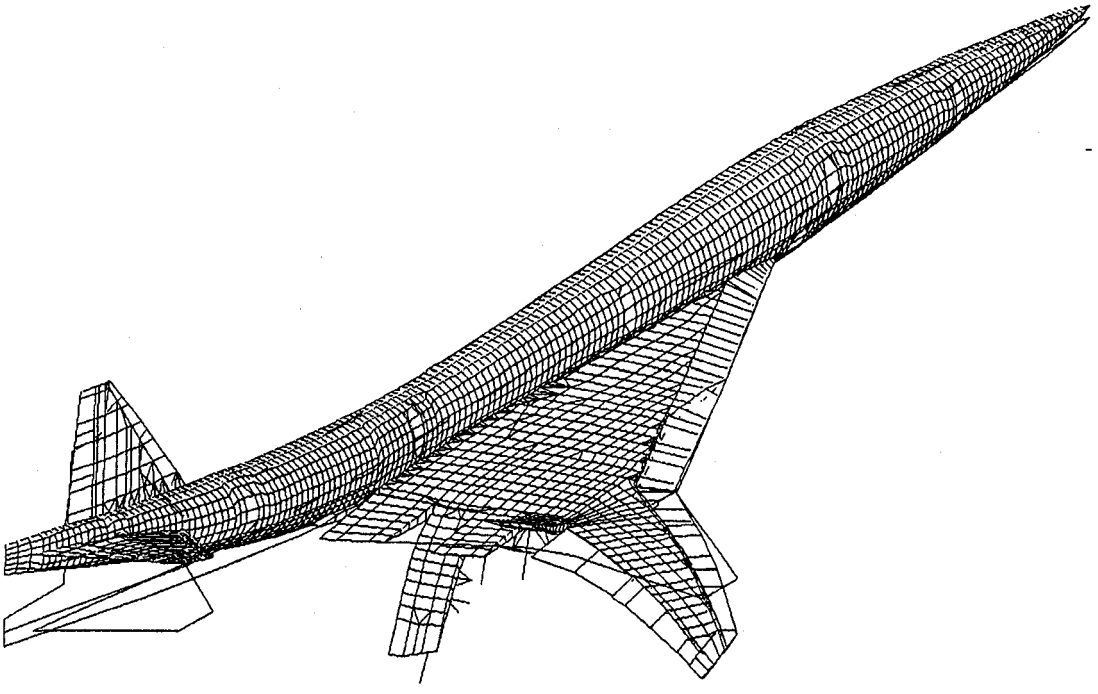

Figure 2-1(d): TCA9UUD Flexible Mode #4. Symmetric, MT-1 Mass Case, Frequency = 1.94 Hz.

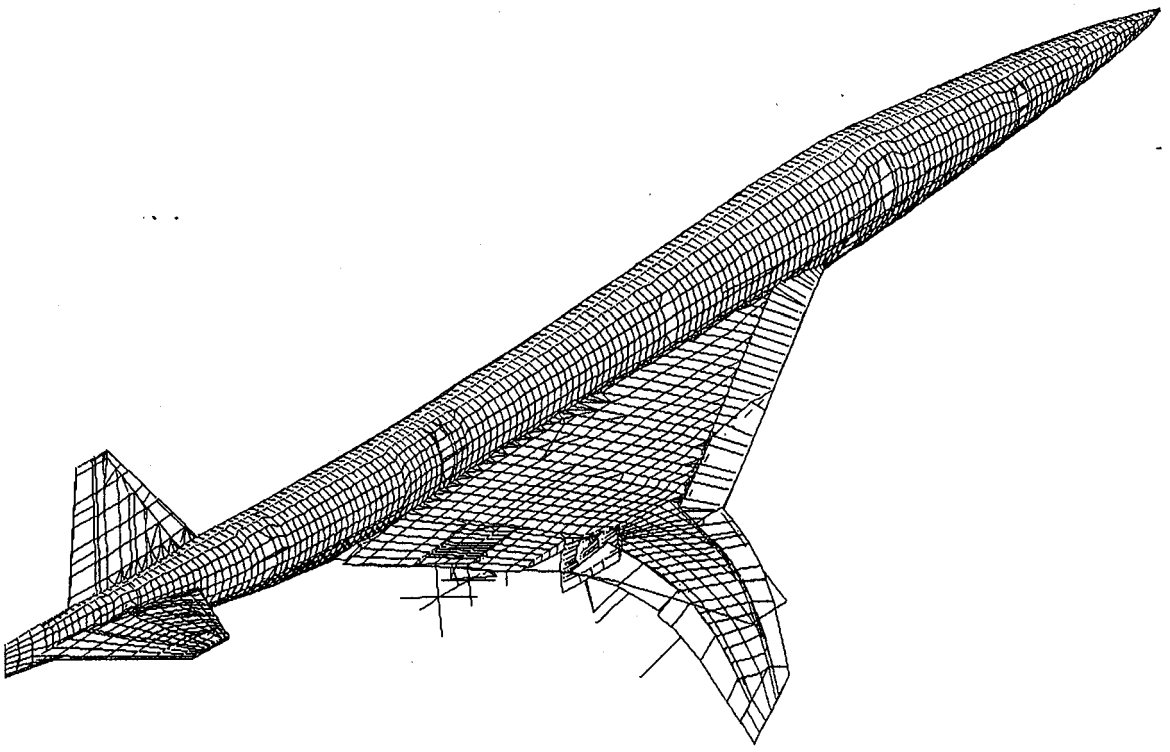

Figure 2-1(e): TCA9UUD Flexible Mode #5. Symmetric, MT-1 Mass Case, Frequency = 2.66 Hz.

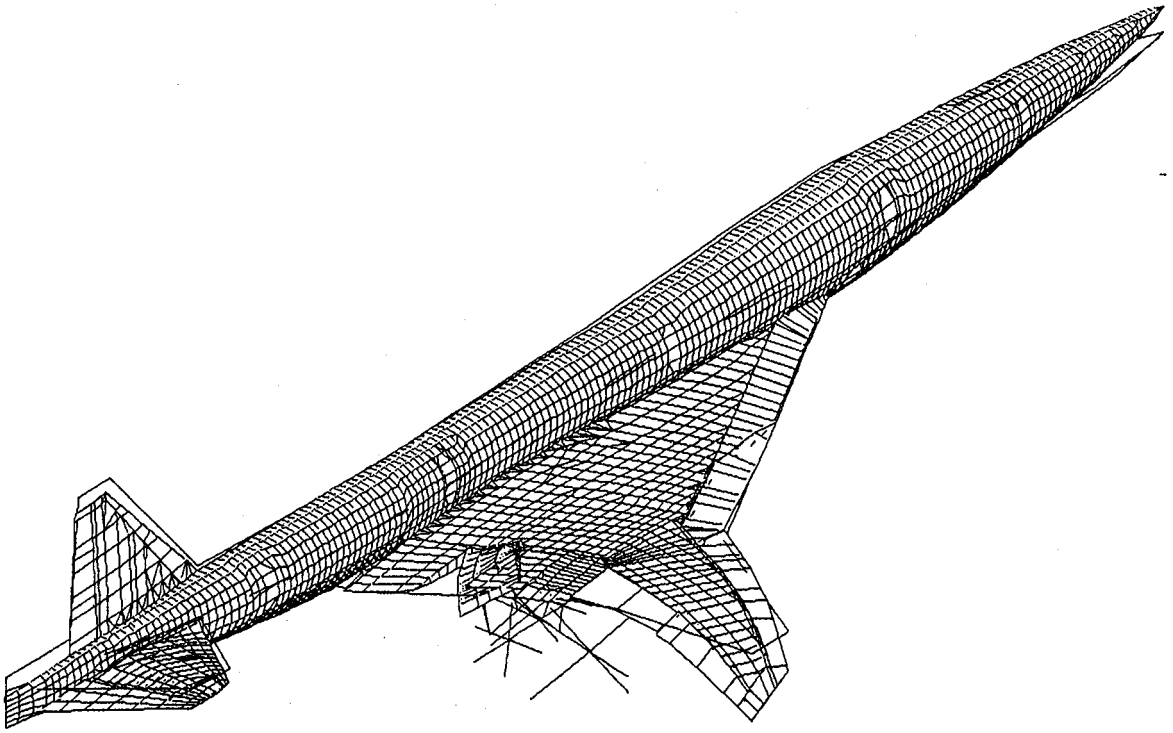

Figure 2-1(f): TCA9UUD Flexible Mode #6. Symmetric, MT-1 Mass Case, Frequency = 2.69 Hz.

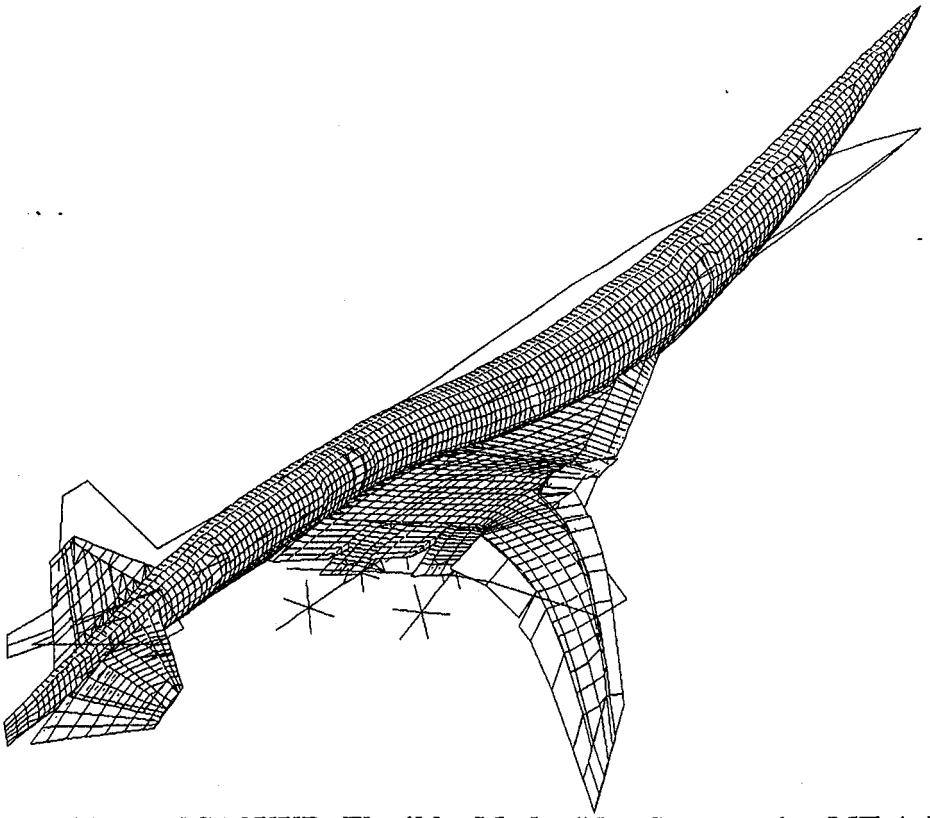

Figure 2-1(g): TCA9UUD Flexible Mode #7. Symmetric, MT-1 Mass Case, Frequency = 2.77 Hz.

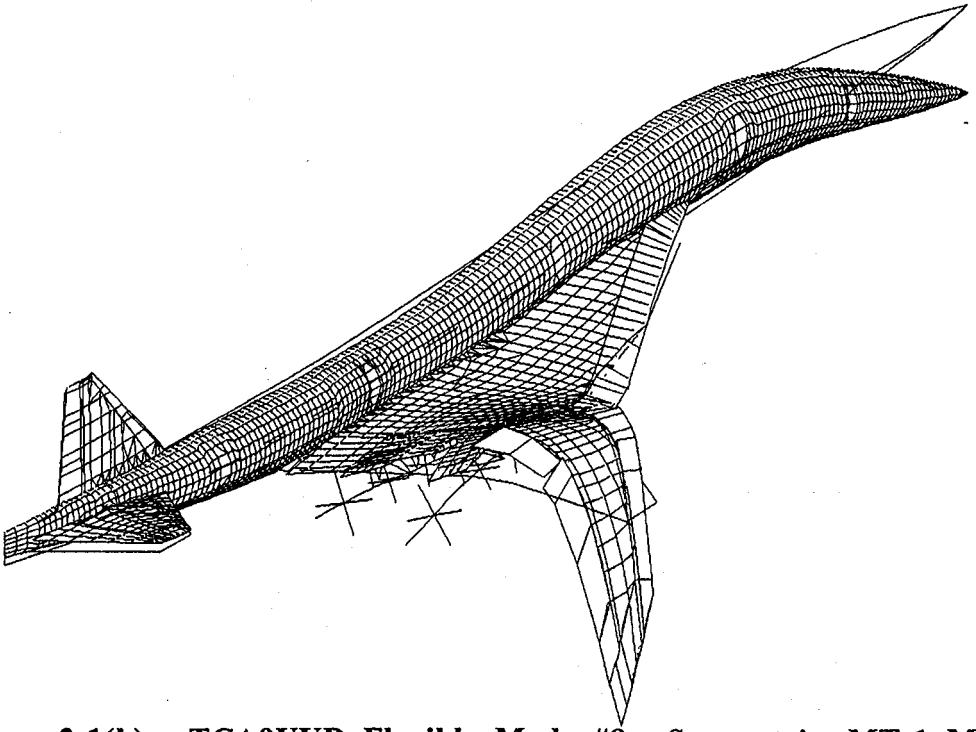

Figure 2-1(h): TCA9UUD Flexible Mode #8. Symmetric, MT-1 Mass Case, Frequency = 3.88 Hz.

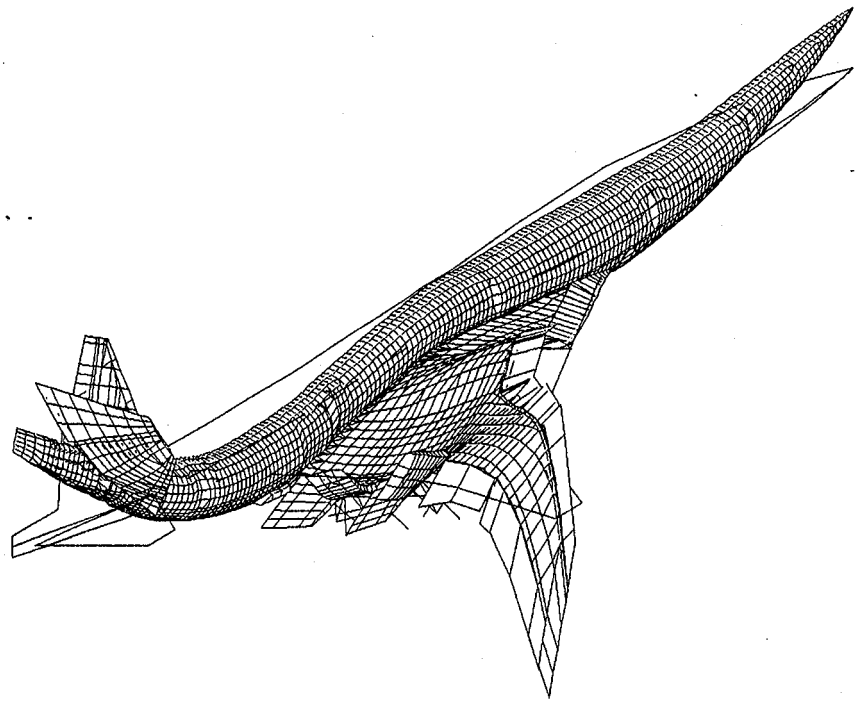

Figure 2-1(i): TCA9UUD Flexible Mode #9. Symmetric, MT-1 Mass Case, Frequency = 4.30 Hz.

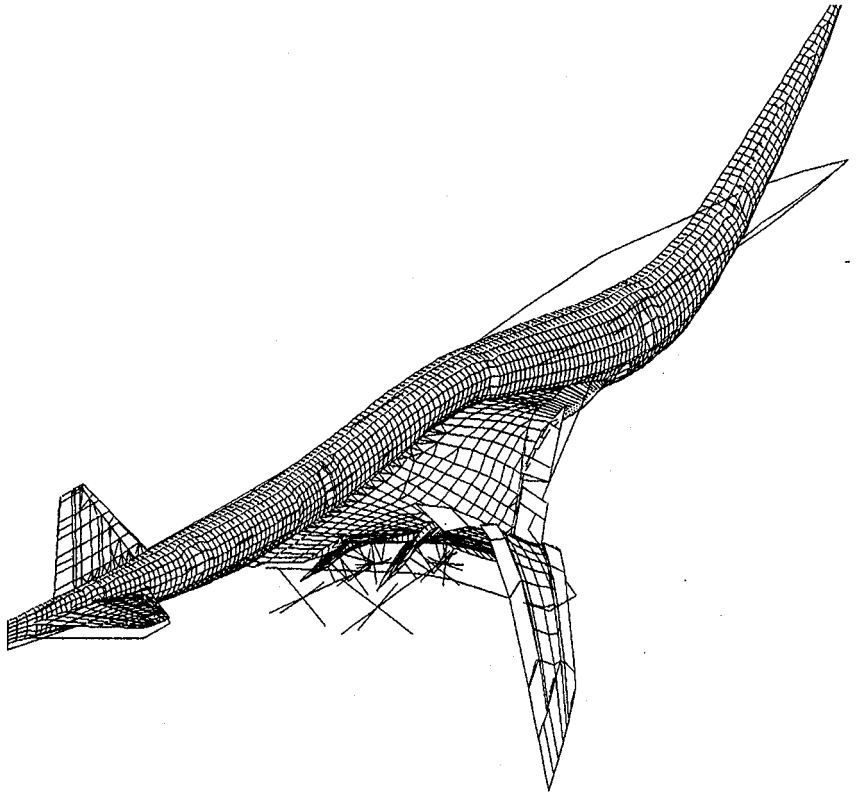

Figure 2-1(j): TCA9UUD Flexible Mode #10. Symmetric, MT-1 Mass Case, Frequency = 4.89 Hz.

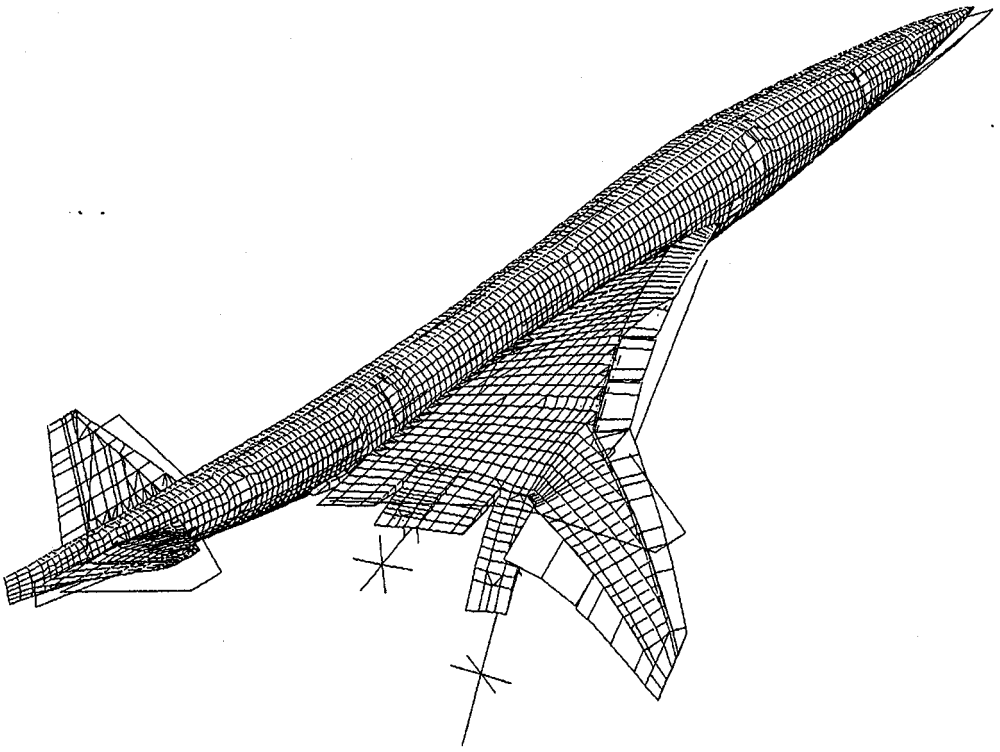

Figure 2-2(a): TCA9UUD Flexible Mode #1. Antisymmetric, MT-1 Mass Case, Frequency = 1.41 Hz.

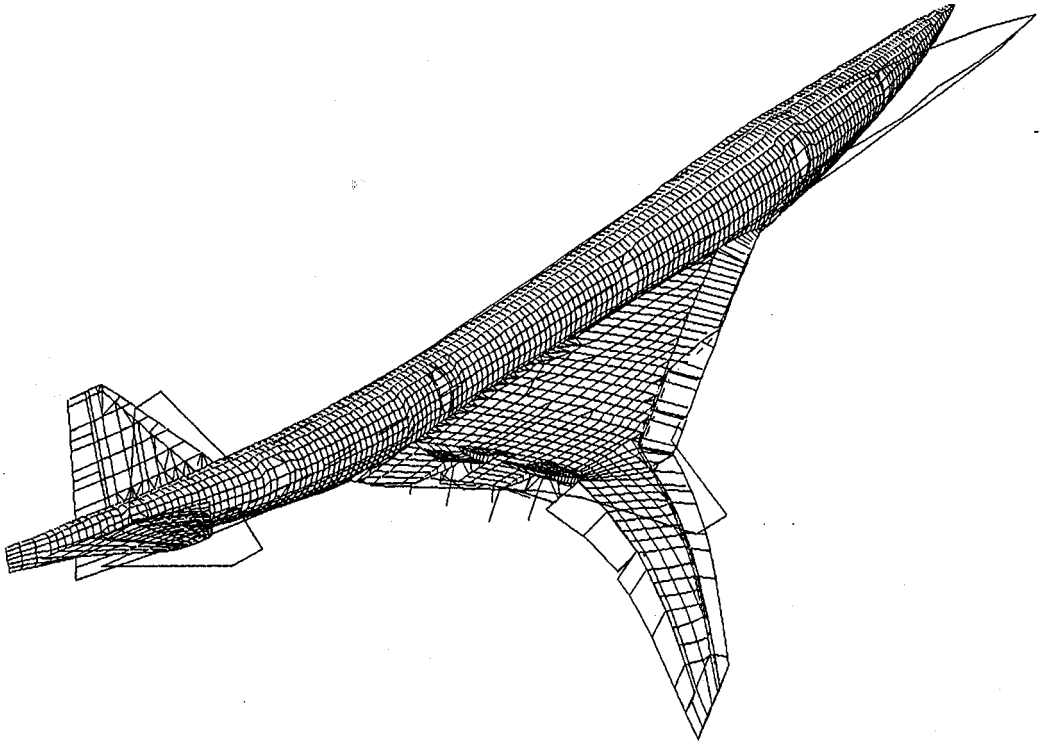

Figure 2-2(b): TCA9UUD Flexible Mode #2. Antisymmetric, MT-1 Mass Case, Frequency = 1.86 Hz.

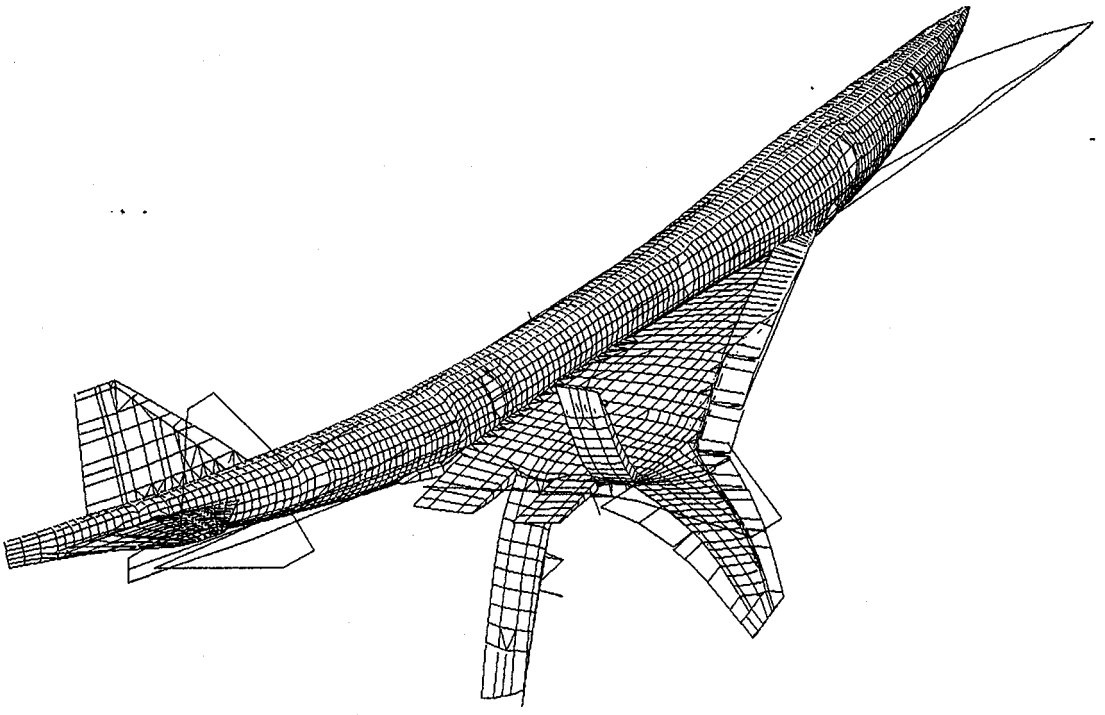

Figure 2-2(c): TCA9UUD Flexible Mode #3. Antisymmetric, MT-1 Mass Case, Frequency = 1.90 Hz.

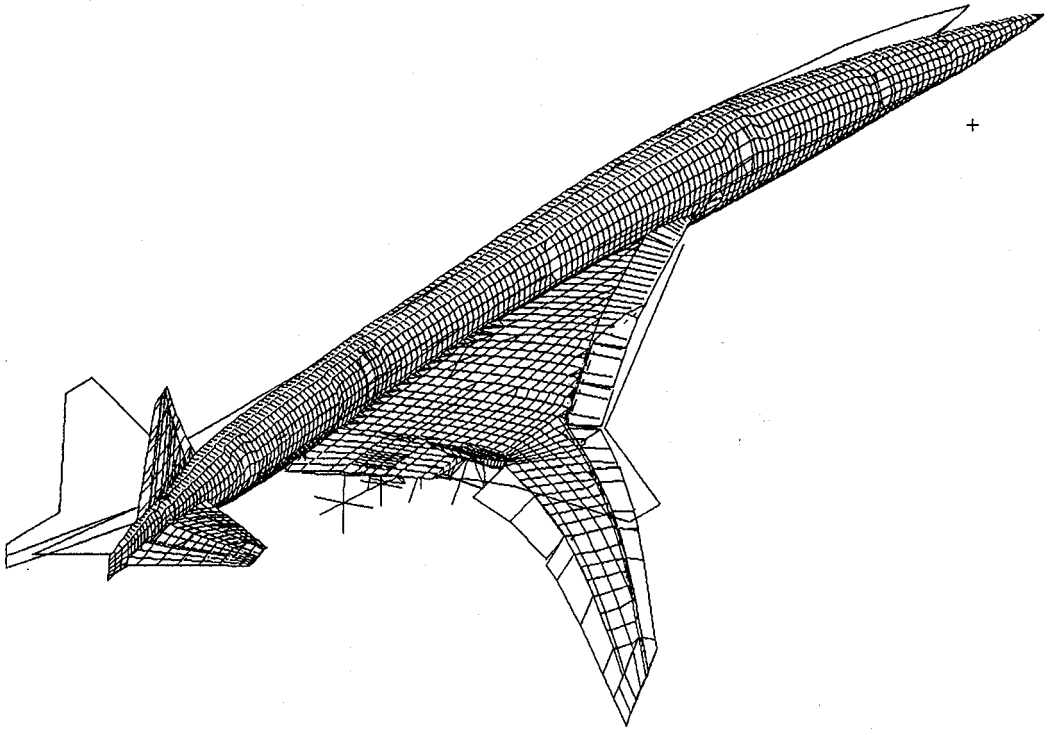

Figure 2-2(d): TCA9UUD Flexible Mode #4. Antisymmetric, MT-1 Mass Case, Frequency = 1.96 Hz.

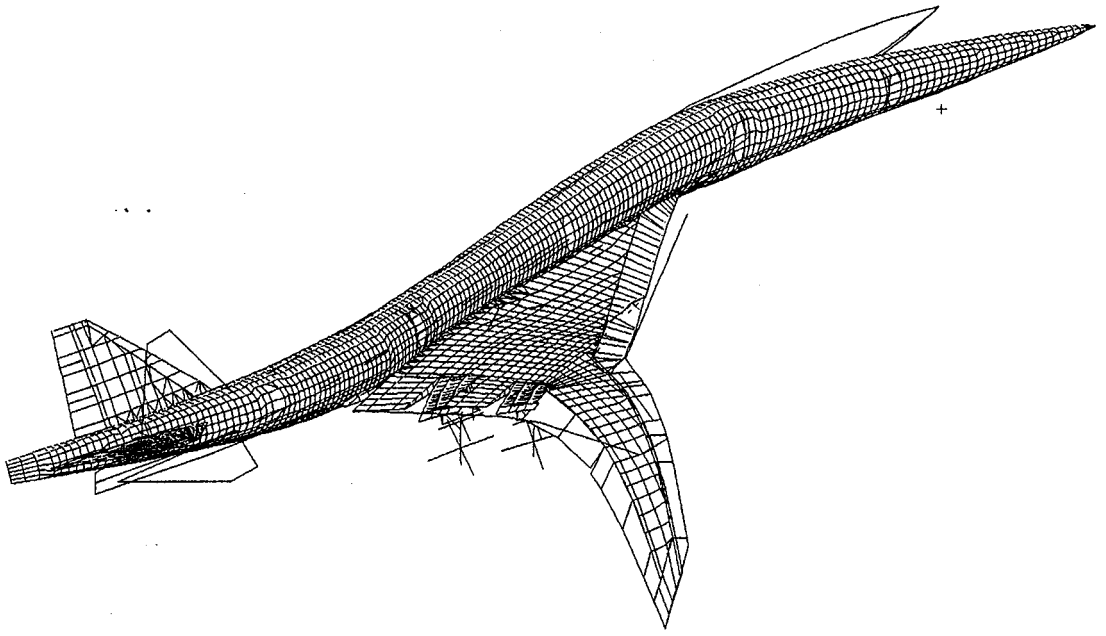

Figure 2-2(e): TCA9UUD Flexible Mode #5. Antisymmetric, MT-1 Mass Case, Frequency = 2.33 Hz.

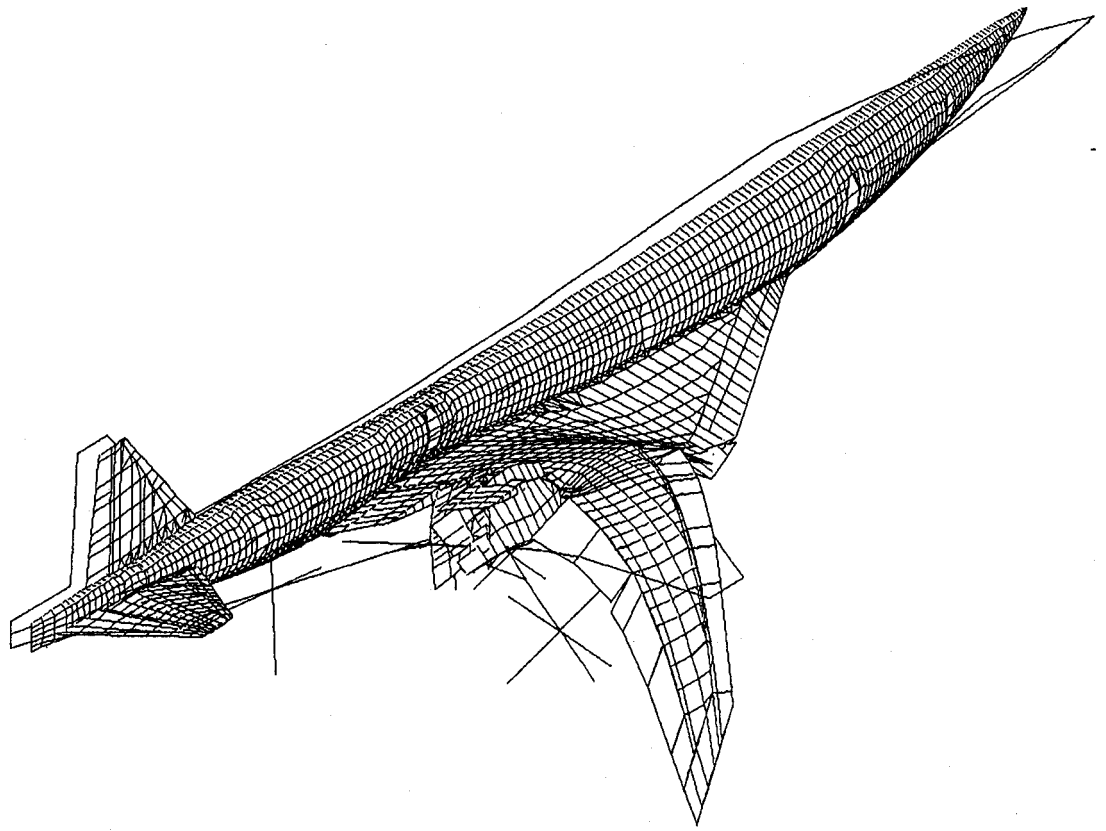

Figure 2-2(f): TCA9UUD Flexible Mode #6. Antisymmetric, MT-1 Mass Case, Frequency = 2.66 Hz.

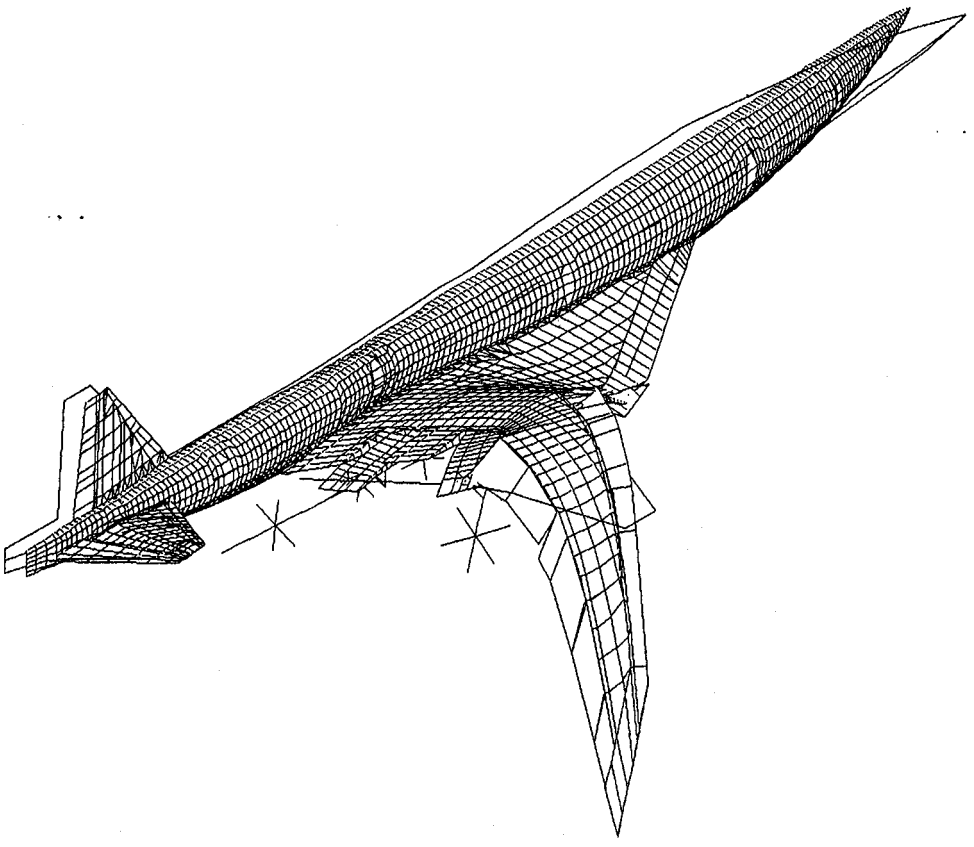

Figure 2-2(g): TCA9UUD Flexible Mode #7. Antisymmetric, MT-1 Mass Case, Frequency = 2.72 Hz.

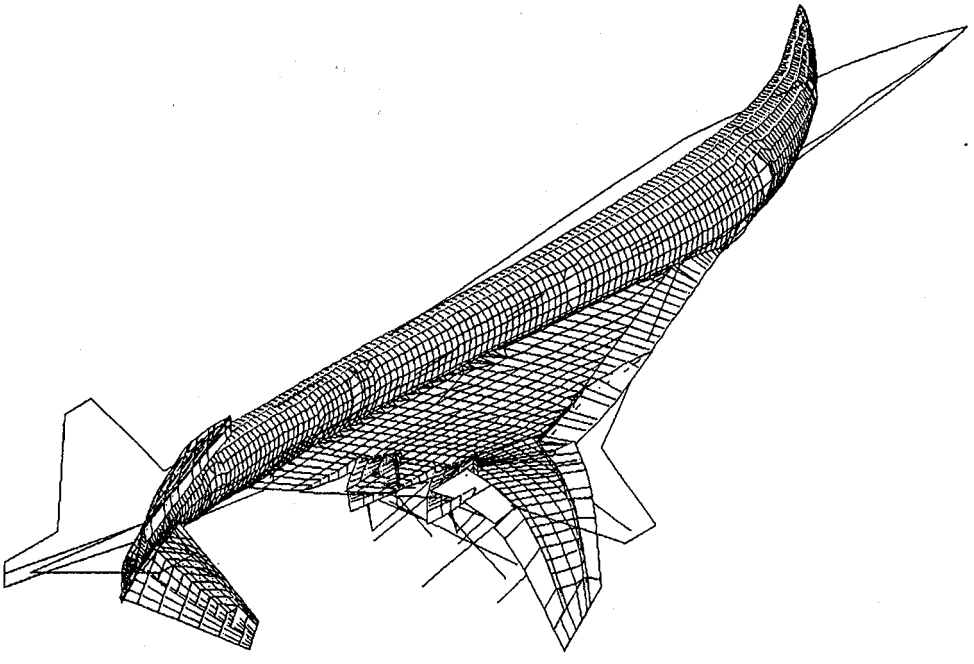

Figure 2-2(h): TCA9UUD Flexible Mode #8. Antisymmetric, MT-1 Mass Case, Frequency = 3.15 Hz.

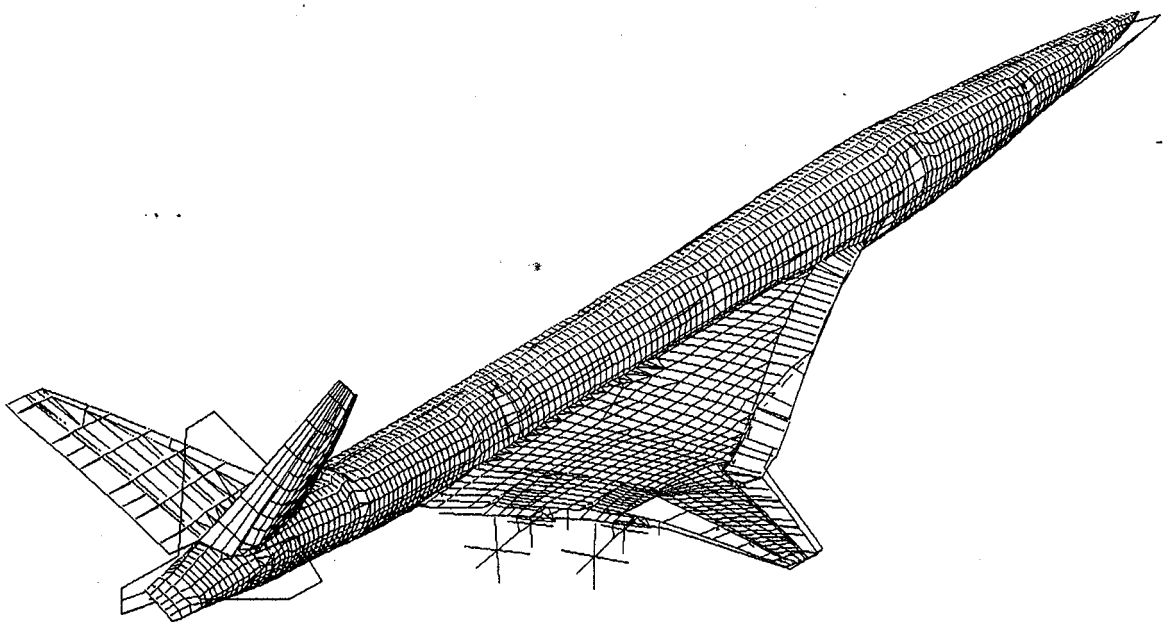

Figure 2-2(i): TCA9UUD Flexible Mode #9. Antisymmetric, MT-1 Mass Case, Frequency = 4.13 Hz.

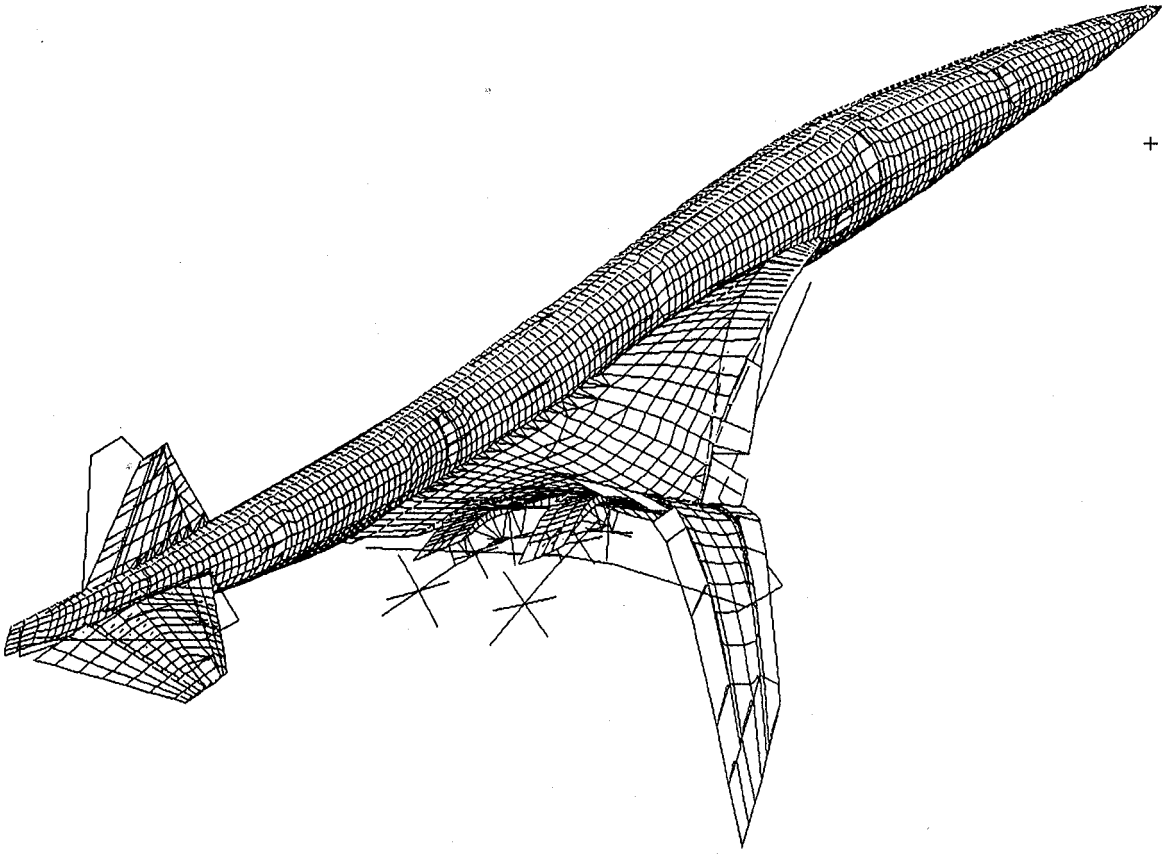

Figure 2-2(j): TCA9UUD Flexible Mode #10. Antisymmetric, MT-1 Mass Case, Frequency = 4.44 Hz.

Baseline Flutter Sized TCA, MT-1 Boundaries

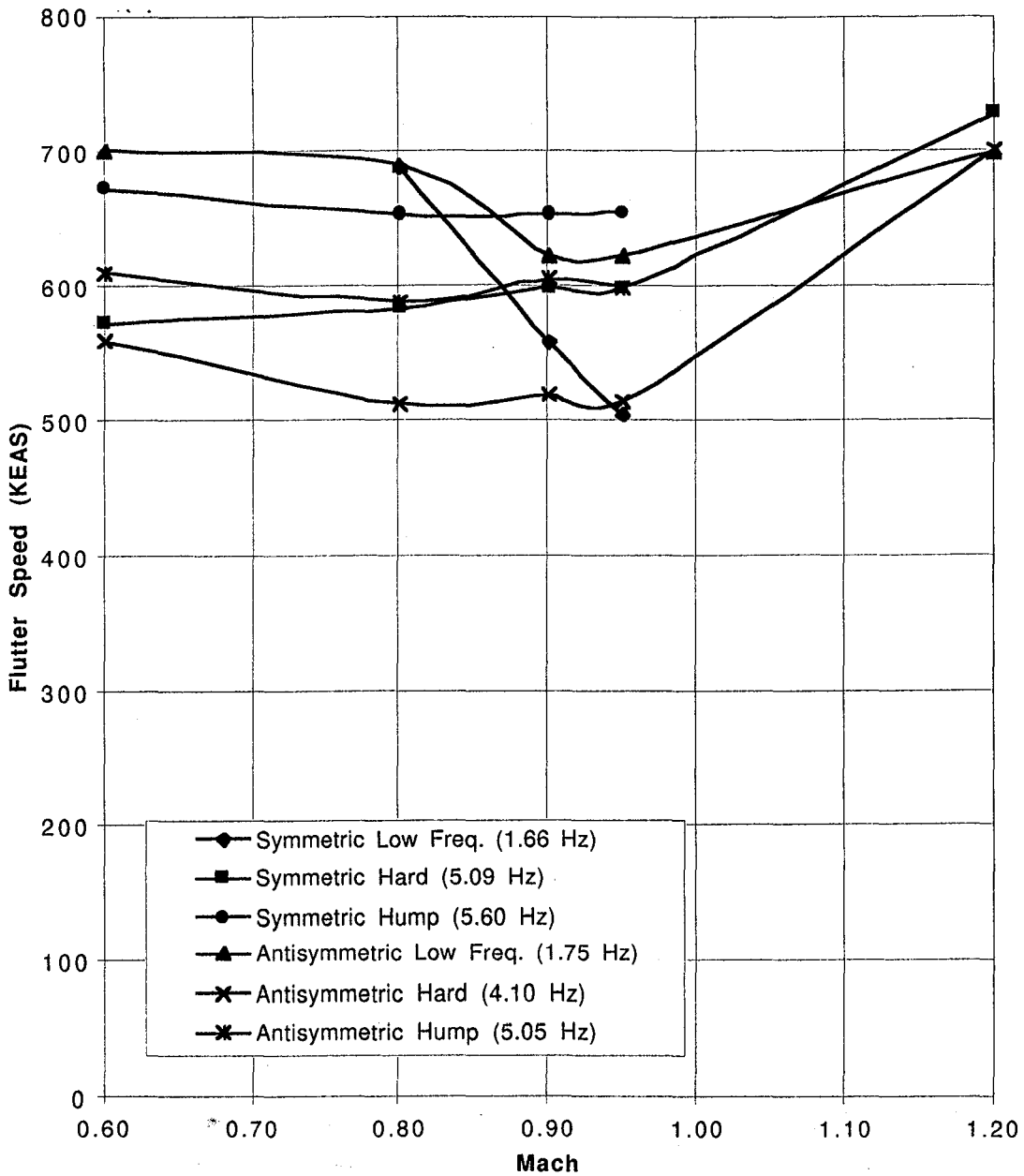

Figure 2-3: Flutter Boundaries of the Baseline Flutter Sized TCA (TCA9UUD) for Mass Case MT-1 in Air.

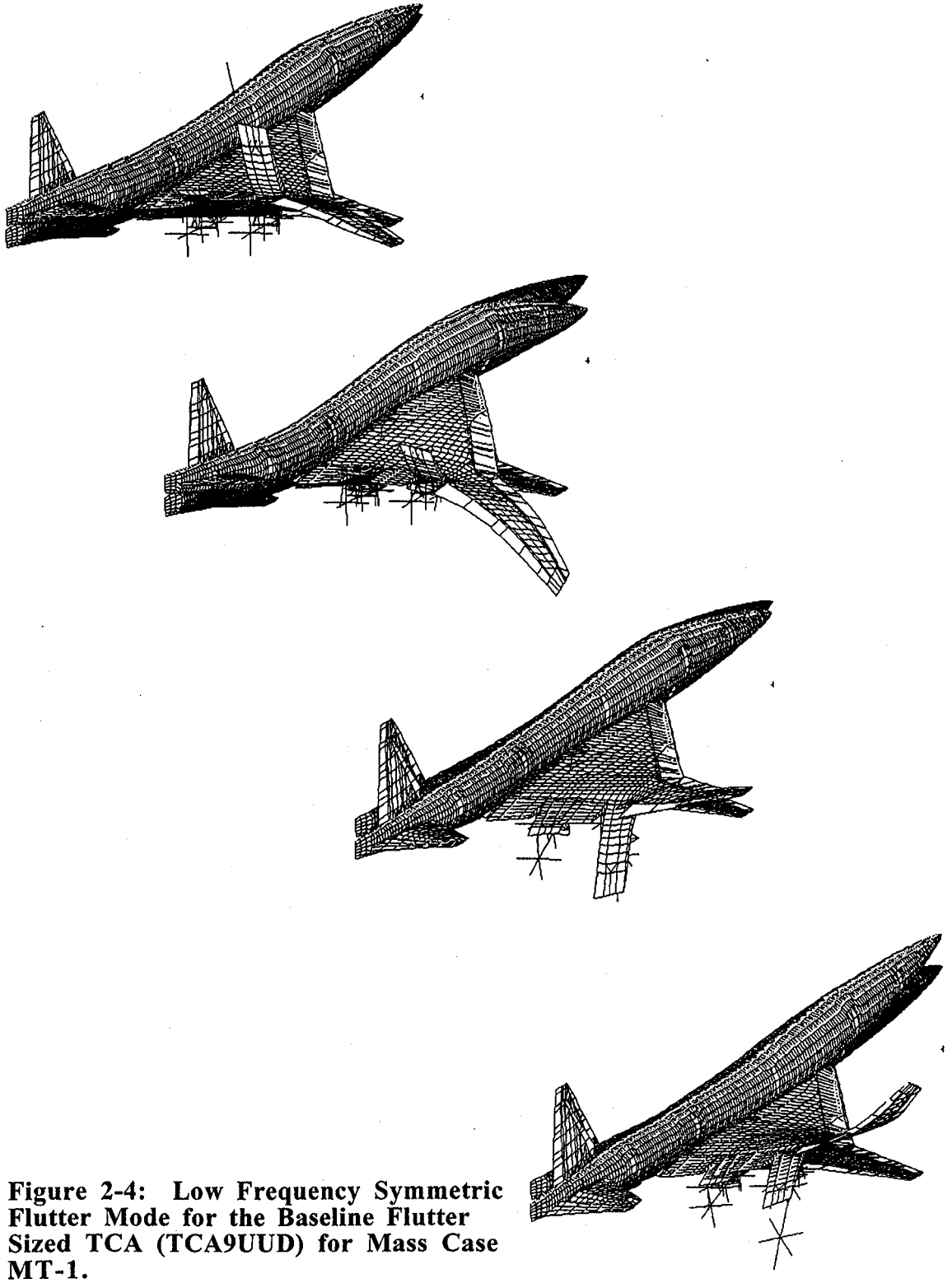

Figure 2-4: Low Frequency Symmetric Flutter Mode for the Baseline Flutter Sized TCA (TCA9UUD) for Mass Case MT-1.

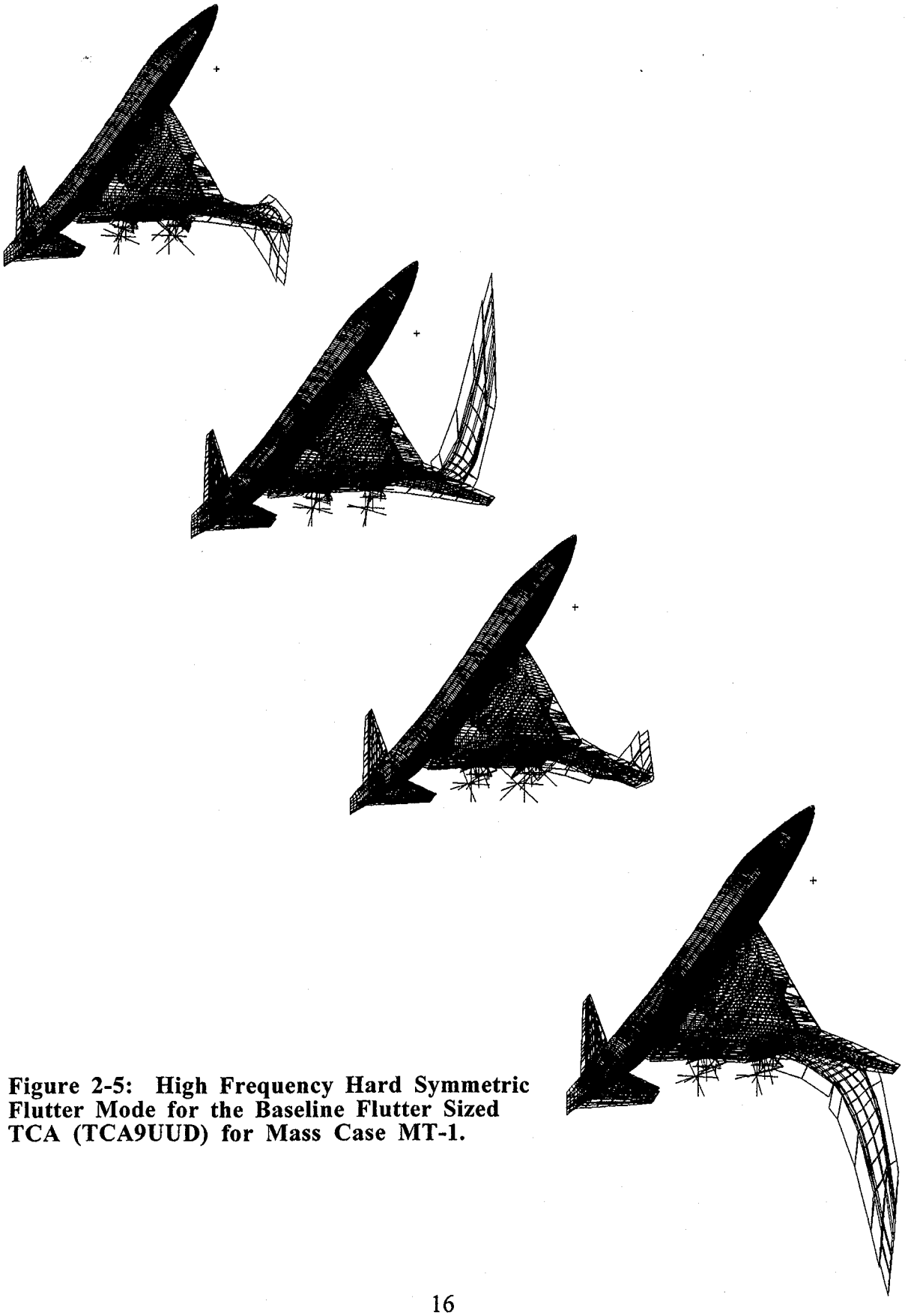

Figure 2-5: High Frequency Hard Symmetric Flutter Mode for the Baseline Flutter Sized TCA (TCA9UUD) for Mass Case MT-1.

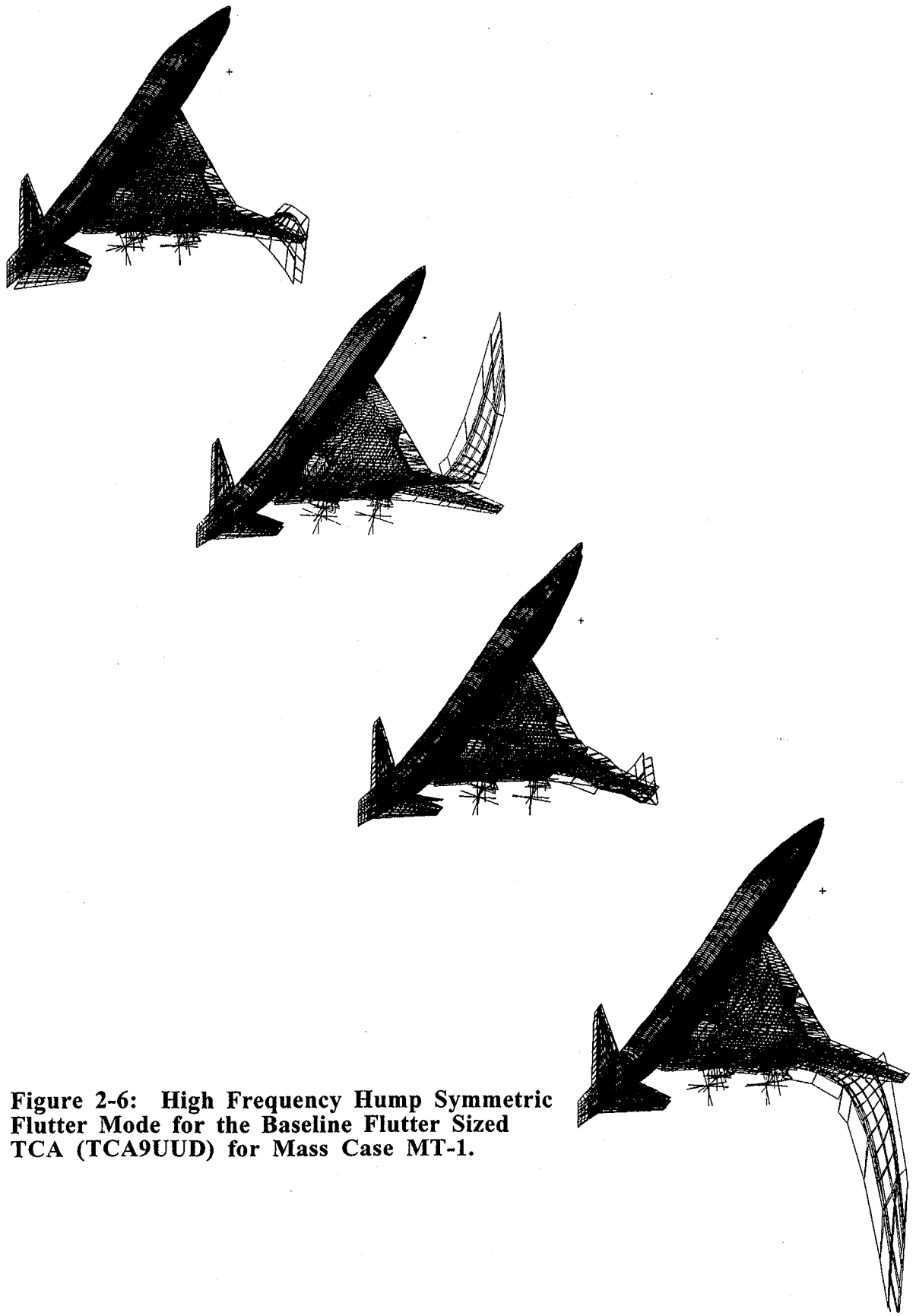

Figure 2-6: High Frequency Hump Symmetric Flutter Mode for the Baseline Flutter Sized TCA (TCA9UUD) for Mass Case MT-1.

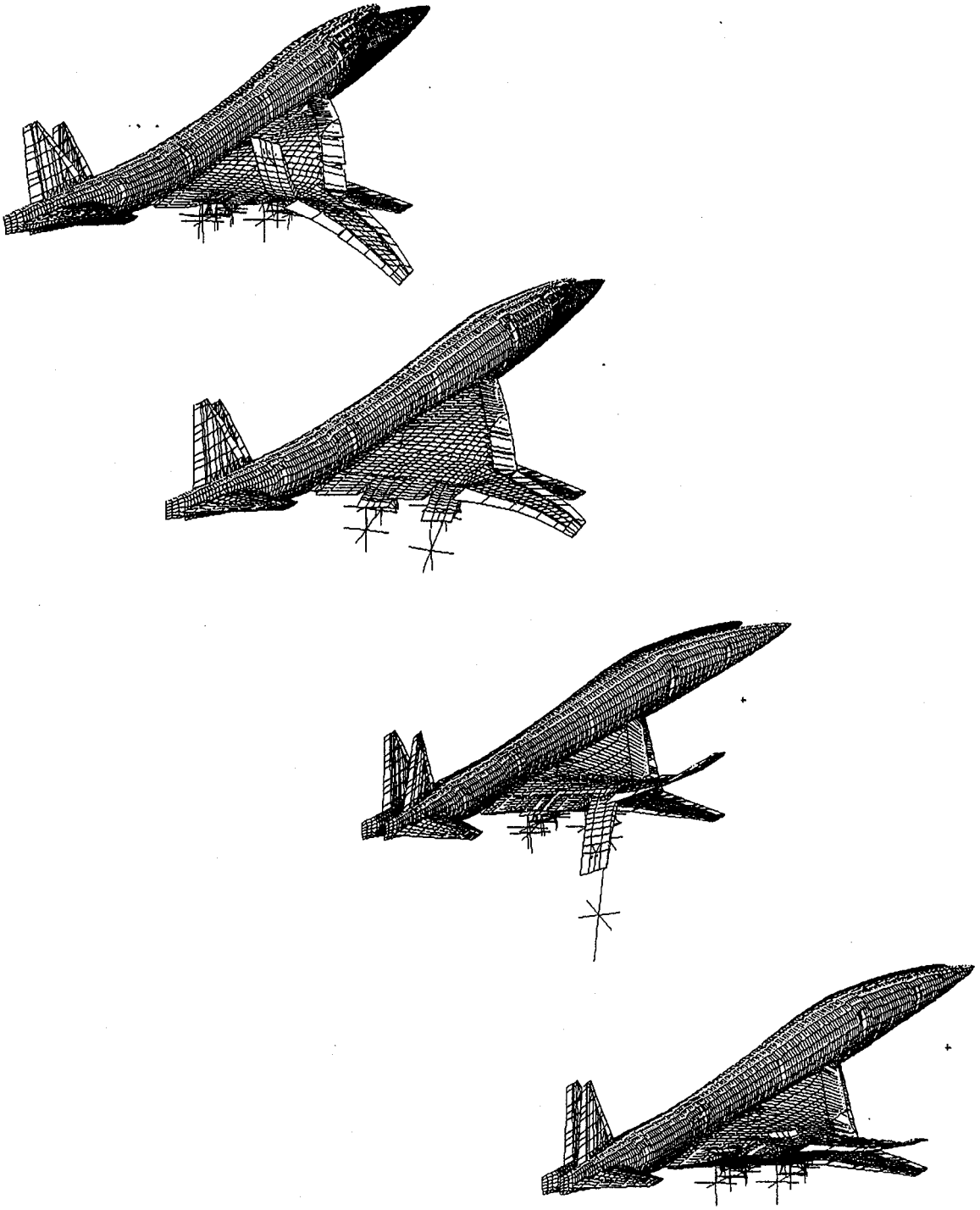

Figure 2-7: Low Frequency Antisymmetric Flutter Mode for the Baseline Flutter Sized TCA (TCA9UUD) for Mass Case MT-1.

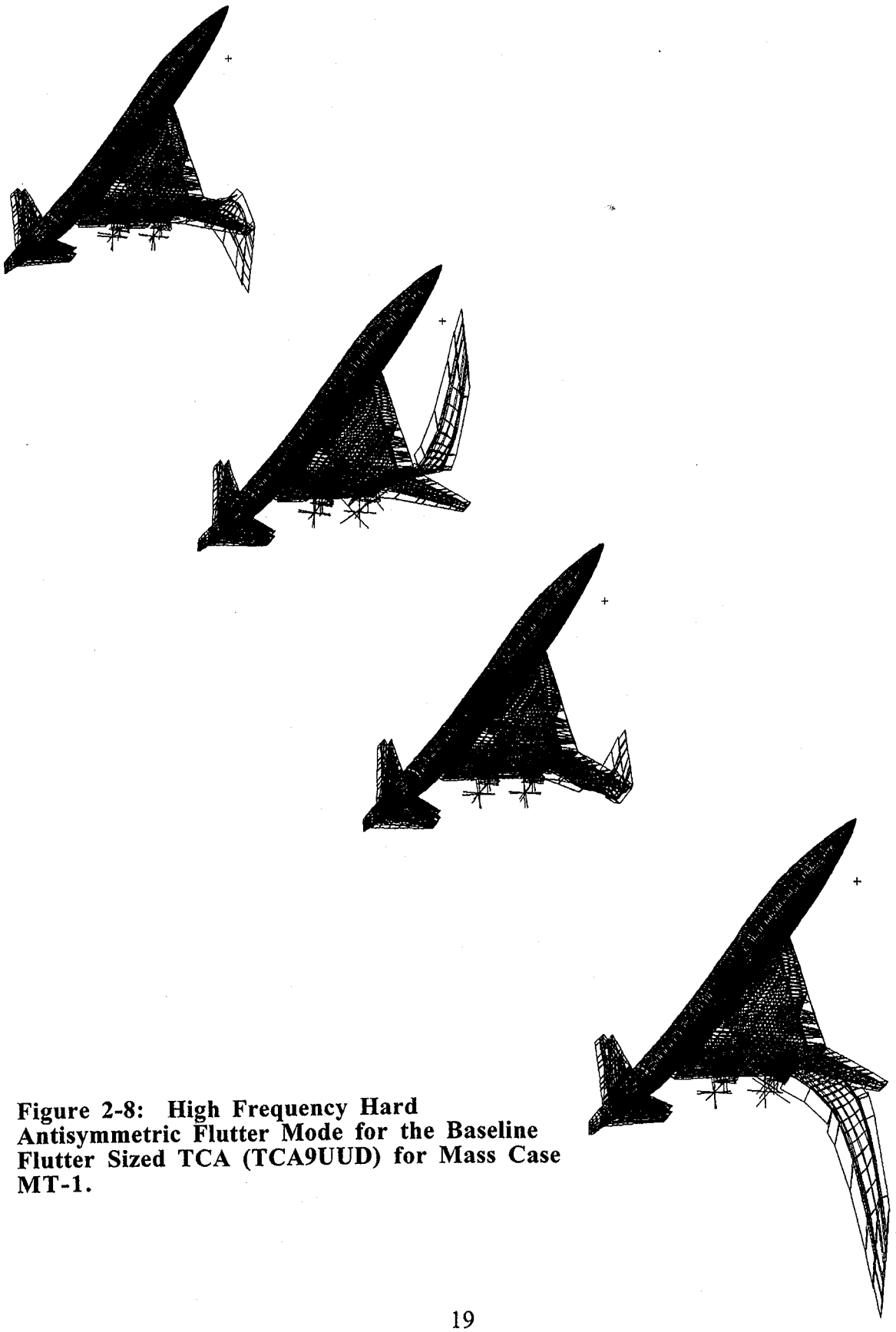

Figure 2-8: High Frequency Hard Antisymmetric Flutter Mode for the Baseline Flutter Sized TCA (TCA9UUD) for Mass Case MT-1.

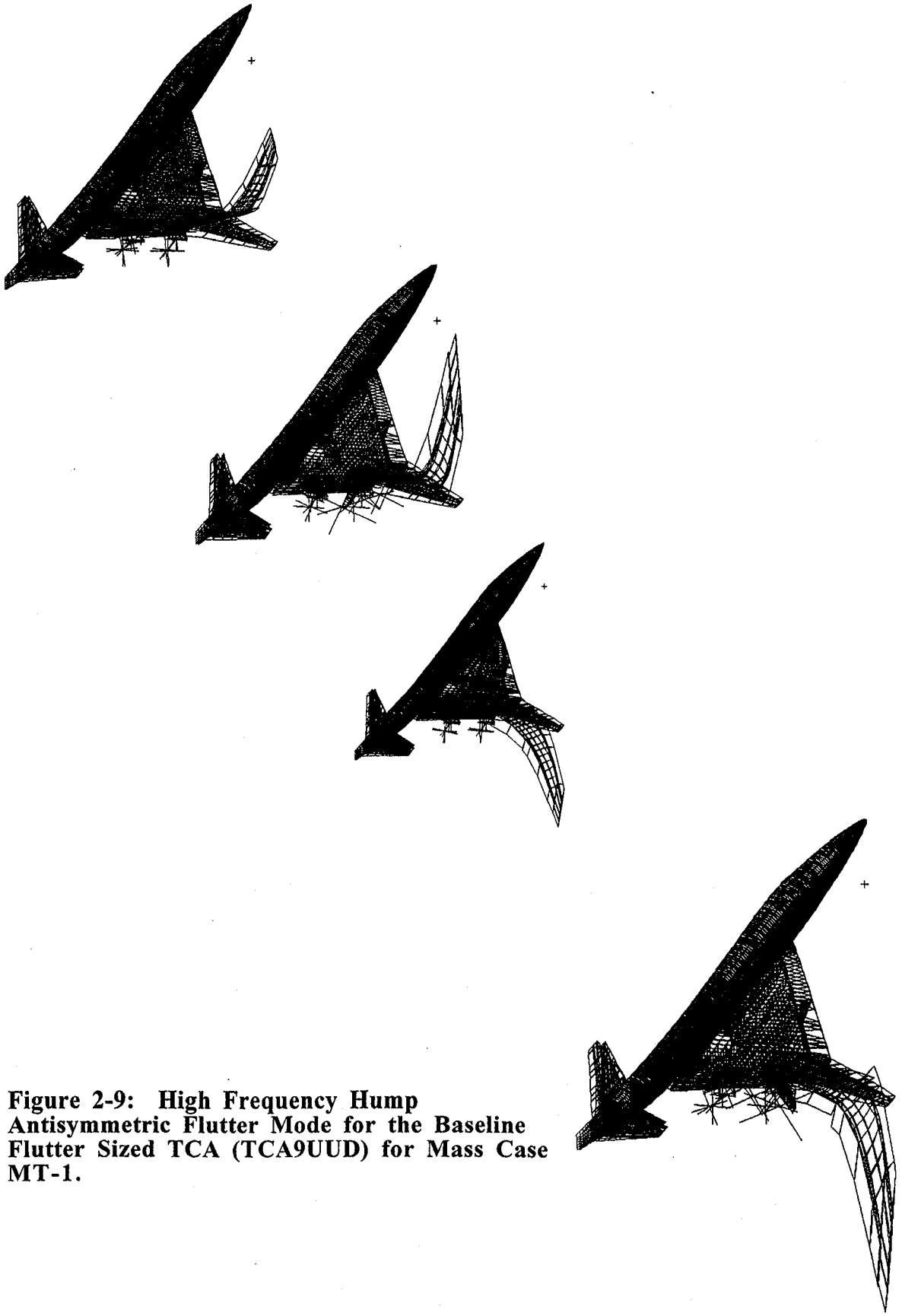

Figure 2-9: High Frequency Hump Antisymmetric Flutter Mode for the Baseline Flutter Sized TCA (TCA9UUD) for Mass Case MT-1.

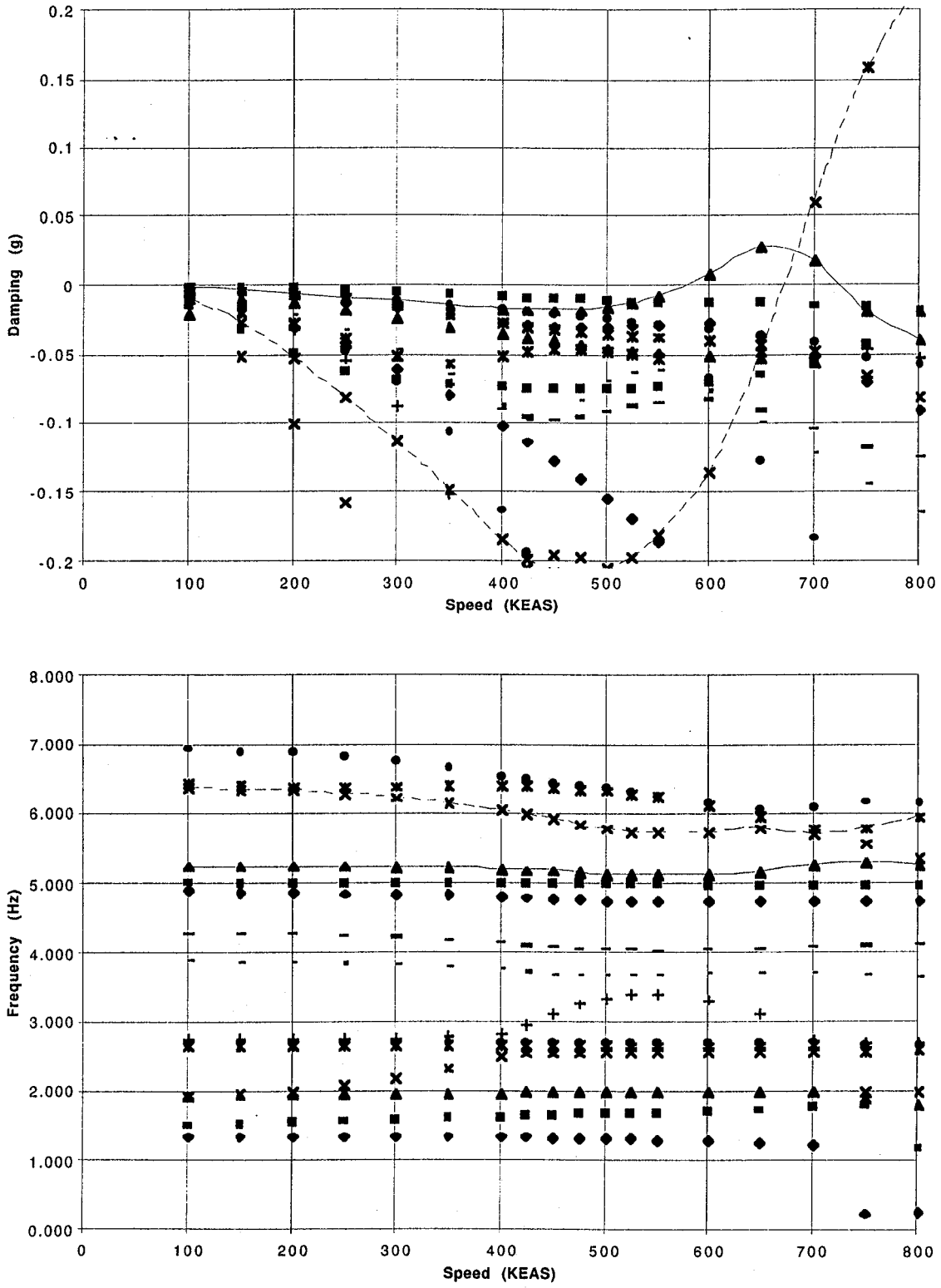

Figure 2-10(a): V-G and V-F Plots for Baseline Flutter Sized TCA. MT-1 Mass Case, Symmetric, Mach 0.60.

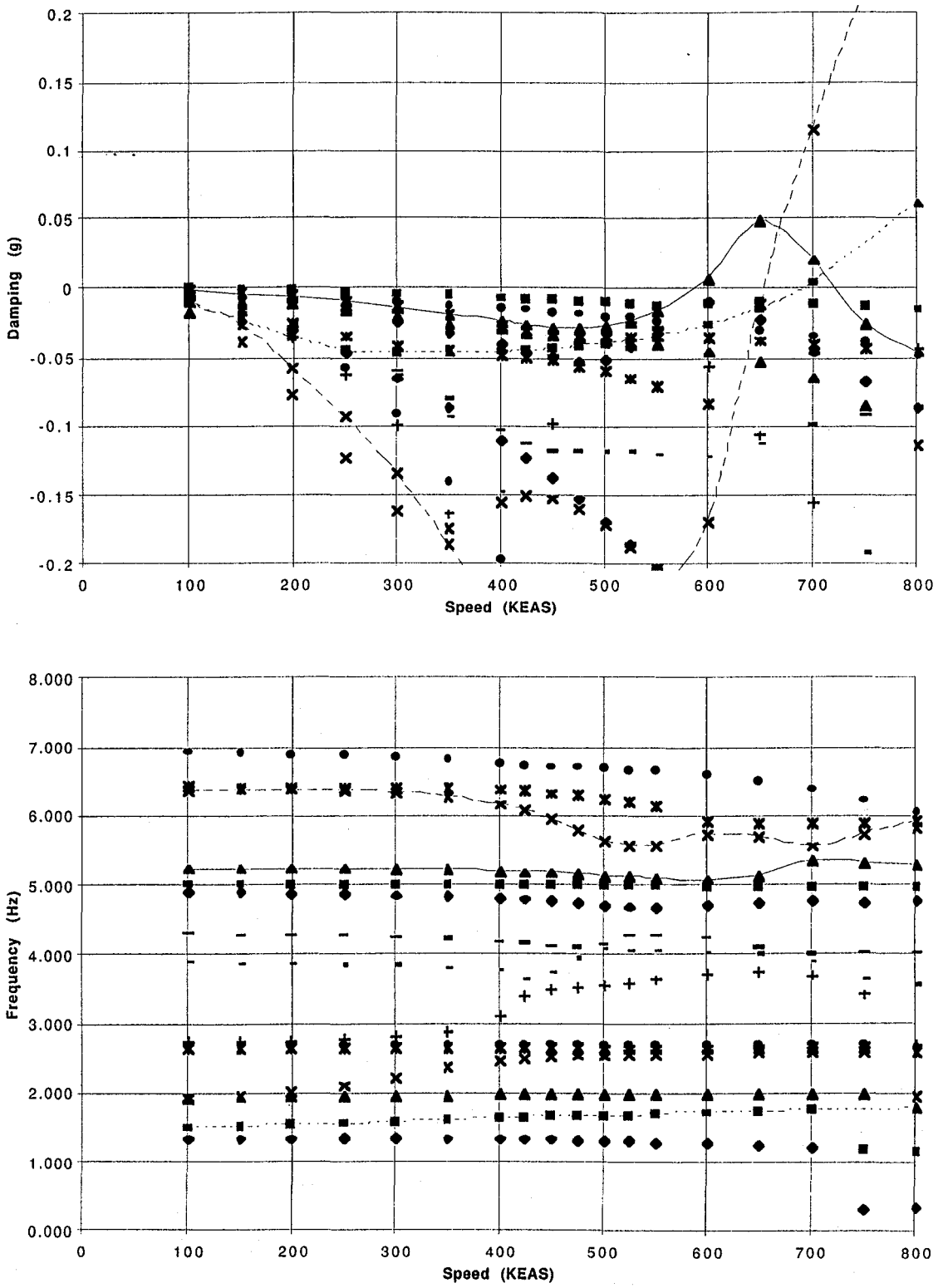

Figure 2-10(b): V-G and V-F Plots for Baseline Flutter Sized TCA. MT-1 Mass Case, Symmetric, Mach 0.80.

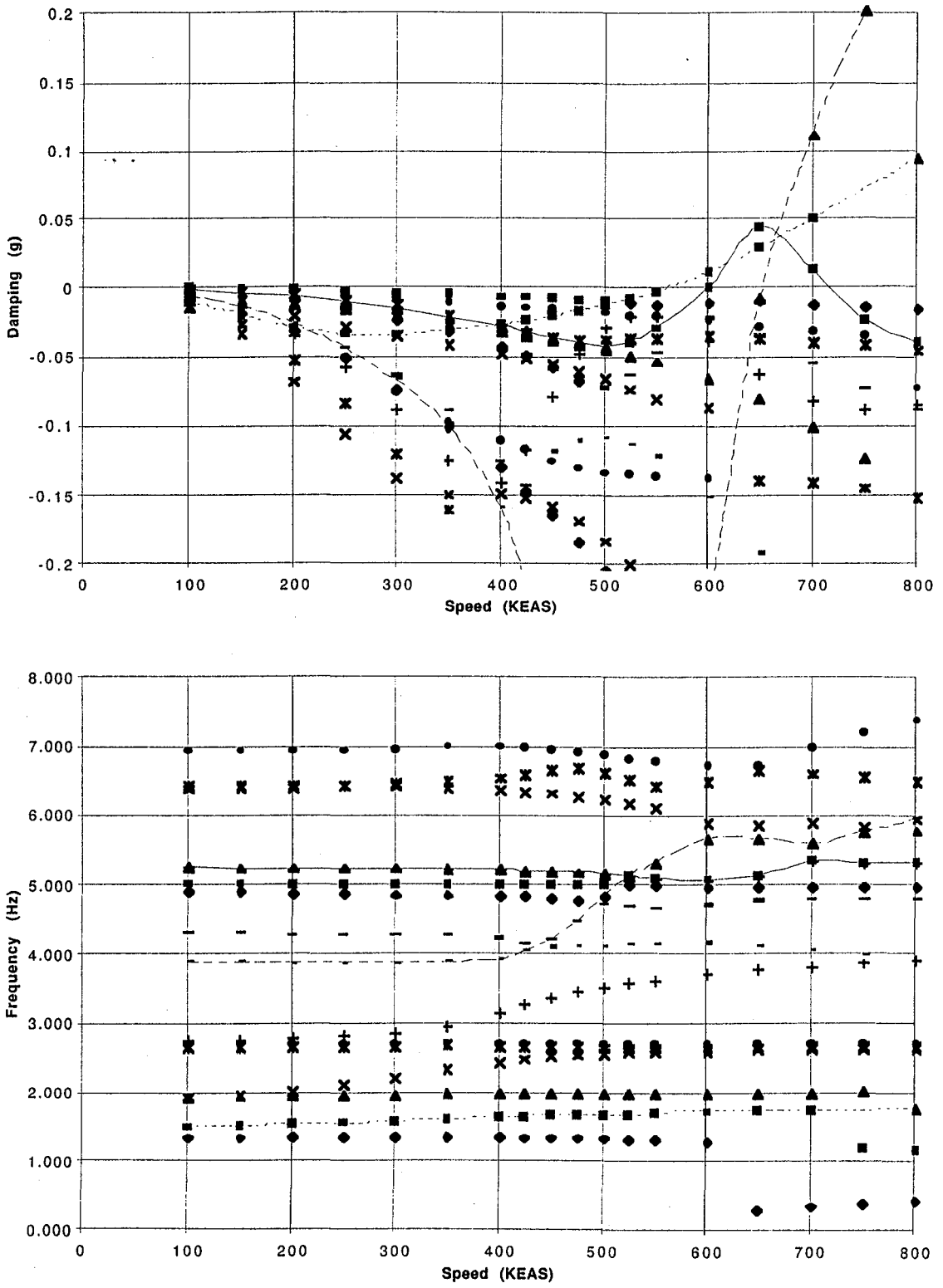

Figure 2-10(c): V-G and V-F Plots for Baseline Flutter Sized TCA. MT-1 Mass Case, Symmetric, Mach 0.90.

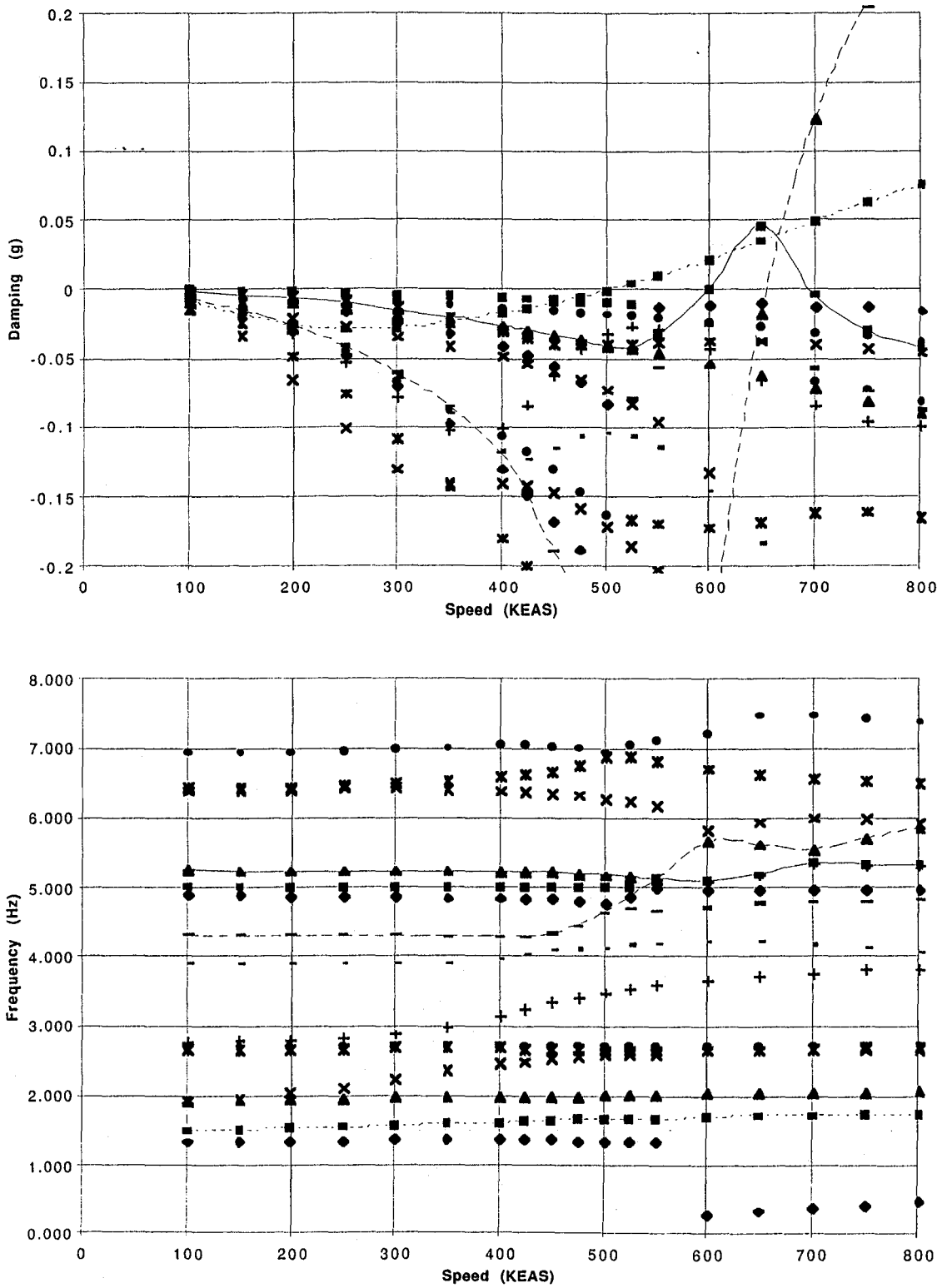

Figure 2-10(d): V-G and V-F Plots for Baseline Flutter Sized TCA. MT-1 Mass Case, Symmetric, Mach 0.95.

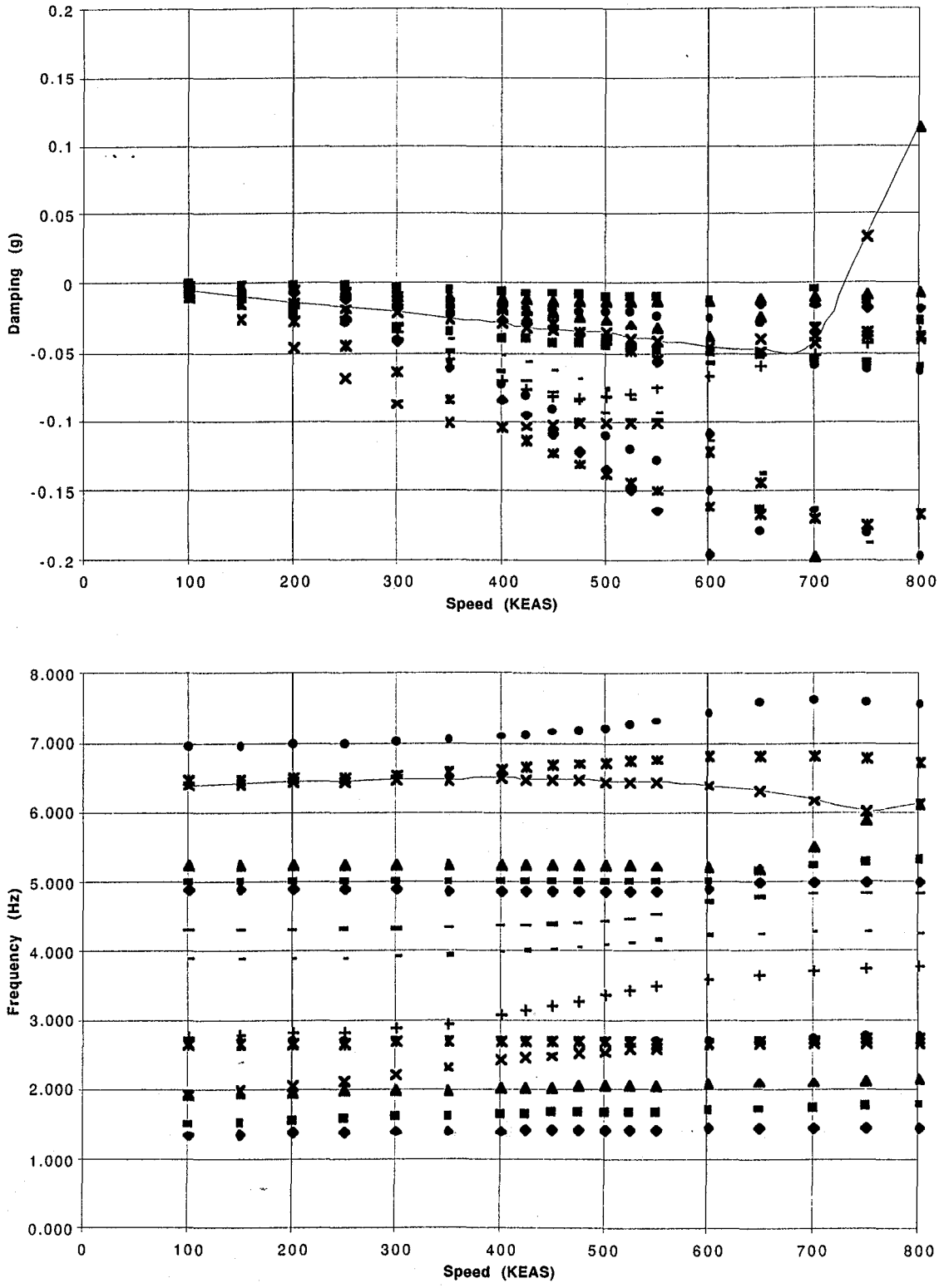

Figure 2-10(e): V-G and V-F Plots for Baseline Flutter Sized TCA. MT-1 Mass Case, Symmetric, Mach 1.20.

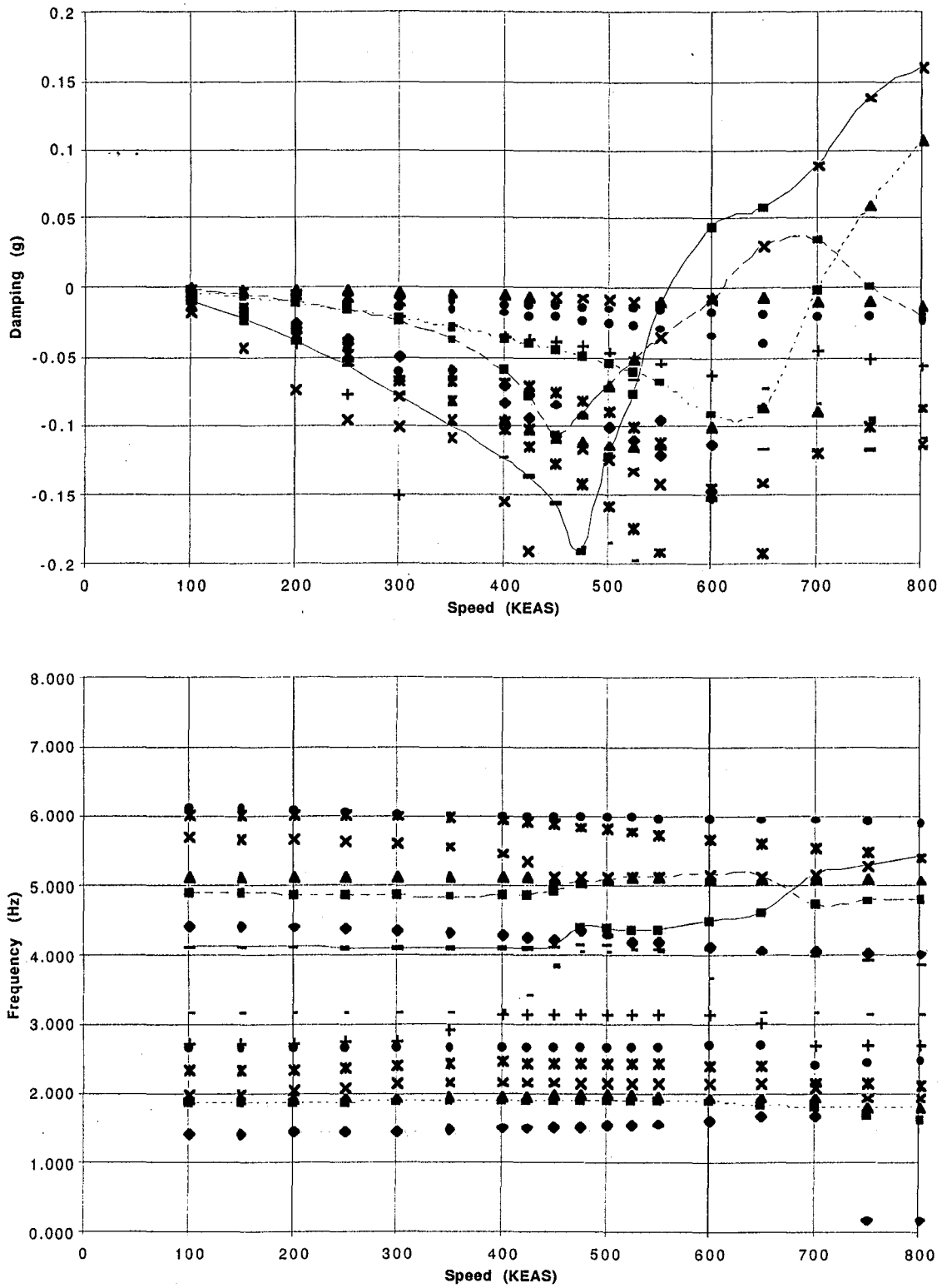

Figure 2-11(a): V-G and V-F Plots for Baseline Flutter Sized TCA. MT-1 Mass Case, Antisymmetric, Mach 0.60.

[redacted]

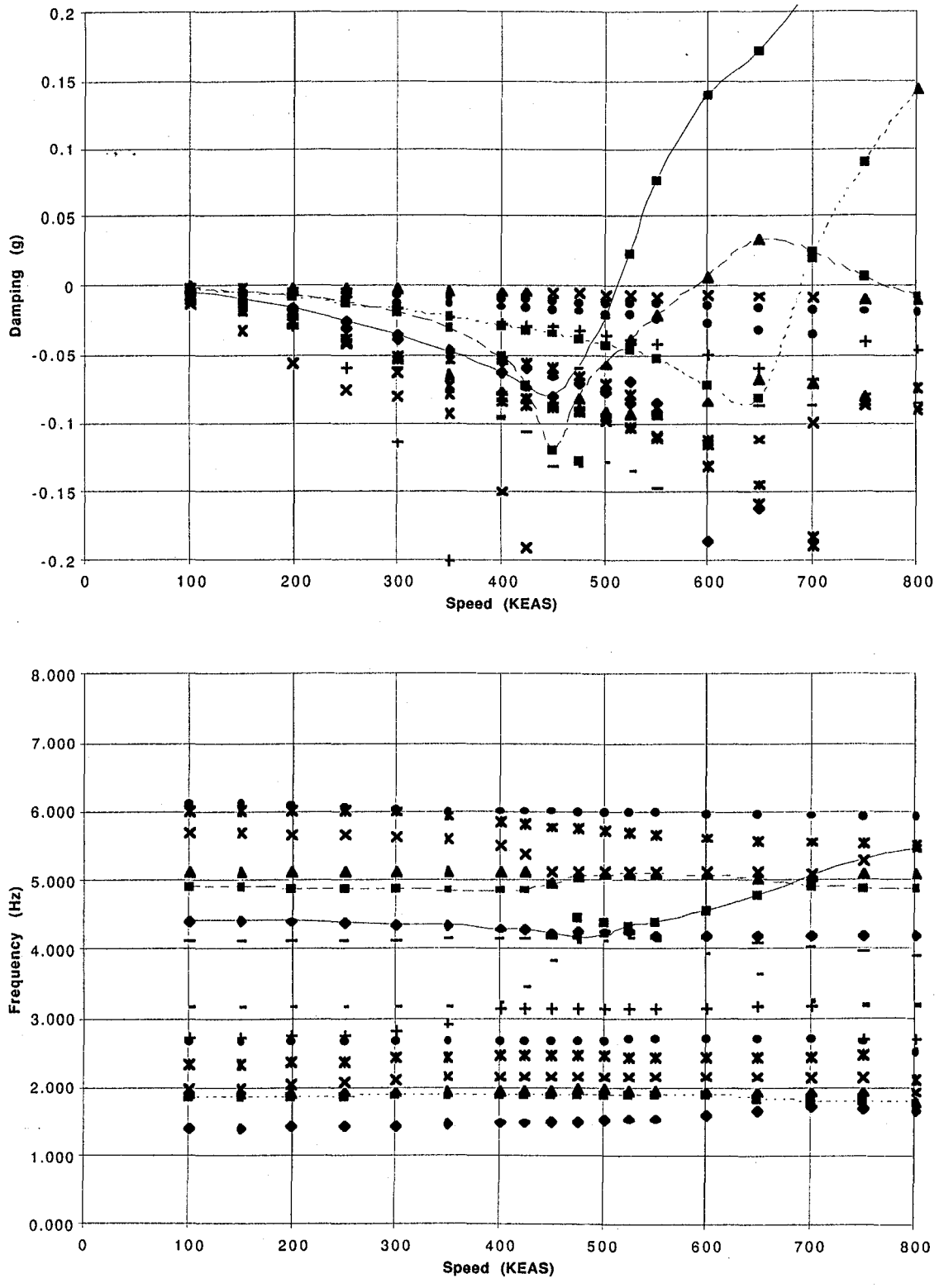

Figure 2-11(b): V-G and V-F Plots for Baseline Flutter Sized TCA. MT-1 Mass Case, Antisymmetric, Mach 0.80.

[redacted]

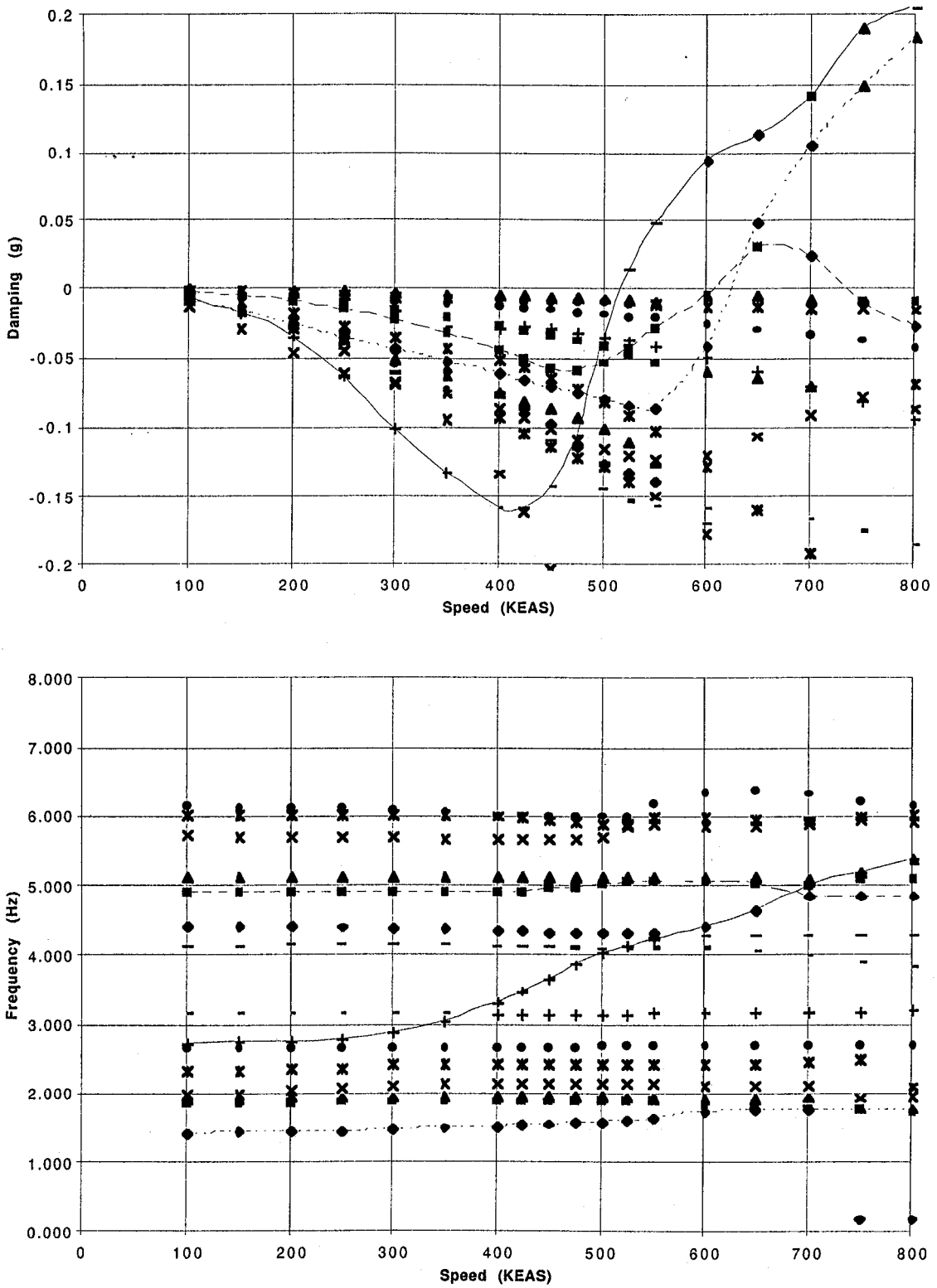

Figure 2-11(c): V-G and V-F Plots for Baseline Flutter Sized TCA. MT-1 Mass Case, Antisymmetric, Mach 0.90.

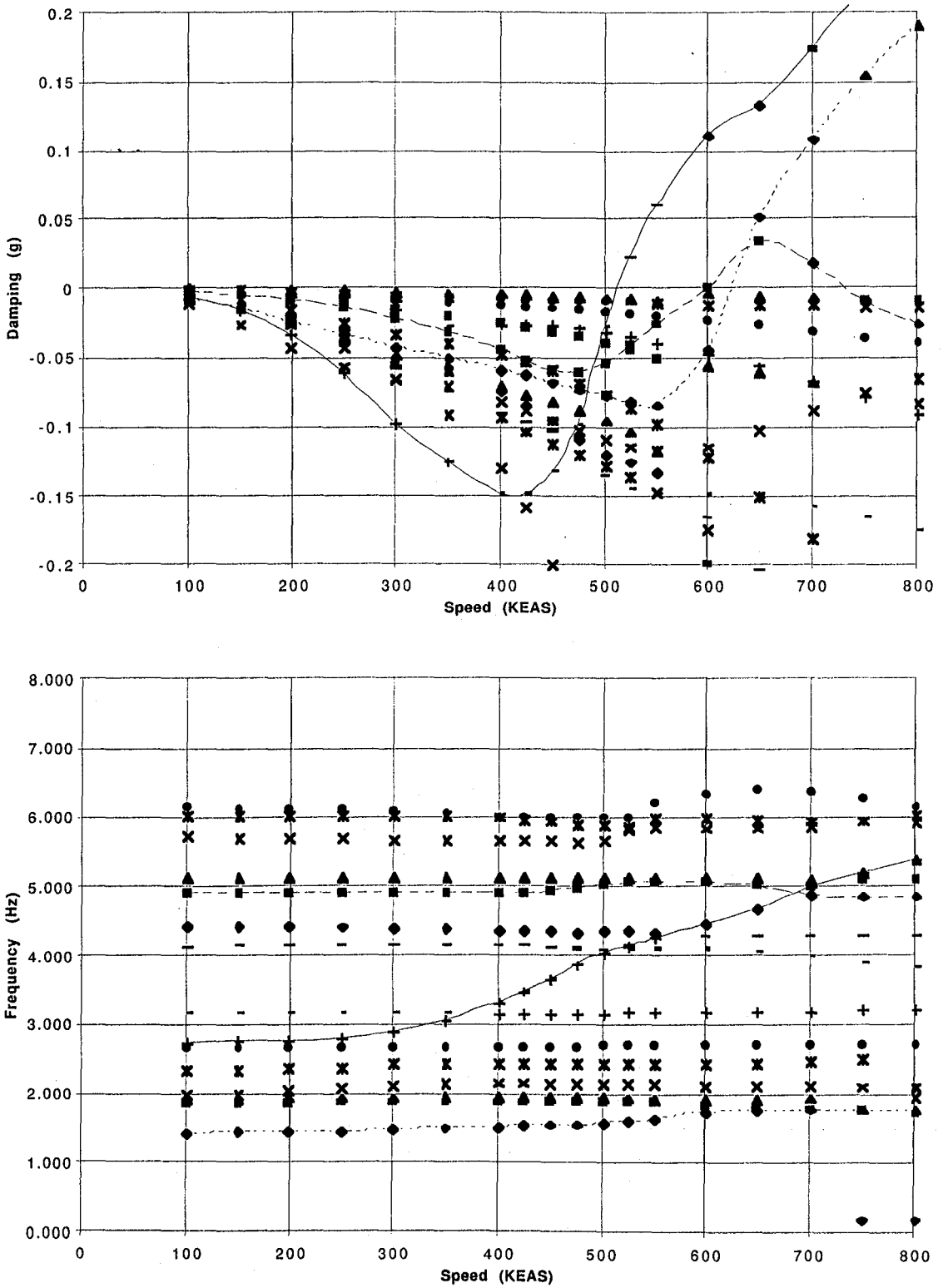

Figure 2-11(d): V-G and V-F Plots for Baseline Flutter Sized TCA. MT-1 Mass Case, Antisymmetric, Mach 0.95.

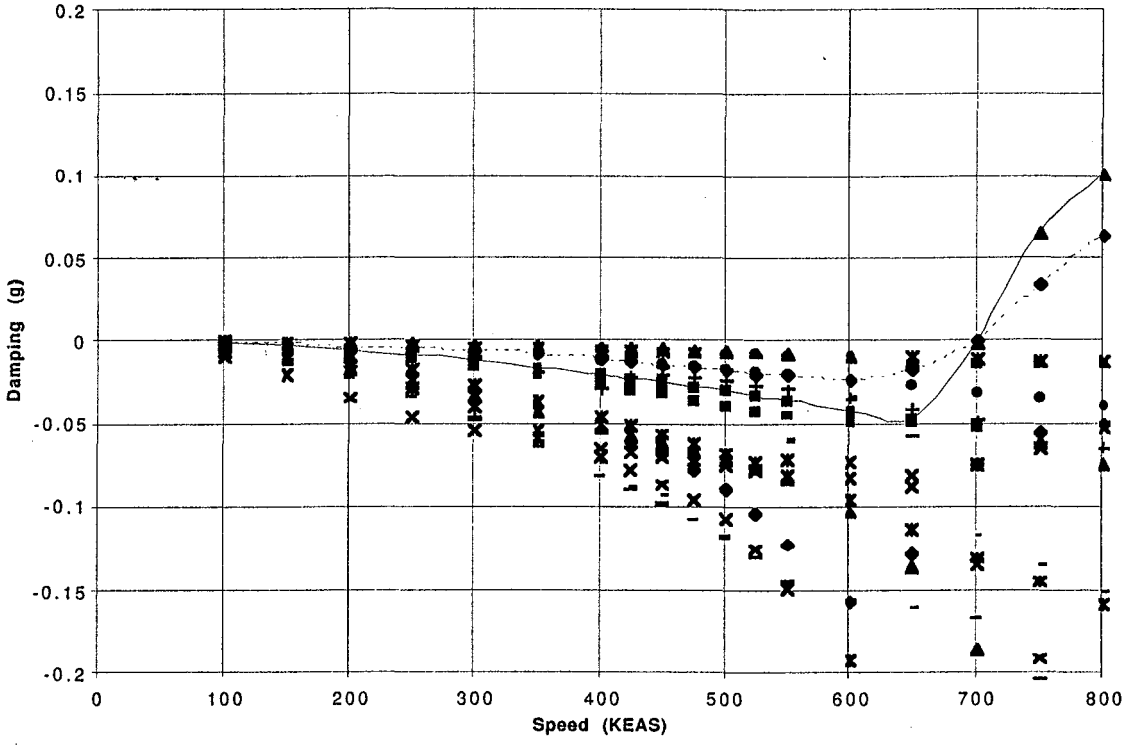

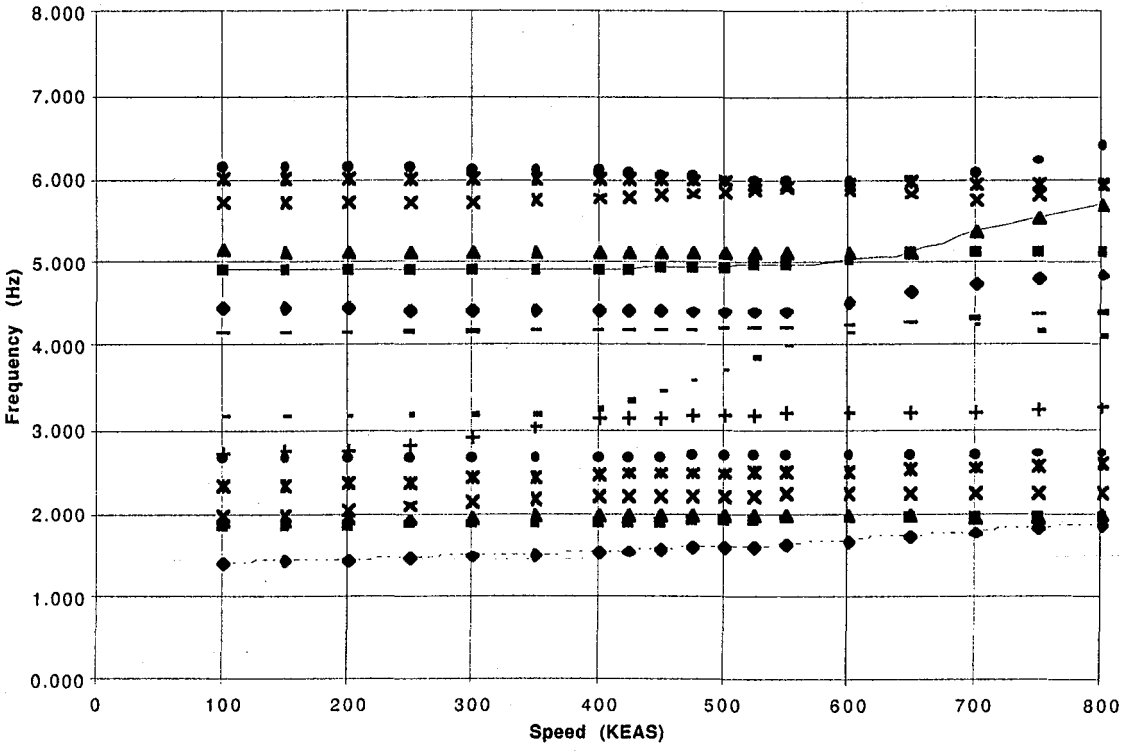

Figure 2-11(e): V-G and V-F Plots for Baseline Flutter Sized TCA. MT-1 Mass Case, Antisymmetric, Mach 1.20.

[redacted]

3. Parametric Flutter Analyses

As discussed in previous sections, the ability to predict the low frequency wing/body/engine/tail (symmetric and antisymmetric) flutter mechanism is deemed to be of greater impact and importance to the HSCT program than any of the high frequency outboard wing modes. The importance of the low frequency flutter mechanisms over the high frequency mechanisms comes from several factors. First, the weight penalty associated with the low frequency flutter mechanism is significantly higher than that attributed to the high frequency flutter modes. Second, it is believed that the low frequency mode involves greater coupling of the fuselage/engines/pylons and wing and thus will be more difficult to predict. Additionally, it was felt that successful testing of the high frequency mechanisms would have been far riskier because the frequencies are much higher, and the flutter crossings are much steeper. The high frequencies are difficult to get away from becuase the frequency scale factor is a function of the length scale factor and the velocity scale factor which are both fixed.

The baseline strength/flutter sized configuration flutter envelope presented in Figure 2-3 clearly shows that this configuration is not appropriate for studying the low frequency flutter mechanisms. It is this observation that prompts the parametric variations described in this section. There are three objectives of these variations:

1) Identify changes to the baseline configuration that will make the low frequency mechanism critical across a significant part of the testing Mach range (0-1.2) and push the flutter speeds of the high frequency mechanisms higher to provide a comfortable margin between the low and high frequency mechanisms.
2) Define the parameters (engine pylon stiffness etc...) that influence the flutter speeds of the low frequency mechanisms to provide input the model design process. This input will be in the form of defining what would the variable parameters be and how much they should vary to significantly effect the flutter speed.
3) Provide asource of information that may help identify a "flutter fix" to help reduce the weight of the TCA configuration, and to identify candidate "flutter stoppers" to help improve test safety.

Each parametric variation performed is described in one of the following subsections. In each case, the results of the variation is compared to the baseline analysis, with emphasis on the MT-1 mass condition and Mach 0.95. Based on these results, the recommended design configuration described in Section 4 was chosen.

3.1 Strength vs. Flutter Sizing

One of the possible variations that was identified early on in this task that might result in a more desireable configuration for wind tunnel testing is the strength-sized model. This model tends to have a lower flutter speed (and hence dynamic pressure), which improves the model scaling parameters, and it also tends to have better separation between the low frequency and high frequency flutter mechanisms. A comparison of the vibration mode frequencies for the first ten modes (symmetric and antisymmetric) for mass case MT-1 of the strength-sized vehicle and the strength+flutter sized vehicle is presented in Table 3.1-1. The general trend, as expected, is that the strength-sized model has slightly lower modal frequencies than the strength+flutter sized model. There are some exceptions in the higher modes (symmetric flexible modes 8 and 10).

The flutter crossing speeds and frequencies for the strength and strength+flutter sized models are compared in Table 3.1-2. There is only a minimal effect on the flutter speed of the high frequency flutter modes (about 30-40 knots), but the flutter speed of the low frequency mechanisms are reduced by about 100 knots. This results in much better separation between the target low frequency mechanisms and the dangerous high frequency mechanisms, resulting in improved model testability. A representative set of v-g and v-f plots for the strength sized model is shown in Figure 3.1-1, for the MT-1 mass condition at Mach 0.95. Based primarily on the improved separation between the low frequency symmetric mechanism and the high frequency antisymmetric mechanism, it was decided that a strength sized airplane would be a good starting point for the wind tunnel model design.

Mode Number	Symmetric		Antisymmetric	
	Flutter Sized	Strength Sized	Flutter Sized	Strength Sized
1	1.326	1.261	1.406	1.296
2	1.485	1.422	1.857	1.752
3	1.893	1.801	1.898	1.822
4	1.942	1.867	1.955	1.884
5	2.664	2.553	2.330	2.252
6	2.686	2.668	2.662	2.595
7	2.768	2.684	2.725	2.623
8	3.880	3.696	3.152	3.086
9	4.298	4.085	4.130	4.015
10	4.891	4.719	4.439	4.205

Table 3.1-1: Modal Frequency Comparison Between Strength and Flutter Sized Models for MT-1 Mass Condition.

		Speed		Frequency	
		Flutter	Strength	Flutter	Strength
Symmetric	Low Freq	505	385	1.664	1.595
	High Freq Hard	656	652	5.596	5.254
	High Freq Hump	600	577	5.085	4.954
Antisymm.	Low Freq	623	534	1.747	1.670
	High Freq Hard	514	478	4.092	3.858
	High Freq Hump	601	572	5.052	4.882

Table 3.1-2: Flutter Crossing Comparison Between Strength and Flutter Sized Models for MT-1 Mass Condition at Mach 0.95.

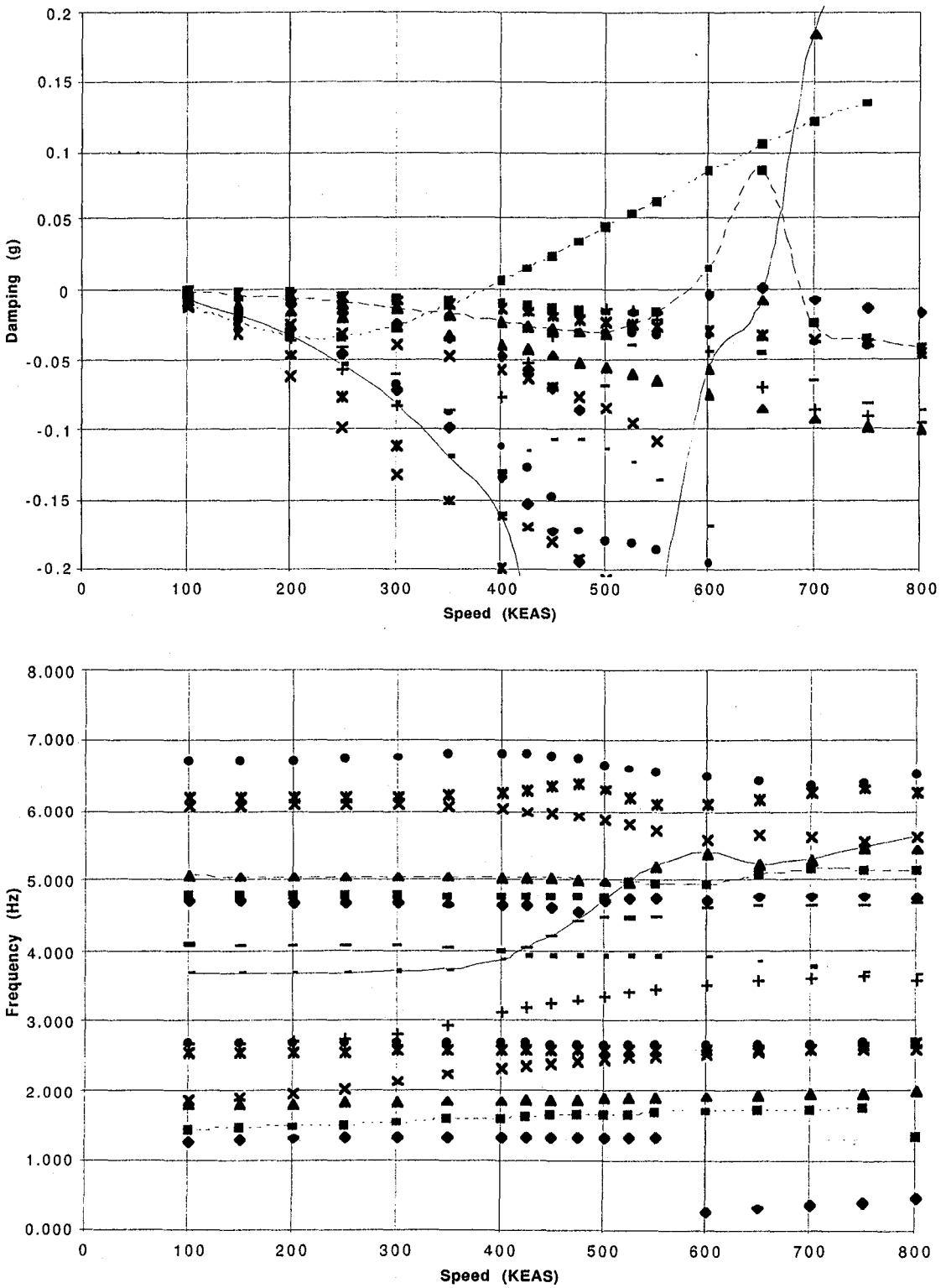

Figure 3.1-1: V-G and V-F Plots for the Strength Sized Model (Symmetric Boundary Condition, MT-1 Mass Case at Mach 0.95 in Air).

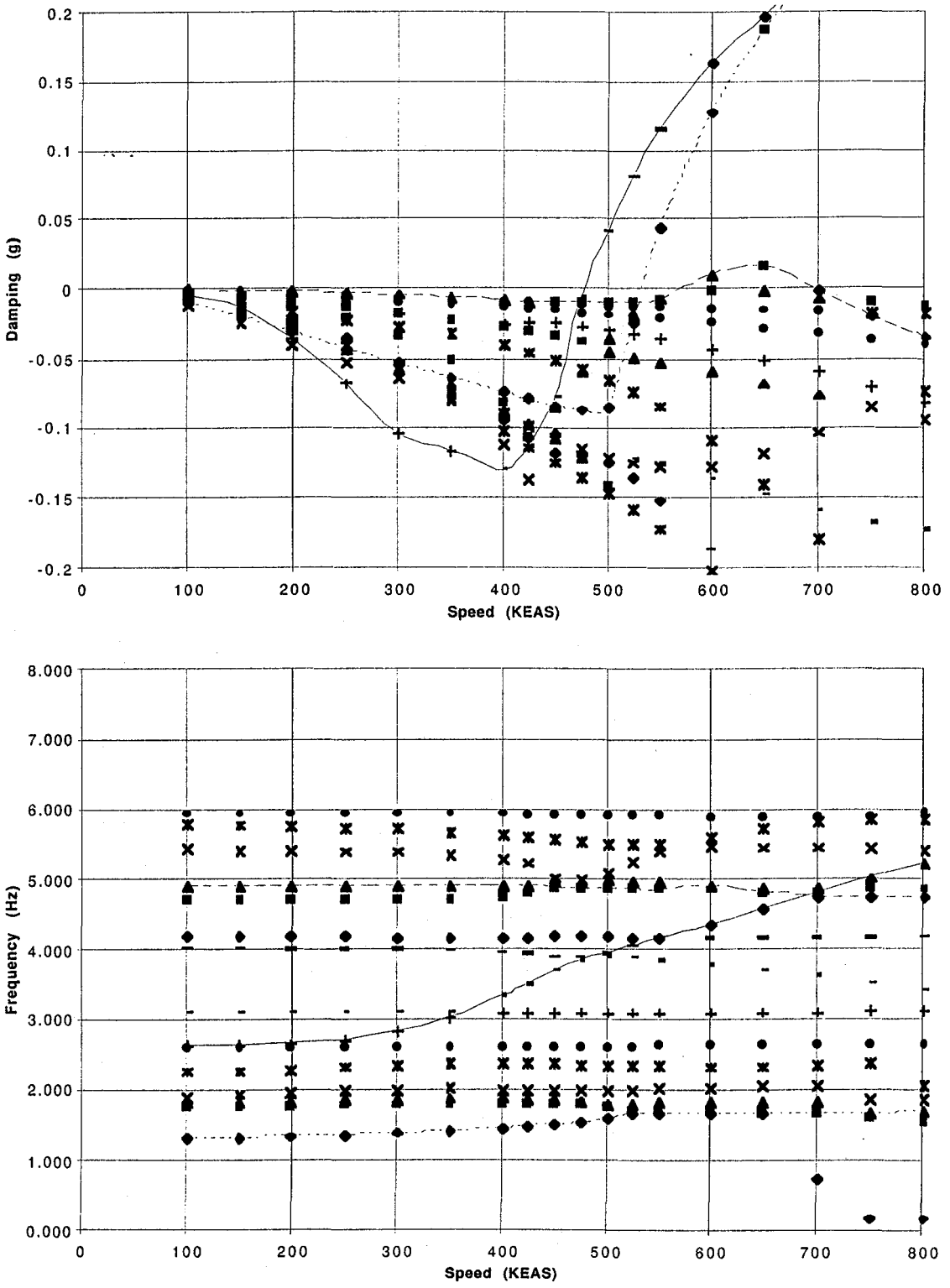

Figure 3.1-2: V-G and V-F Plots for the Strength Sized Model (Antisymm. Boundary Condition, MT-1 Mass Case at Mach 0.95 in Air).

3.2 Fuselage Mass

Since a significant amount of instrumentation and hardware will be mounted in the fuselage of the FFM model (cable mount pulleys, snubber brackets, servovalves, canard/tail/rudder actuators, wing carry-through brackets, etc...), it is likely that the fuselage will be overweight. In order to address this possibility up front and evaluate the impact on the flutter mechanisms of interest, a flutter analysis was performed on the TCA where the fuselage mass properties were doubled. Since the finite element model of the TCA is very complicated, it was not considered feasible to double the mass of each element individually, since this would require tracking down and modifying each element/property/material in the fuselage. In order to avoid this complexity, the doubling of the fuselage mass was accomplished by dividing the fuselage into a series of bays, and defining an additional node along the fuselage centerline for each bay. A concentrated mass (CONM2) was then defined for each bay, with a mass equal to the mass of the fuselage section associated with that bay. These mass elements were then attached to the existing fuselage elements using RBE3 elements. This results in a fuselage with unchanged stiffness properties, but doubled mass (one unit of mass from the detailed FEM, and one unit from the additional CONM2 elements). A vibration analysis indicated that no significant problems with local modes were generated by using this approach.

The modal frequencies for the baseline and the heavy fuselage configurations are compared in Table 3.2-1. As expected, the added mass tended to reduce all the vibration frequencies for both the symmetric and antisymmetric conditions. Note that the ordering of symmetric modes 5 and 6 changed with the addition of the extra fuselage mass.

Flutter speeds and frequencies for the baseline and the heavy fuselage configurations are compared in Table 3.2-2. The high frequency modes were barely affected, while significant changes occurred to the low frequency symmetric and antisymmetric modes. These differences can be understood by considering the representative v-g and v-f plots for the heavy fuselage condition shown in Figures 3.2-1 and 3.2-2. Symmetric and antisymmetric analysis for the MT-1 mass case are shown. Very little change is seen in the high frequency modes, while the low frequency modes were shifted somewhat. The flutter crossing of the low frequency symmetric mode was reduced significantly although the modes interacting did not change. For the antisymmetric low frequency mode, the character of the interaction changed a little, with an initial interaction between the first two vibration modes occurring around 450 KEAS, and a secondary interaction involving the third flexible mode occurring around 700 KEAS.

Figure 3.2-3 shows a direct comparison of the flutter crossings by plotting the v-g traces the two configurations on one graph. All the symmetric mechanisms are shown in the upper half of the Figure, and all the antisymmetric mechanisms are shown in the lower half of the Figure.

Since the primary mode of interest (the symmetric low frequency mode) was not changed in character, since the fuselage mass variation improves model buildability, and since the separation between the low and high frequency modes was improved, it is recommended that the fuselage mass of the FFM be doubled.

Mode Number	Symmetric		Antisymmetric	
	Baseline	Heavy Fuse.	Baseline	Heavy Fuse.
1	1.326	1.148	1.406	1.391
2	1.485	1.407	1.857	1.602
3	1.893	1.887	1.898	1.865
4	1.942	1.917	1.955	1.921
5	2.664	2.486	2.330	2.112
6	2.686	2.664	2.662	2.646
7	2.768	2.689	2.725	2.701
8	3.880	3.516	3.152	3.023
9	4.298	4.055	4.130	4.049
10	4.891	4.515	4.439	4.393

Table 3.2-1: Modal Frequency Comparison Between Baseline and Heavy Fuselage Models for MT-1 Mass Condition.

		Speed		Frequency	
		Baseline	Heavy Fuse.	Baseline	Heavy Fuse.
Symmetric	Low Freq	505	388	1.664	1.606
	High Freq Hard	656	646	5.596	5.439
	High Freq Hump	600	616	5.085	5.086
Antisymm.	Low Freq	623	468	1.747	1.576
	High Freq Hard	514	515	4.092	4.077
	High Freq Hump	601	602	5.052	5.046

Table 3.2-2: Flutter Crossing Comparison Between Baseline and Heavy Fuselage Models for MT-1 Mass Condition at Mach 0.95.

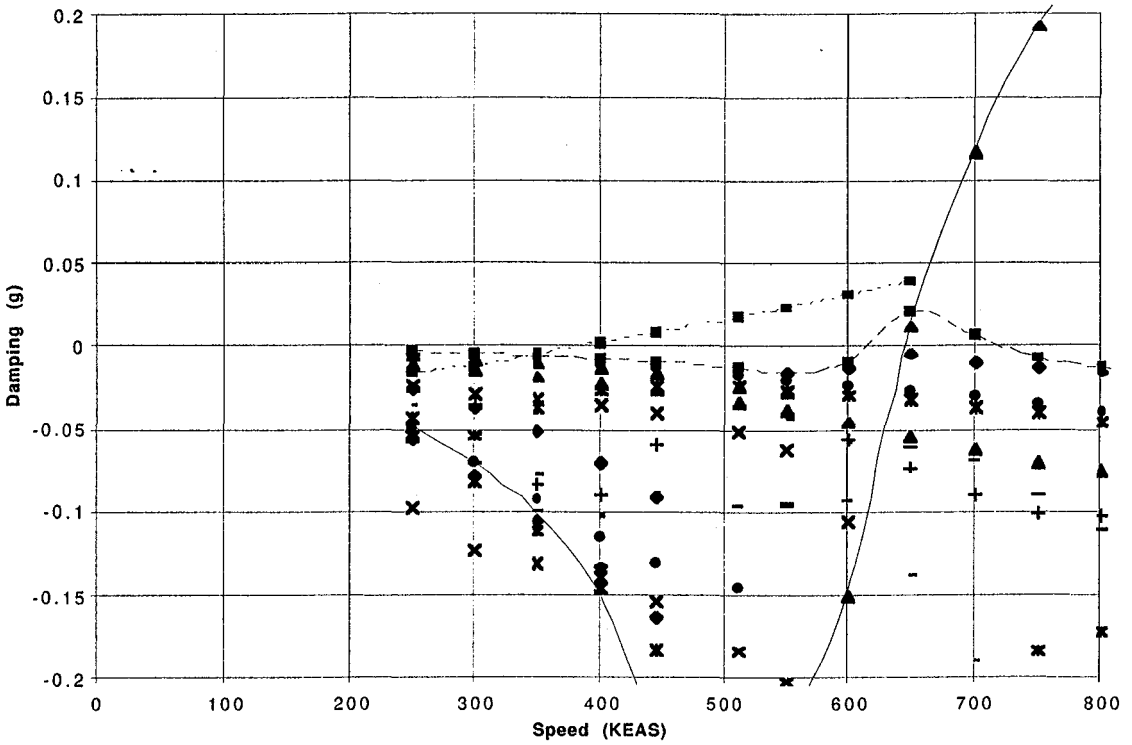

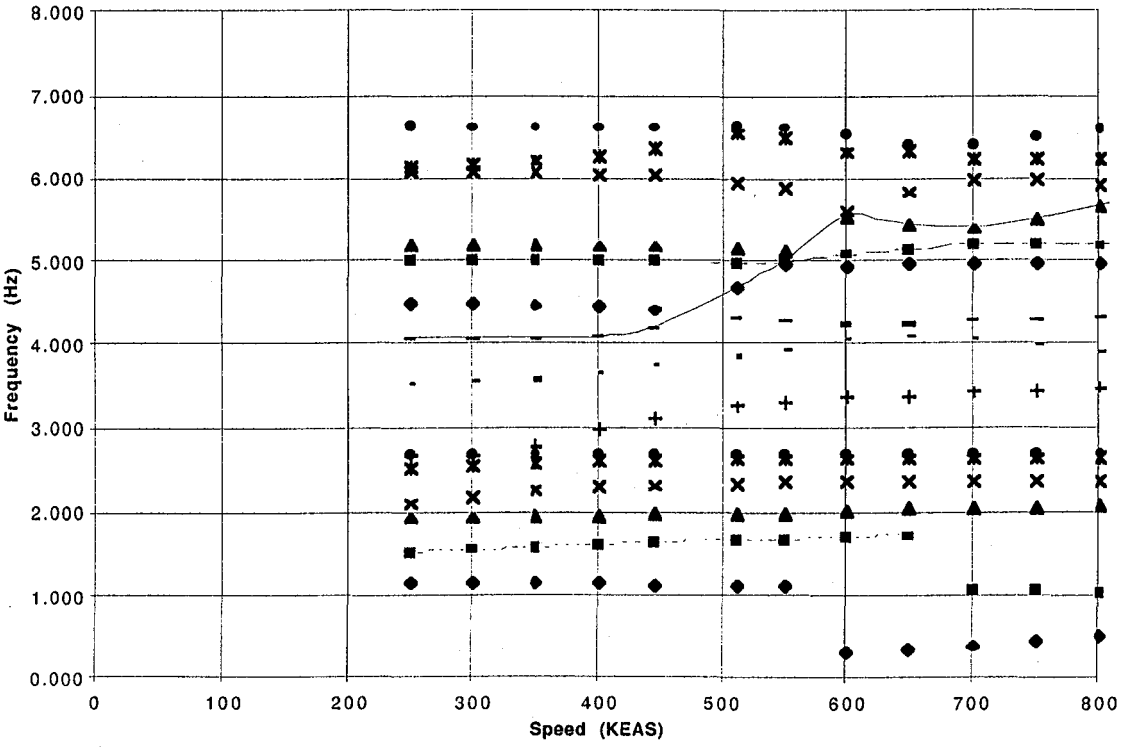

Figure 3.2-1: V-G and V-F Plots for the Heavy Fuselage Condition. Symmetric Boundary Condition, Mass Case MT-1, Mach 0.95.

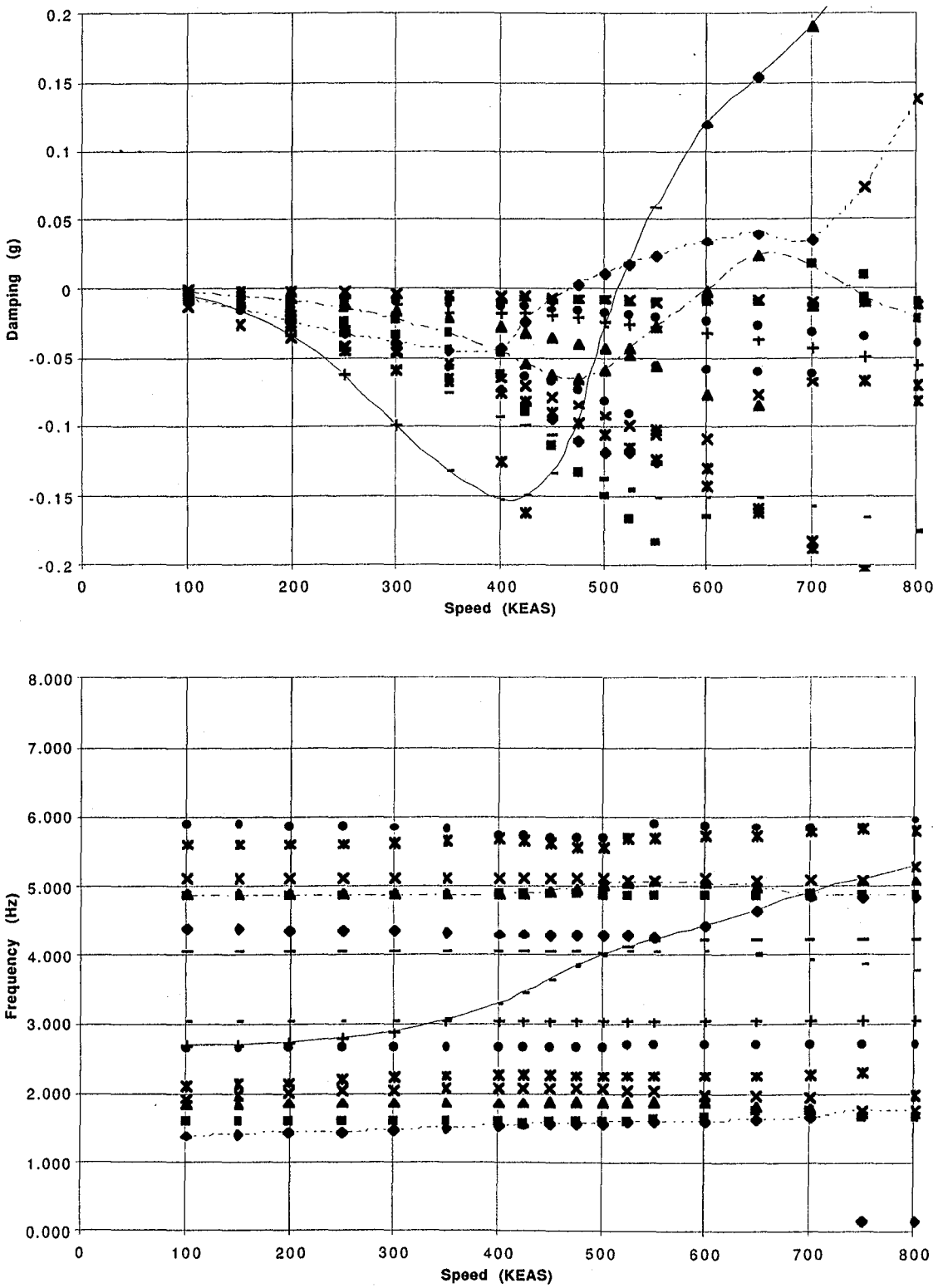

Figure 3.2-2: V-G and V-F Plots for the Heavy Fuselage Condition. Symmetric Boundary Condition, Mass Case MT-1, Mach 0.95.

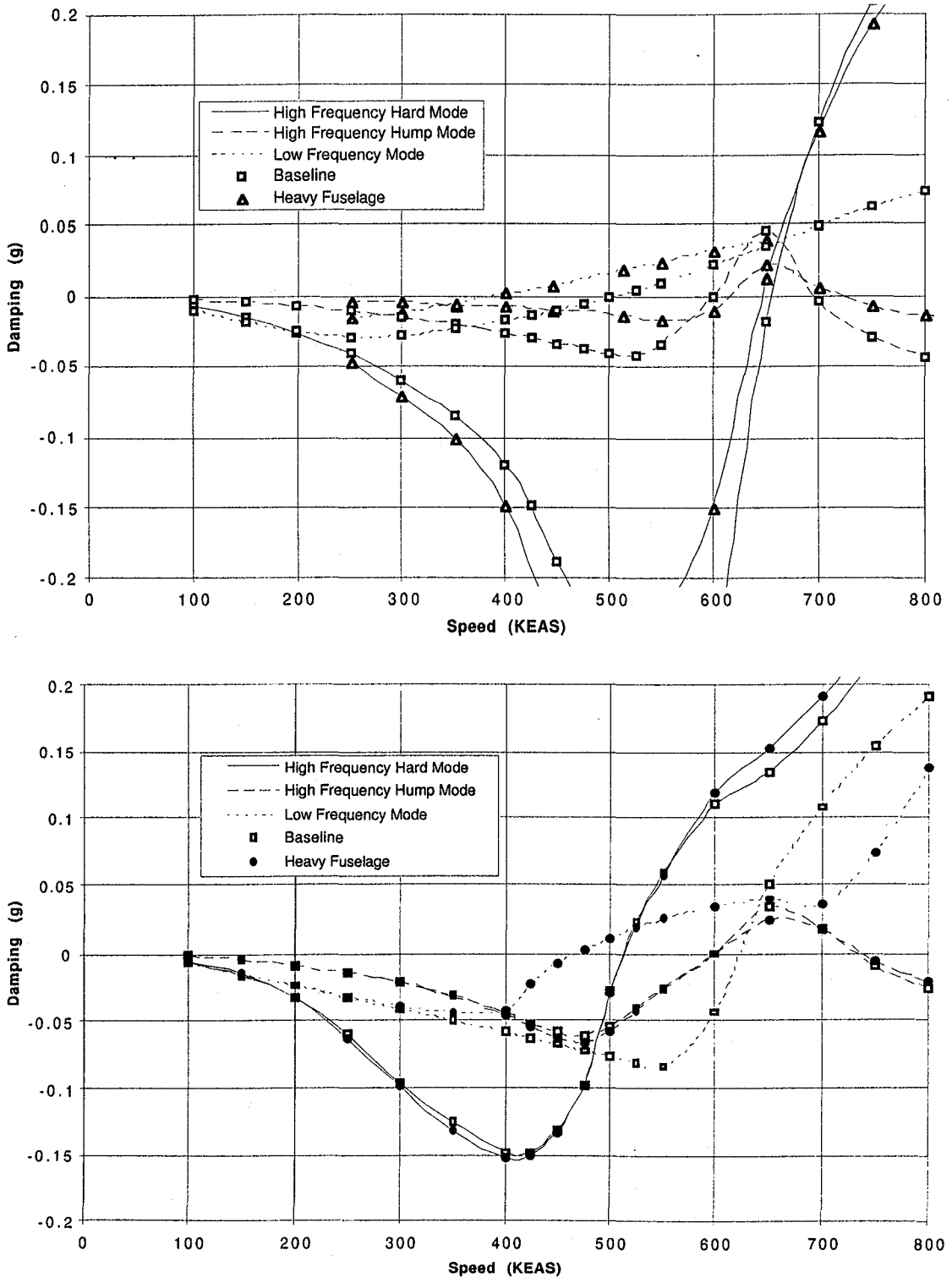

Figure 3.2-3: Comparison of V-G Curves for Flutter Modes as Fuselage Mass is Doubled. MT-1 Mass Case at Mach 0.95. Top=Symmetric, Bottom=Antisymmetric.

3.3 Tail Aerodynamics

Since the control concept for the HSCT vehicle is still under debate, and the final airplane may include a horizontal stabilizer (tail), canard, or both, a preliminary analysis of the effects of tail aerodynamics on the flutter mechanisms of interest was performed. In this analysis, the effects of the horizontal stabilizer aerodynamics were investigated by performing a flutter analysis with the tail panels removed, and another analysis with a weighting factor applied to the tail aerodynamics to double the tail forces. The results of this study are presented in Table 3.3-1 and in Figure 3.3-1. Only symmetric analyses were performed for this variation.

From Table 3.3-1 and Figure 3.3-1, it can clearly be seen that tail aerodynamics have a destabilizing effect on the low frequency flutter mode. In fact, when the tail aerodynamics were removed, no flutter was obtained for the low frequency mode. Doubling the tail aerodynamics resulted in approximately 5% reduction in flutter speed. Effects on the high frequency symmetric flutter mechanisms were minimal.

		Flutter Speed		
		No Tail Aero	Baseline	Double Aero
Symmetric	Low Freq	N/F	505	480
	High Freq Hard	659	656	676
	High Freq Hump	618	600	618

Table 3.3-1: Flutter Crossing Comparison Between Baseline and Heavy Fuselage Models for MT-1 Mass Condition at Mach 0.95.

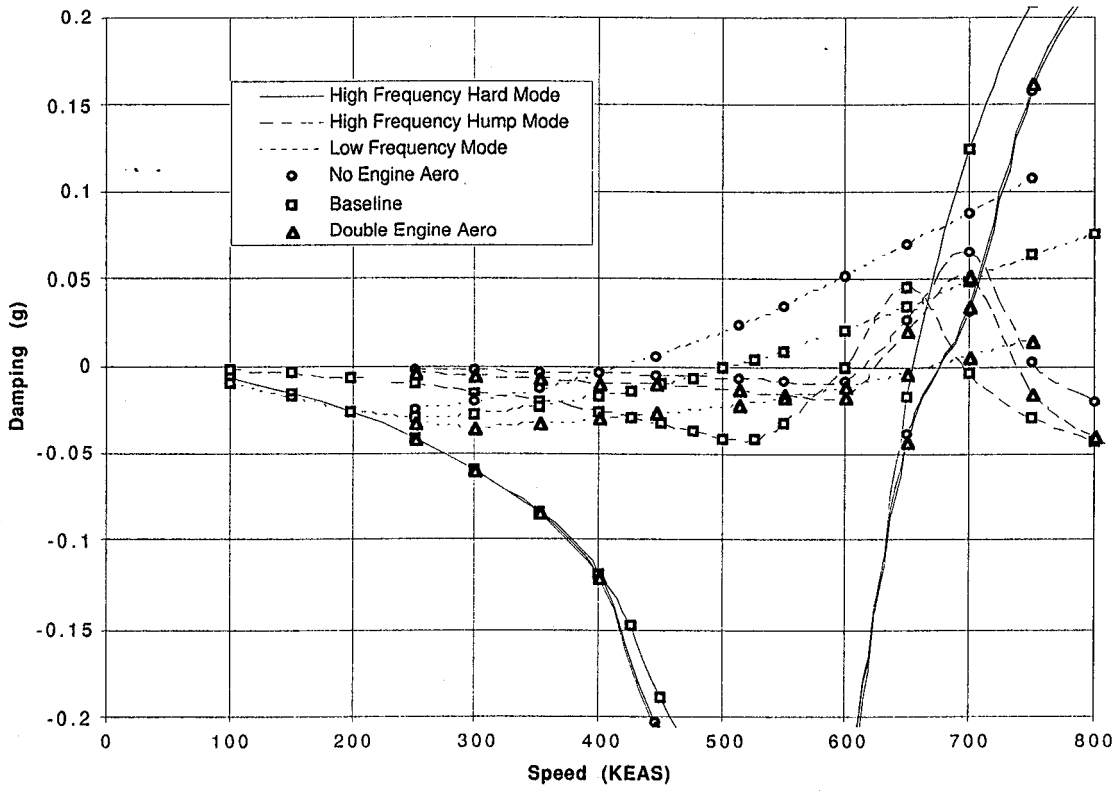

Figure 3.3-1: Comparison of V-G Curves for Flutter Modes as Tail Aerodynamics are Varied. MT-1 Mass Case at Mach 0.95. Symmetric Analysis Only.

3.4 Pylon Stiffness

Since the low frequency flutter mechanisms have a significant amount of outboard engine paticipation, analyses were also conducted to investigate the effect of engine mounting stiffness. Through experimenting on the finite element model, it was determined that significant changes in the cantilevered engine pitching frequencies could be obtained by varying the area of the rod elements connecting the pylon to the aft spar of the wing.

Through a cantilevered engine-only vibration analysis, it was determined that doubling the area of these rod elements resulted in approximately a 10% increase in the frequency of the first engine pitching mode. In order to cover a reasonable range of stiffnesses, analyses were conducted with the rod areas set to zero, one, two, and three times the baseline value.

The vibration frequencies for each configuration are shown in Table 3.4-1. As expected, reducing the rod areas resulted in frequency reductions, and increasing the rod areas increases the vibration mode frequencies. The frequency variation is obviously nonlinear with the changes in the rod areas, and reducing the rod areas to zero has a much greater effect than doubling or tripling the areas.

The flutter crossing speeds at Mach 0.95 for mass case MT-1 are tabulated in Table 3.4-2. The pylon stiffness variations have a profount impact on the low frequency mechanisms, with reduced pylon stiffness resulting in improved stability. Increasing the rod areas reduces the flutter speed of each low frequency mode. The common misconception that adding structural stiffness increases flutter speed is not true in this case because adding rod area tends to result in configurations where the first few modal frequencies are closer together than the baseline model. Since the frequencies are closer together, the flutter interaction occurs at a lower dynamic pressure. This tendency was seen in several other variations, where increasing the frequency of the low-frequency modes tends to lower the flutter speed.

A direct comparison between the flutter behavior of the different pylon stiffness variations can be seen in Figures 3.4-1 through 3.4-3. Figure 3.4-1 shows V-G curves for the low frequency symmetric and antisymmetric modes. Figure 3.4-2 shows the same information for the high frequency hard flutter modes, and Figure 3.4-3 shows the behavior of the high frequency hump modes.

The flutter behavior of the TCA is clearly very sensitive to the stiffness of the engine mounting structure, and could be used to place the low frequency flutter modes in a desireable test regime. However, it was felt that the degree of sensitivity was such that it might be difficult to control. It is recommended that variations in pylon stiffness be included as a parametric sensitivity for wind tunnel testing, but that other means be used to develop a "testable" configuration. Due to the large stabilizing influence of softening the pylon, it is also recommended that a decoupler pylon be investigated as a flutter stopper. These variations also offer the possibility of tailoring the TCA flutter behavior to alleviate the flutter weight penalty, but must be carefully considered due to robustness concerns and possible impact on other constraints such as loads dynamic response, engine unstart, etc.

Mode	Symmetric				Antisymmetric			
	Zero Area	Baseline	Double Area	Triple Area	Zero Area	Baseline	Double Area	Triple Area
1	1.030	1.326	1.342	1.348	1.049	1.406	1.441	1.455
2	1.234	1.485	1.508	1.518	1.227	1.857	1.912	1.919
3	1.465	1.893	1.953	1.985	1.730	1.898	1.985	2.009
4	1.715	1.942	2.098	2.181	1.926	1.955	2.,022	2.100
5	2.212	2.664	2.738	2.768	2.174	2.330	2.348	2.355
6	2.230	2.686	2.765	2.779	2.222	2.662	2.723	2.747
7	2.746	2.768	2.806	2.855	2.598	2.725	2.785	2.822
8	3.803	3.880	3.903	3.915	2.867	3.152	3.232	3.273
9	4.201	4.298	4.334	4.354	4,116	4.130	4.133	4.135
10	4.798	4.891	4.913	4.925	4.334	4.439	4.476	4.497

Table 3.4-1: Vibration Mode Frequency Comparison For Pylon Stiffness Variations. MT-1 Mass Condition at Mach 0.95.

		Flutter Speed			
		Zero Rod Area	Baseline	Double Rod Area	Triple Rod Area
Symmetric	Low Freq	702 1.402	505 1.664	463 1.741	447 1.776
	High Freq Hard	660 5.534	656 5.596	656 5.622	656 5.635
	High Freq Hump	573 4.837	600 5.085	603 5.128	604 5.147
Antisymm.	Low Freq	N/F	623 1.747	587 1.789	578 1.815
	High Freq Hard	497 3.986	514 4.092	520 4.122	523 4.136
	High Freq Hump	573 4.840	601 5.052	606 5.085	608 5.102

Table 3.4-2: Flutter Crossing Comparison For Pylon Stiffness Variations. MT-1 Mass Condition at Mach 0.95.

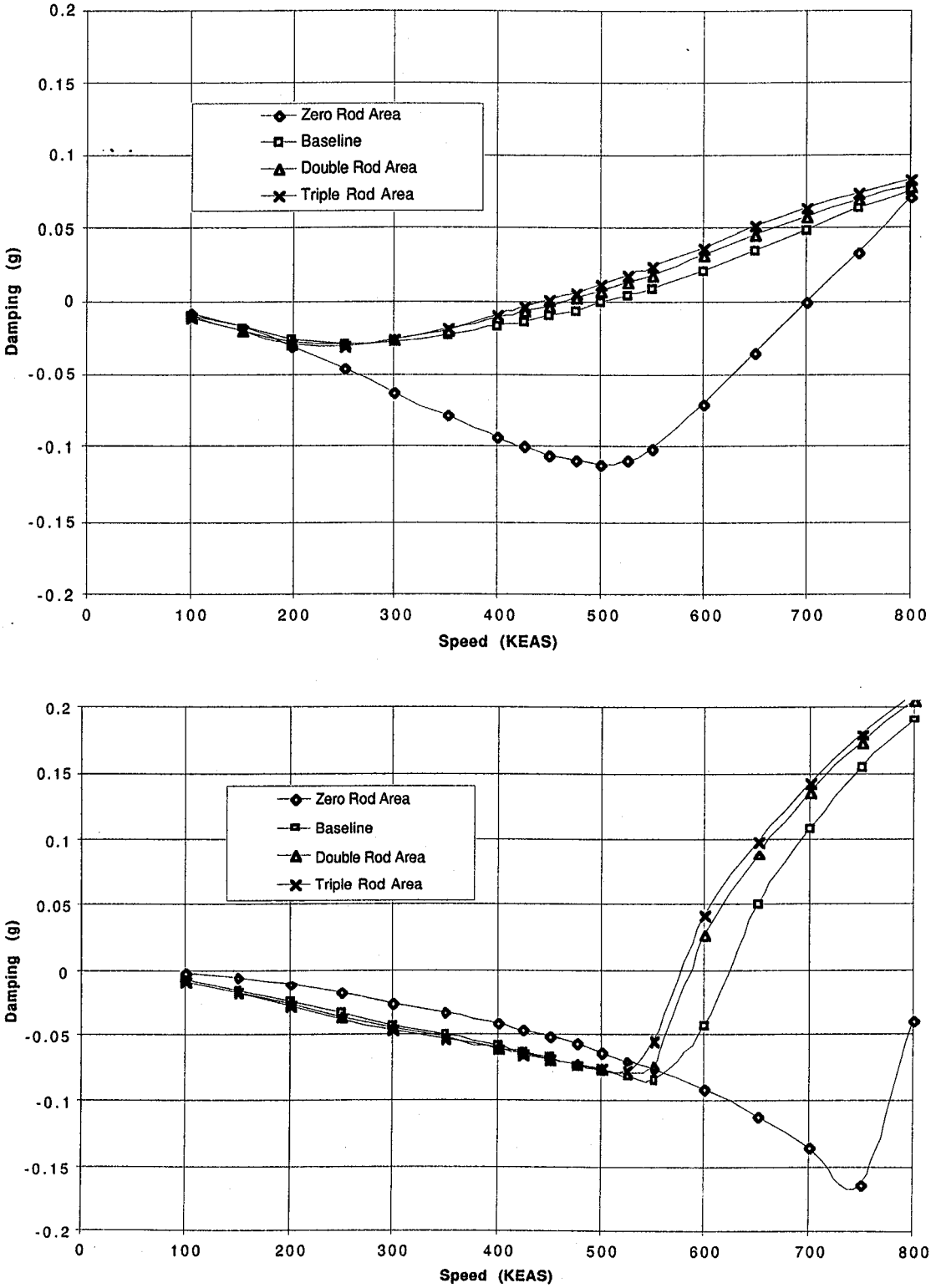

Figure 3.4-1: Comparison of V-G Curves for Low Frequency Flutter Modes as Pylon Stiffness is Varied. MT-1 Mass Case at Mach 0.95. Top=Symmetric, Bottom=Antisymmetric.

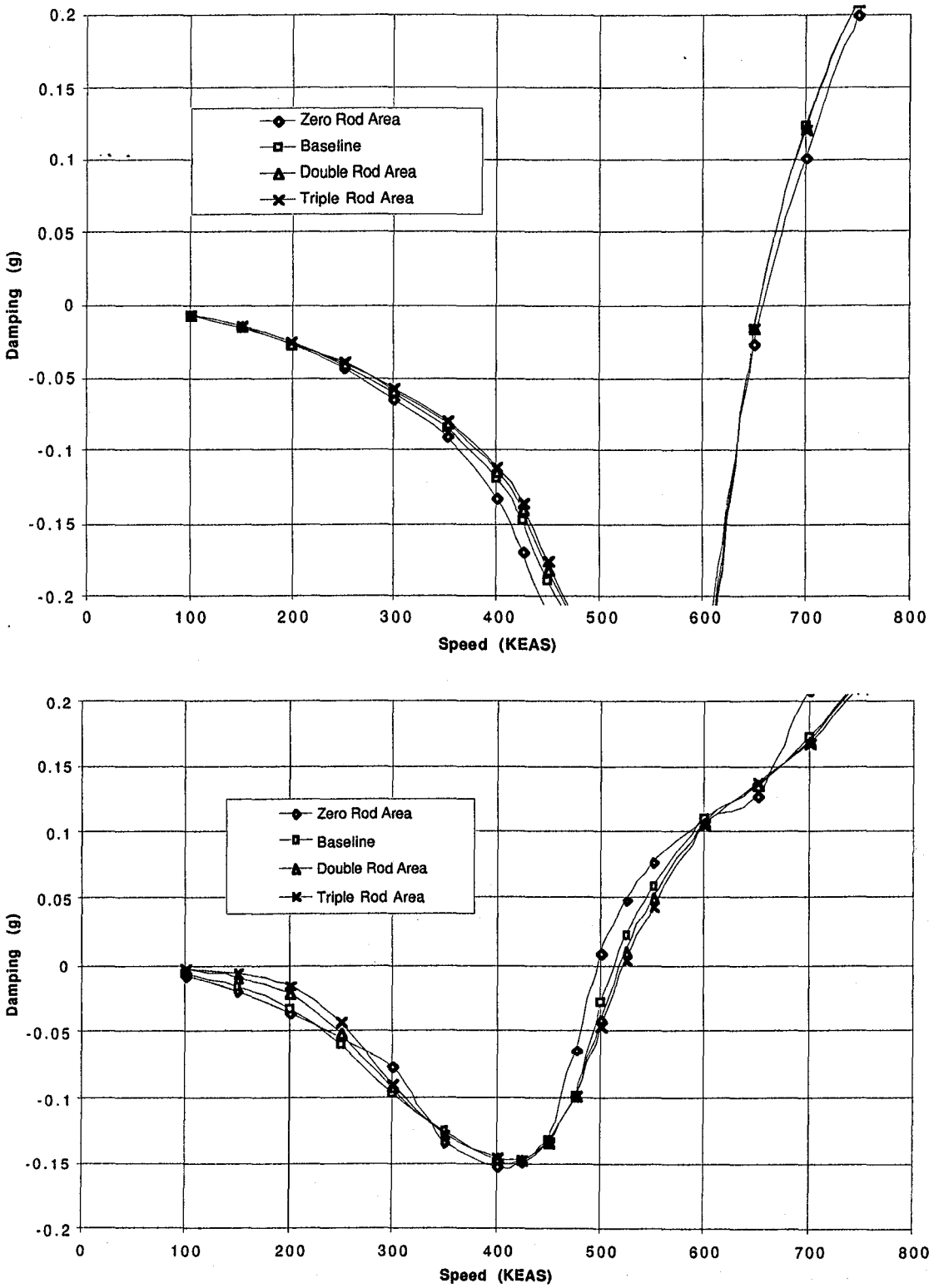

Figure 3.4-2: Comparison of V-G Curves for High Frequency Hard Flutter Modes as Pylon Stiffness is Varied. MT-1 Mass Case at Mach 0.95. Top=Symmetric, Bottom=Antisymmetric.

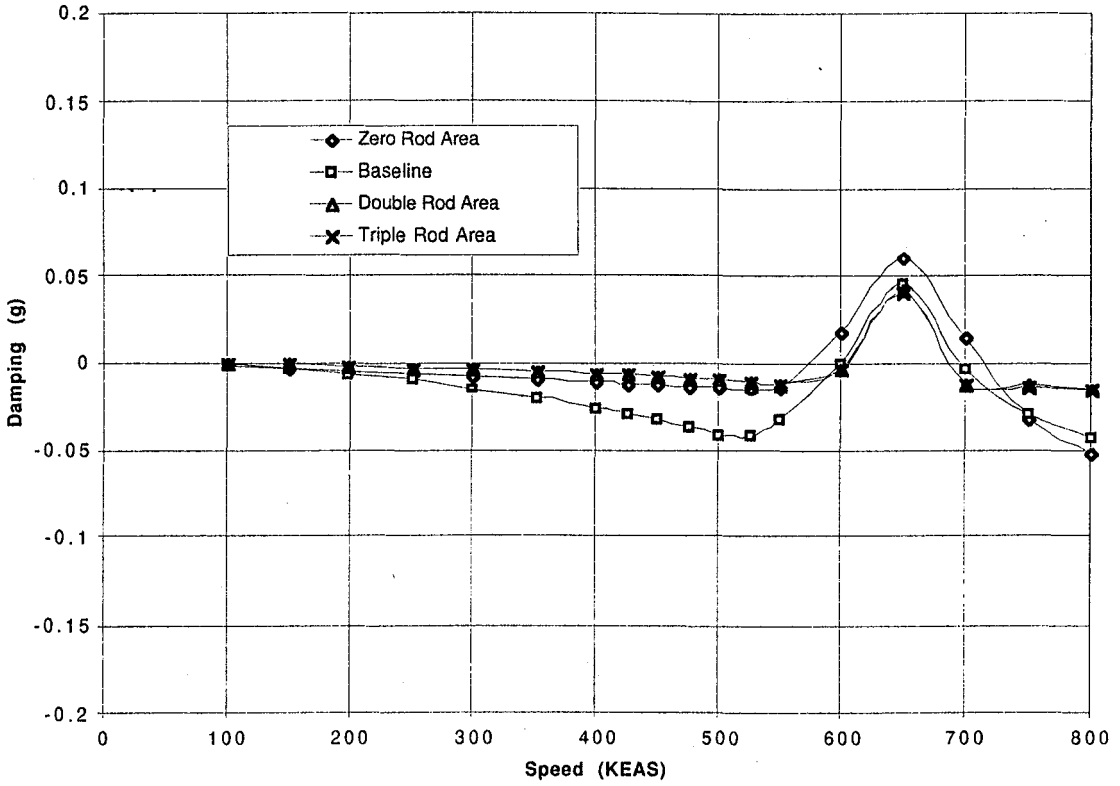

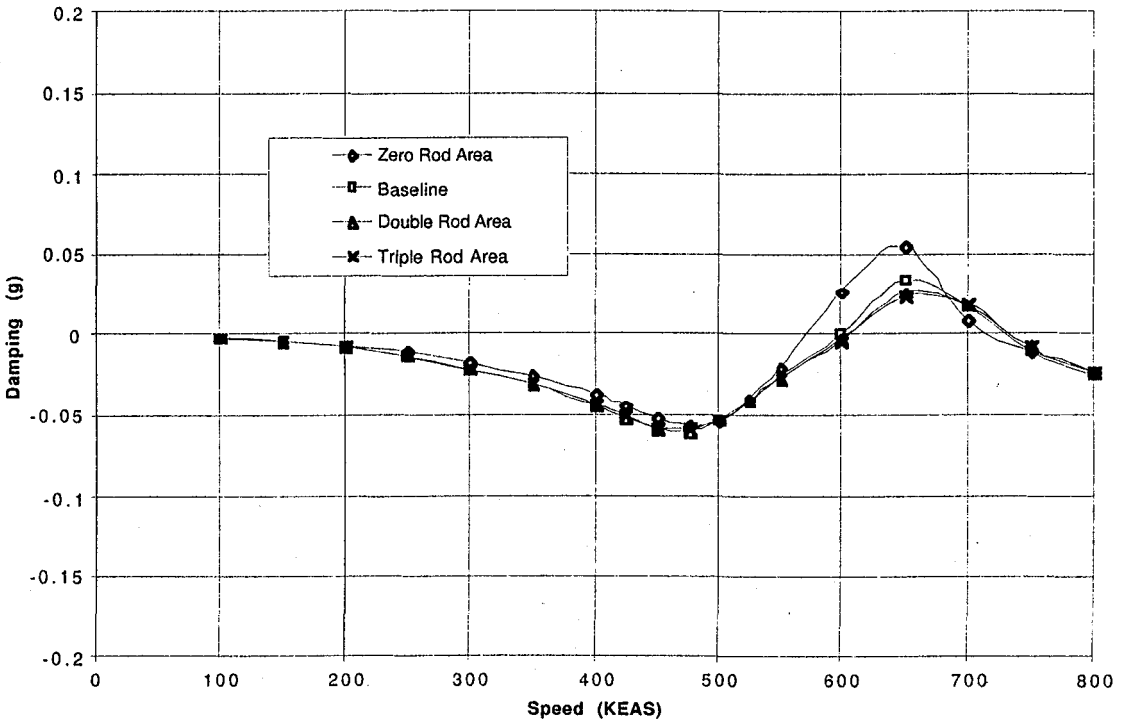

Figure 3.4-3: Comparison of V-G Curves for High Frequency Hump Flutter Modes as Pylon Stiffness is Varied. MT-1 Mass Case at Mach 0.95. Top=Symmetric, Bottom=Antisymmetric.

3.5 Engine Aerodynamics

During the DITS design effort for the TCA, engine aerodynamics was identified as an unknown area. The MSC/NASTRAN based flutter analysis process used to design the TCA at Boeing Long Beach has limitations on the types of aerodynamic representations that are supported. While the aerodynamic options are certainly adequate for lifting surfaces, they leave something to be desired for computing aerodynamic loads on engines. Traditionally, engines are modeled as either slender bodies (no flow through), ring-wings (100% flow-through), or cruciforms. The supersonic aerodynamics in MSC/NASTRAN do not support slender bodies, so the decision was to use a cruciform engine aerodynamic model, and analysis was also performed without engine aerodynamics. Neither of these approaches will likely give the correct answer, but an indication of the sensitivity of the flutter mechanisms to the presence or absence of engine aerodynamics can be obtained with a good degree of confidence.

In order to evaluate the impact of engine aerodynamics on the flutter mechanisms, flutter analyses were performed with the engine panels removed (no aero), in the baseline configuration with doublet lattice engine panels, and with weighting factors applied to double the magnitude of the engine aerodynamics from the baseline. These conditions are referred to as "no engine aerodynamics", "baseline", and "double engine aerodynamics". The flutter crossing results are tabulated in Table 3.5-1. It is clear that engine aerodynamics have almost no effect on the antisymmetric mechanisms or on the symmetric high frequency mechanisms, but have a dramatic effect on the symmetric low frequency mechanism. Including engine aerodynamics increases the aerodynamic damping, resulting in higher flutter speeds and improved stability.

A graphical view of the effects of engine aerodynamics on the flutter behavior of the TCA can be seen in Figures 3.5-1 and 3.5-2.

Again, the primary conclusion of this study is that engine aerodynamics should be investigated using the wind tunnel model. Due to the inadequacy of the available aerodynamic tools for accurately predicting engine airloads, this is not considered a viable tool for tailoring the flutter behavior of the FFM model. Since the low frequency symmetric flutter mechanism was so strongly affected by engine aerodynamics, and since this mechanism was a significant weight driver for the TCA airplane, this wind tunnel mode has the potential to give us significant insight into a parameter that might save thousands of pounds in the airplane design.

		Flutter Speed		
		No Engine Aero	Baseline	Double Engine Aero
Symmetric	Low Freq	418 1.631	505 1.664	666 1.732
	High Freq Hard	678 5.636	656 5.596	678 5.594
	High Freq Hump	612 5.081	600 5.085	623 5.038
Antisymm.	Low Freq	610 1.709	623 1.747	625 1.788
	High Freq Hard	514 4.095	514 4.092	514 4.090
	High Freq Hump	590 5.072	601 5.052	605 5.015

Table 3.5-1: Flutter Crossing Comparison For Engine Aerodynamics Variations. MT-1 Mass Condition at Mach 0.95.

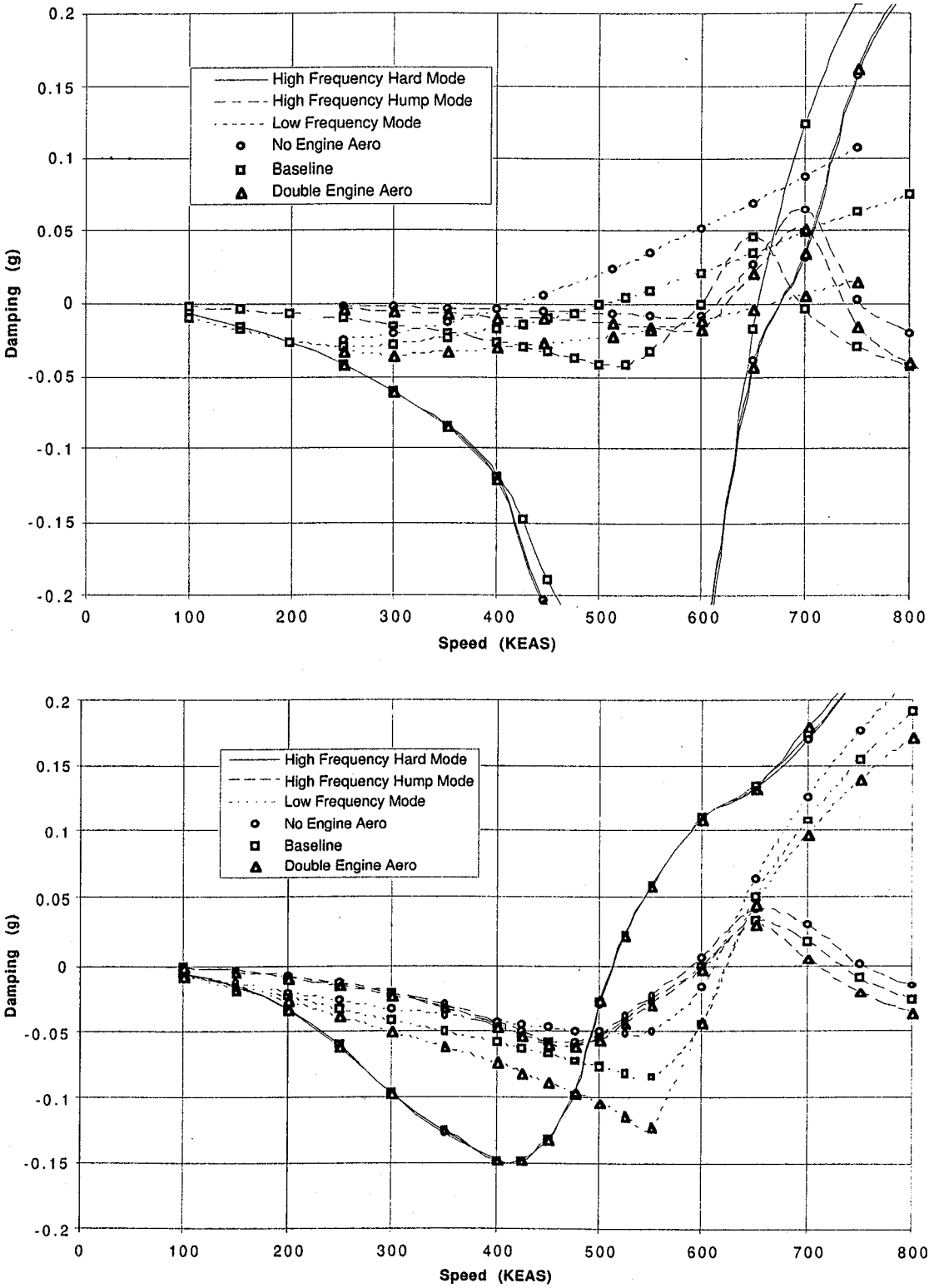

Figure 3.5-2: Comparison of V-G Curves for Flutter Modes as Engine Aerodynamics is Varied. MT-1 Mass Case at Mach 0.95. Top=Symmetric, Bottom=Antisymmetric.

3.6 Engine CG Position

Since the mounting concept used for the TCA engines places the engines fairly far aft on a very thin mounting structure, the vibration modes have very low frequencies, and are very sensitive to the streamwise engine position. In order to evaluate the impact of streamwise engine position on the flutter behavior of the TCA, flutter analyses were performed with the engine masses shifted forward and aft by 5 and 10 feet, which corresponds roughly to distances of 10% and 20% of the nacelle length. The engine aerodynamic panels were not modified, and the engine mounting points were not moved.

The vibration mode frequencies for the symmetric and antisymmetric boundary conditions using the MT-1 mass case are summarized in Table 3.6-1. For most vibration modes, shifting the engine masses forward caused a frequency increase, while shifting the masses at caused a frequency reduction. Some exceptions are symmetric mode 8 and antisymmetric mode 9.

aft

The resulting flutter boundary information is summarized in Table 3.6-2, which shows the flutter (zero damping) speeds and frequencies of the six "interesting" mechanisms. The results are again somewhat counter-intuitive, but are consistent with the results from pylon stiffness variations. A forward shift in the engine CG, which raises the first few modal frequencies, causes a flutter speed reduction in the low frequency mechanisms, while an aft shift in the CG raises the flutter speeds. The effect is quite dramatic, with a five foot shift (equivalent to about three inches in model scale) changing the flutter speed by 150-200 KEAS. In fact, shifting the engine CG aft by five feet completely eliminates the low frequency antisymmetric mechanism. The effect on the high frequency mechanisms was much smaller, and did not show a clear trend.

The tabular results of Table 3.6-2 are shown graphically in Figures 3.6-1 through 3.6-3, which show the V-G traces of the relevant flutter mechanisms for all the engine position variations.

These results indicate that testing variations of the FFM with different engine CG positions will give significant insight into the HSCT-unique engine flutter mechanisms, and potentially allow us to save a large amount of weight on future configurations. Engine CG position also shows great promise as a flutter stopping mechanism, and should be further investigated by the FFM design/build team.

Mode	Symmetric					Antisymmetric				
	120" Fwd	60" Fwd	Base-line	60" Aft	120" Aft	120" Fwd	60" Fwd	Base-line	60" Aft	120" Aft
1	1.402	1.387	1.326	1.138	0.923	1.629	1.566	1.406	1.164	0.937
2	1.637	1.592	1.485	1.358	1.112	1.931	1.930	1.857	1.420	1.095
3	2.425	2.190	1.893	1.564	1.461	2.360	2.171	1.898	1.792	1.486
4	2.617	2.492	1.942	1.766	1.477	2.437	2.376	1.955	1.902	1.562
5	2.824	2.750	2.664	1.979	1,492	2.578	2.470	2.330	1.979	1.761
6	3.290	3.420	2.686	1.991	1.756	2.832	2.772	2.662	2.043	1.957
7	3.365	3.528	2.768	2.768	2.763	3.373	3.489	2.725	2.614	2.554
8	3.477	3.822	3.880	3.870	3.754	3.571	3.825	3.152	2.827	2.750
9	3.839	4.162	4.298	4.287	4.205	3.667	4.128	4.130	4.124	4.094
10	4.316	4.342	4.891	4.884	4.747	4.092	4.276	4.439	4.410	4.219

Table 3.6-1: Vibration Frequency Comparison For Engine CG Position Variations. MT-1 Mass Condition at Mach 0.95.

		Flutter Speed				
		10 Ft Fwd	5 Ft Fwd	Baseline	5 Ft Aft	10 Ft Aft
Symmetric	Low Freq	393 2.331	360 2.028	505 1.664	713 1.341	748 0.780
	High Freq Hard	569 4.515	635.7 4.697	656 5.596	648 5.248	636 5.018
	High Freq Hump	505 3.581	591 4.404	600 5.085	532 3.545	524 3.497
Antisym.	Low Freq	423 3.461	458 1.931	623 1.747	N/F	N/F
	High Freq Hard	587 4.661	539 4.391	514 4.092	509 4.059	488 3.918
	High Freq Hump	543 3.955	497 4.019	601 5.052	607 5.223	594 4.987

Table 3.6-2: Flutter Crossing Comparison For Engine CG Position Variations. MT-1 Mass Condition at Mach 0.95.

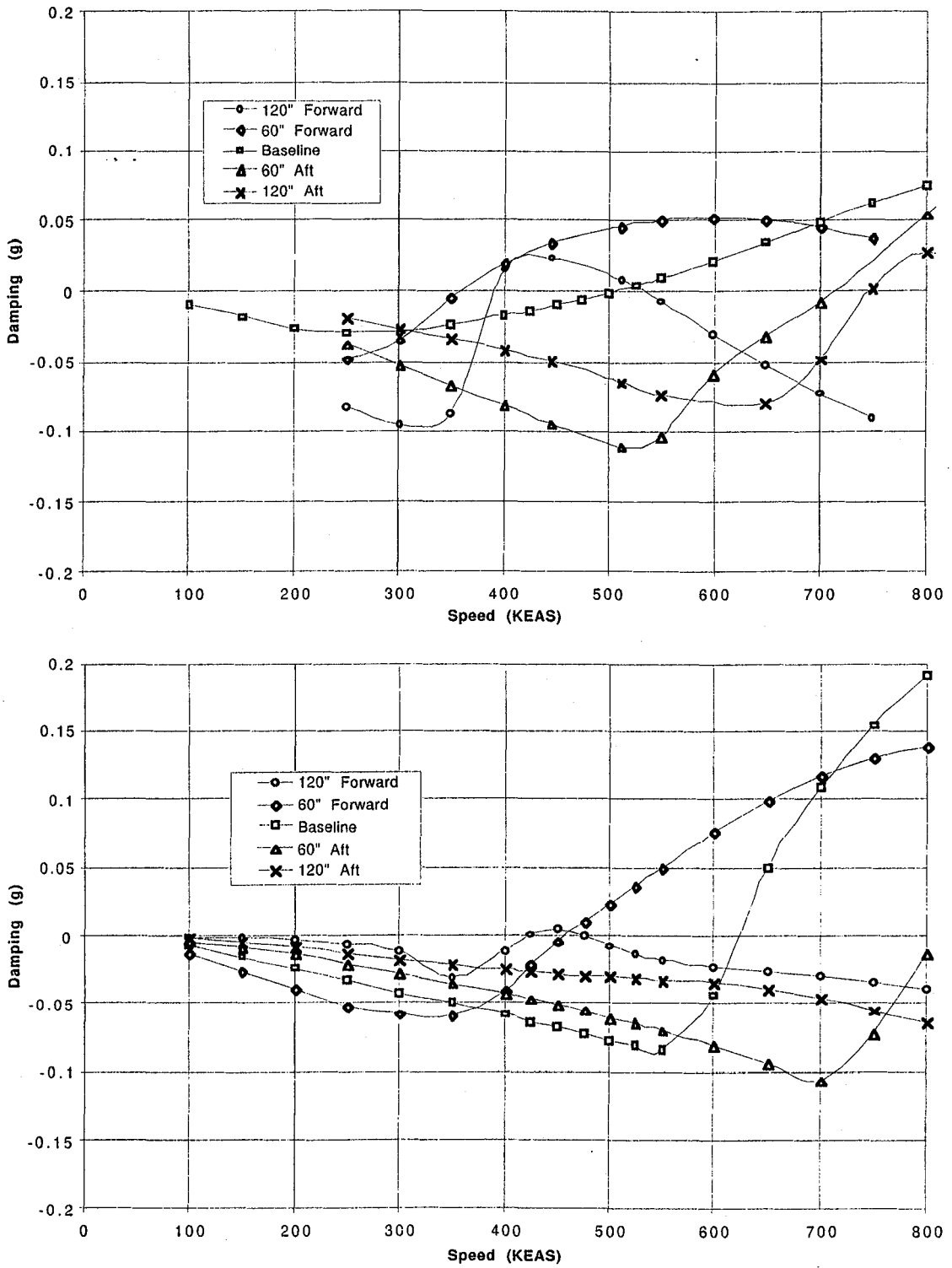

Figure 3.6-1: Comparison of V-G Curves for Low Frequency Flutter Modes as Engine CG Position is Varied. MT-1 Mass Case at Mach 0.95. Top=Symmetric, Bottom=Antisymmetric.

[redacted]

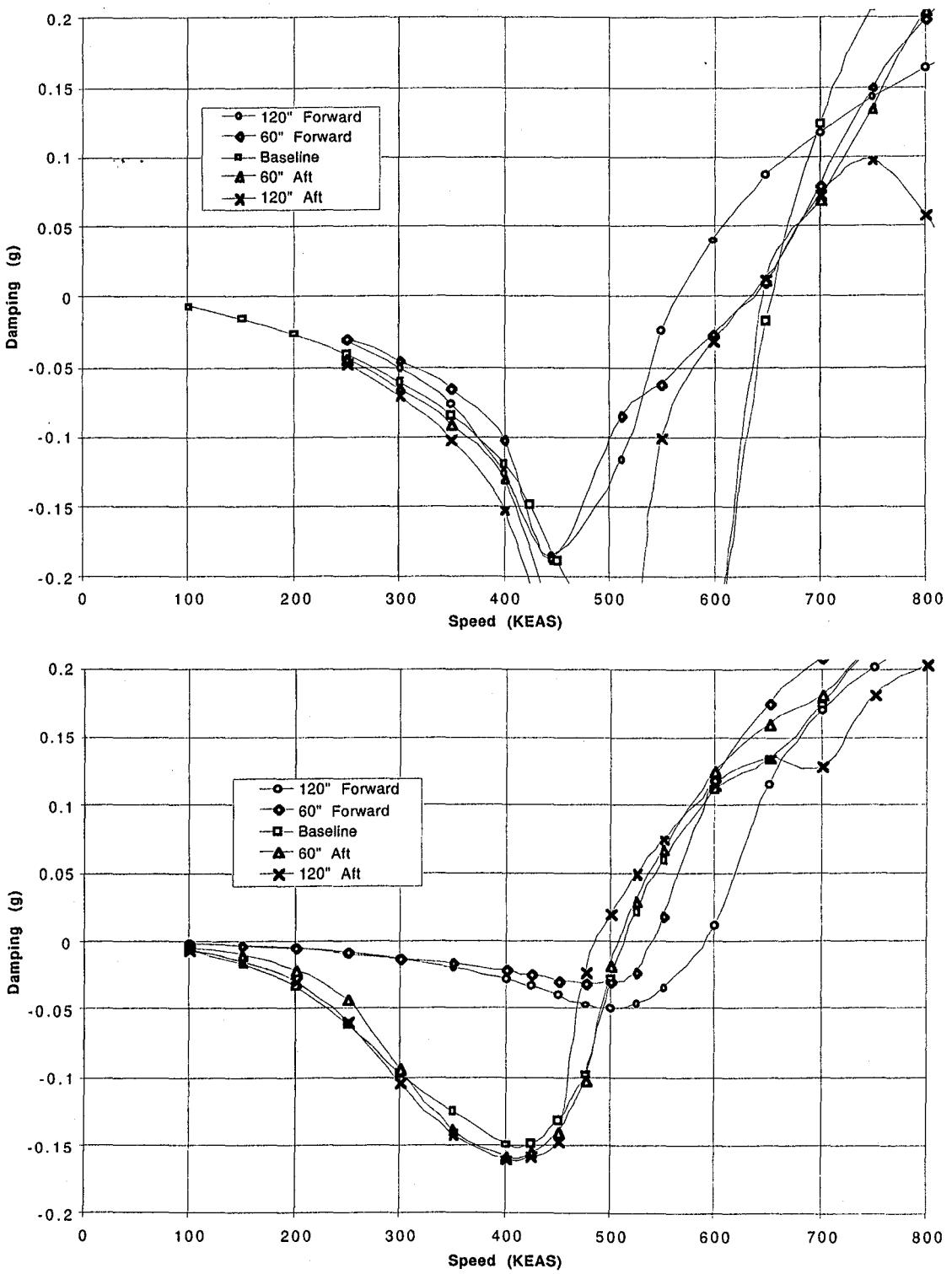

Figure 3.6-2: Comparison of V-G Curves for High Frequency Hard Flutter Modes as Engine CG Position is Varied. MT-1 Mass Case at Mach 0.95. Top=Symmetric, Bottom=Antisymmetric.

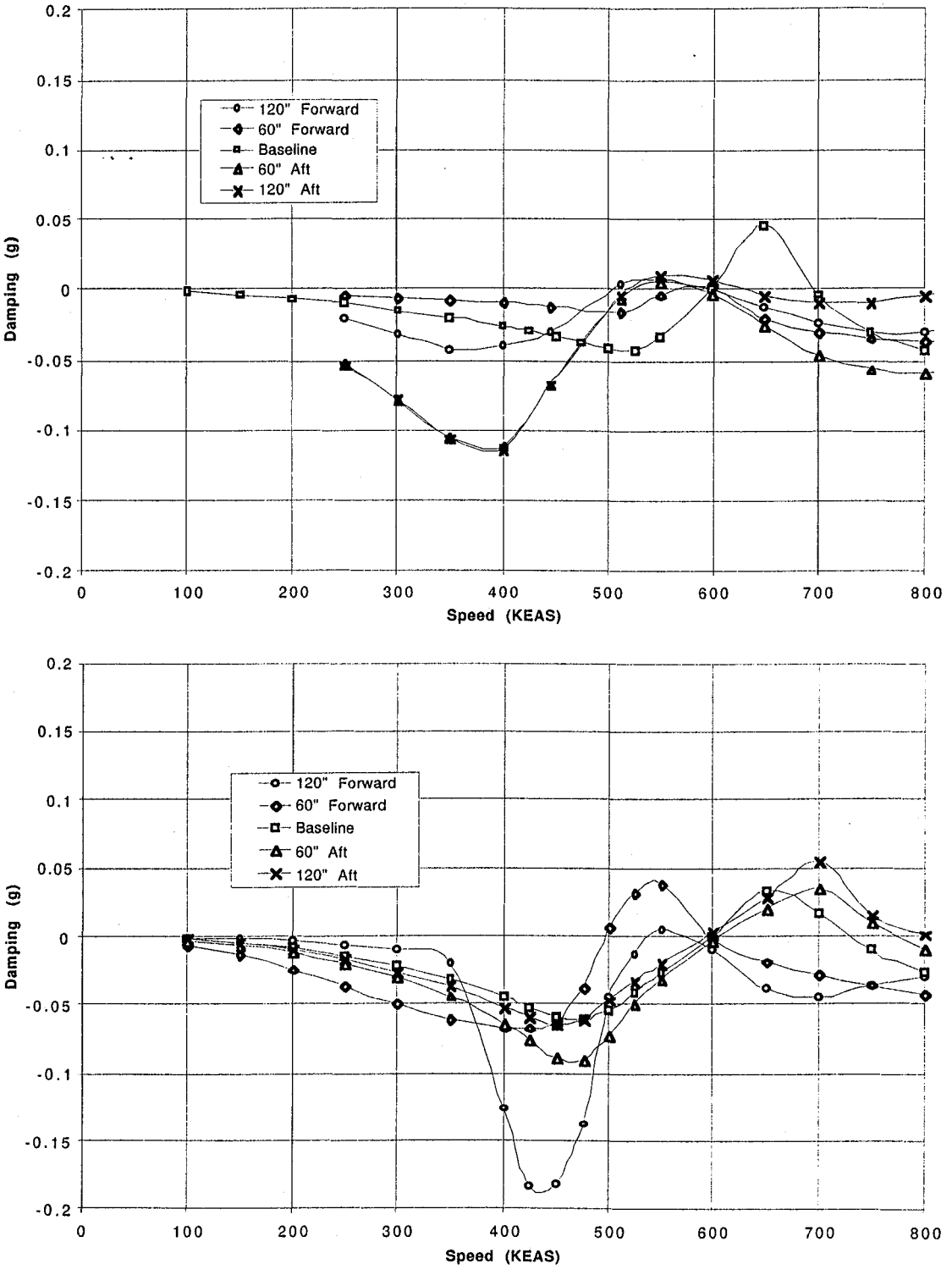

Figure 3.6-3: Comparison of V-G Curves for High Frequency Hump Flutter Modes as Engine CG Position is Varied. MT-1 Mass Case at Mach 0.95. Top=Symmetric, Bottom=Antisymmetric.

3.7 Engine Mass and Inertia

The final parametric variation associated with the engines was an investigation of the effects of variations in engine mass properties on the flutter mechanisms of the TCA. In order to accomplish this, the individual mass elements making up the engines were duplicated, resulting in a baseline set of mass elements and a separate set of mass elements representing a perturbation. Flutter analyses were performed with the perturbation masses set to -50%, -20%, +20%, and +50% of the baseline mass distribution. This results in total engine masses of 50%, 80%, 100%, 120%, and 150% of the baseline nacelle weight. All masses associated with the nacelle (including the inlet, engine, and nozzle) were included in the perturbation.

The effect of the engine mass variations on the vibration frequencies of the TCA is summarized in Table 3.7-1. As expected, a mass reduction leads to an increase in modal frequencies, and a mass increase leads to a reduction in modal frequency.

Flutter crossings for the MT-1 mass condition at Mach 0.95 are tabulated in Table 3.7-2. Again consistent with the other engine studies, the low frequency modes' flutter speeds tend to vary inversely with the first few modal frequencies. As the engine mass is increased, the first few modal frequencies are reduced, and the flutter speed for the low frequency modes in increased. As engine mass is reduced, the first few modal frequencies are raised, and the flutter speed drops. The high frequency hard flutter modes (both symmetric and antisymmetric) were not significantly affected by the engine mass variations, but the high frequency hump modes showed some sensitivity, but no clear trends.

The sensitivity of the individual flutter mechanisms to engine mass variations are shown graphically in Figures 3.7-1 through 3.7-3.

It is recommended that engine mass variations be tested to help understand the flutter mechanisms of interest. However, it is not felt that this variation is likely to result in a viable flutter stopping mechanism, since it requires mass to be magically added to the engines to improve stability, which would be very difficult if not impossible. Adding ballast to the engines might be a method to help alleviate flutter problems in future HSCT configurations (where conventional flutter wisdom might suggest ballasting a wingtip leading edge), but must be carefully considered due to its impact on other constraints such as loads dynamic response, engine unstart, etc.

Mode	Symmetric					Antisymmetric				
	-50%	-20%	Base.	+20%	+50%	-50%	-20%	Base.	+20%	+50%
1	1.380	1.362	1.326	1.278	1.199	1.540	1.483	1.406	1.333	1.239
2	1.577	1.537	1.485	1.446	1.400	1.932	1.920	1.857	1.711	1.541
3	2.112	1.978	1.893	1.801	1.661	2.106	2.003	1.898	1.858	1.819
4	2.367	2.133	1.942	1.845	1.794	2.296	2.068	1.955	1.939	1.921
5	2.805	2.782	2.664	2.440	2.194	2.489	2.399	2.330	2.259	2.154
6	3.332	2.968	2.686	2.457	2.201	2.830	2.760	2.662	2.444	2.194
7	3.374	3.003	2.768	2.749	2.725	3.362	2.990	2.725	2.665	2.600
8	3.985	3.940	3.880	3.819	3.717	3.733	3.374	3.152	3.015	2.894
9	4.404	4.362	4.298	4.218	4.021	4.147	4.135	4.130	4.123	4.052
10	4.958	4.940	4.891	4.589	4.153	4.530	4.500	4.439	4.371	4.124

Table 3.7-1: Vibration Frequency Comparison For Engine Mass Variations. MT-1 Mass Condition at Mach 0.95.

		Flutter Speed				
		-50%	-20%	Baseline	+20%	+50%
Symmetric	Low Freq	380 1.949	428 1.803	505 1.664	562 1.553	646 1.428
	High Freq Hard	666 5.574	657 5.449	656 5.596	681 5.469	676 5.295
	High Freq Hump	511 3.612	N/F	600 5.085	586 4.670	521 4.227
Antisym.	Low Freq	478 1.911	458 1.931	623 1.747	703 1.673	749 1.653
	High Freq Hard	528 4.203	539 4.391	514 4.092	506 4.030	513 4.293
	High Freq Hump	N/F	690 5.530	601 5.052	562 4.669	499 3.899

Table 3.7-2: Flutter Crossing Comparison For Engine Mass Variations. MT-1 Mass Condition at Mach 0.95.

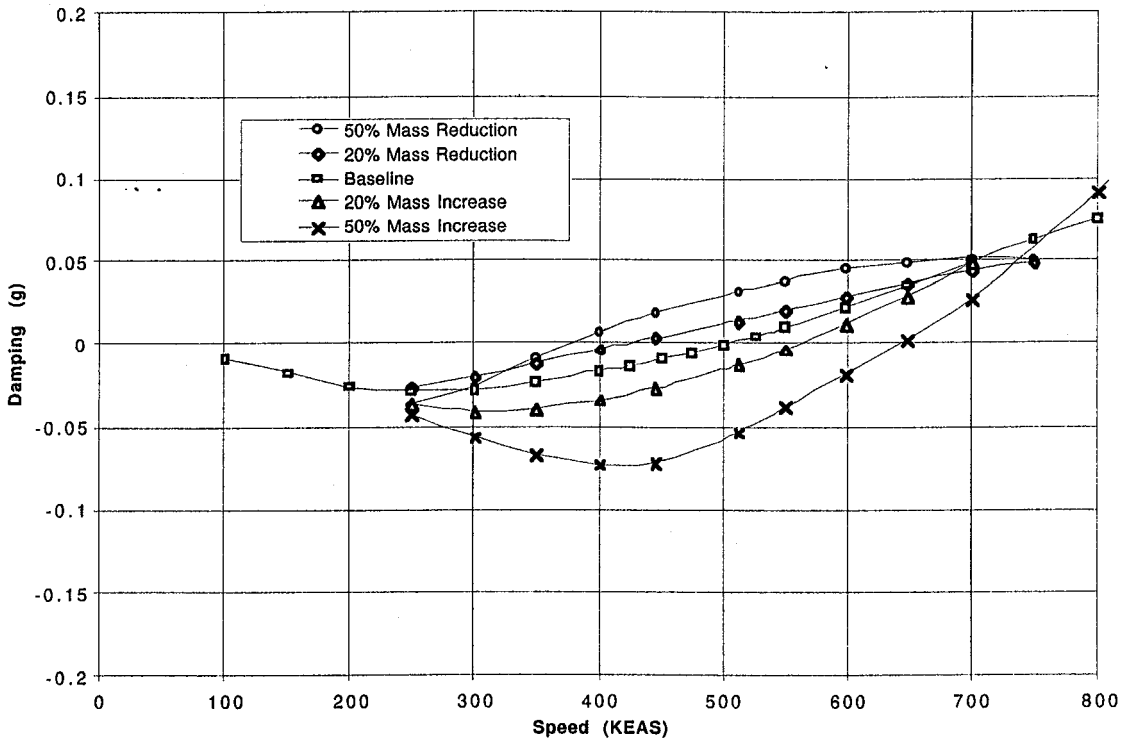

1.8 Hz Antisymmetric Mode Sensitivity to Engine Mass Properties

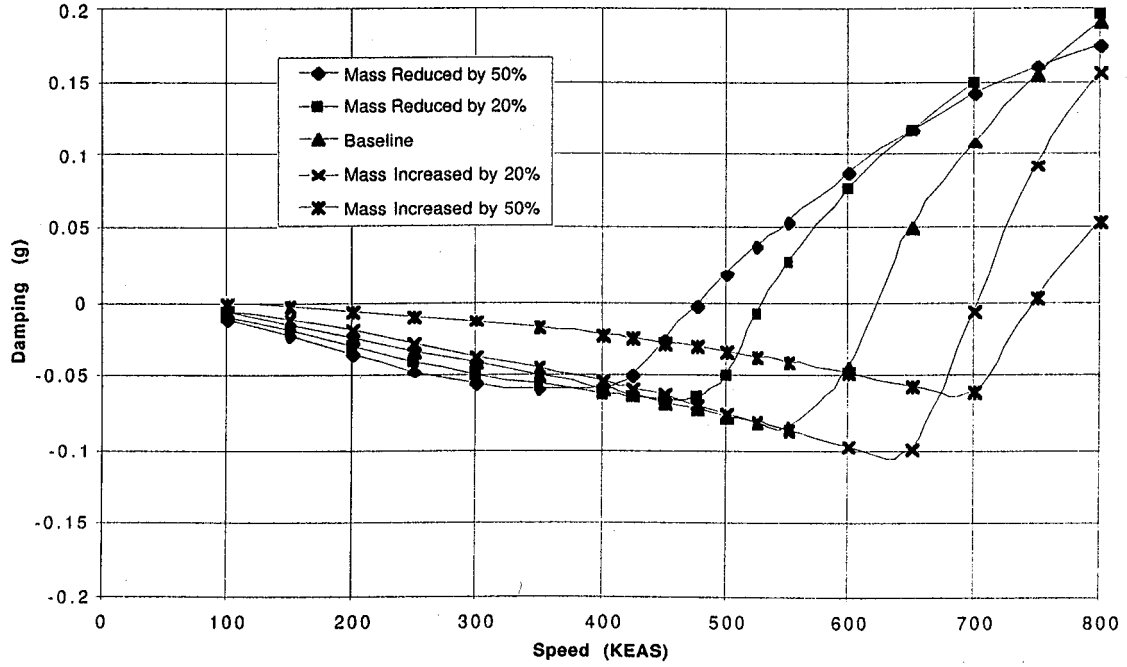

Figure 3.7-1: Comparison of V-G Curves for Low Frequency Flutter Modes as Engine Mass is Varied. MT-1 Mass Case at Mach 0.95. Top=Symmetric, Bottom=Antisymmetric.

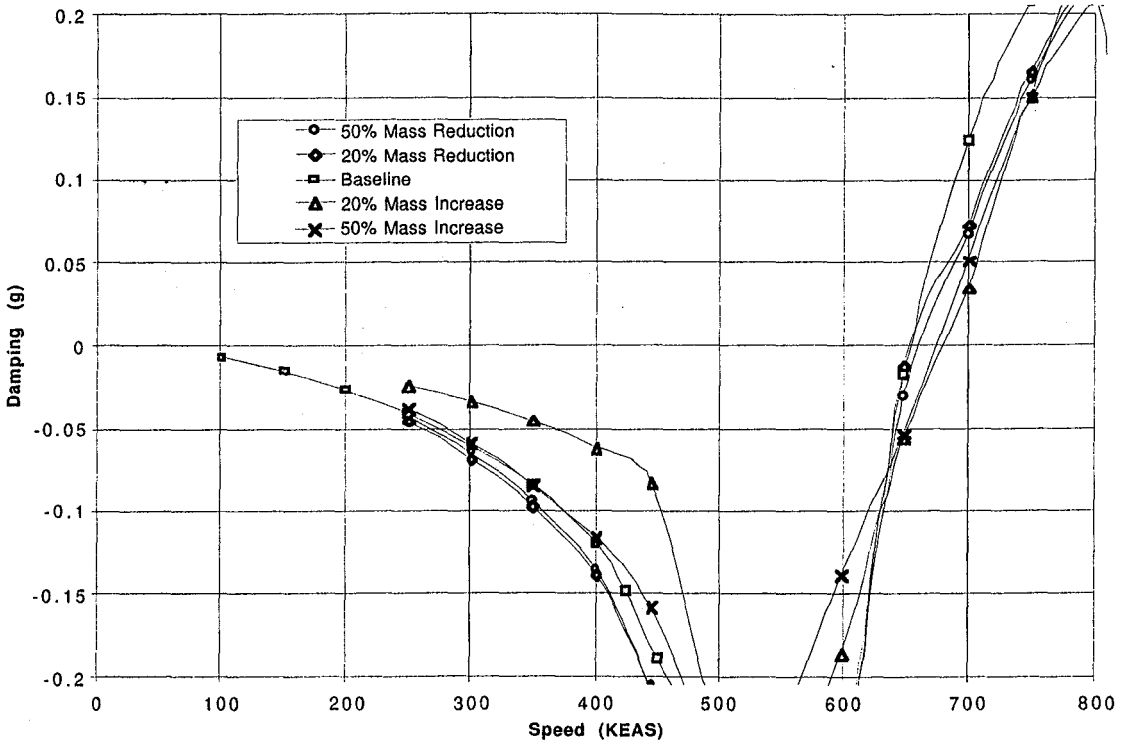

5 Hz Antisymmetric Mode Sensitivity to Engine Mass Properties

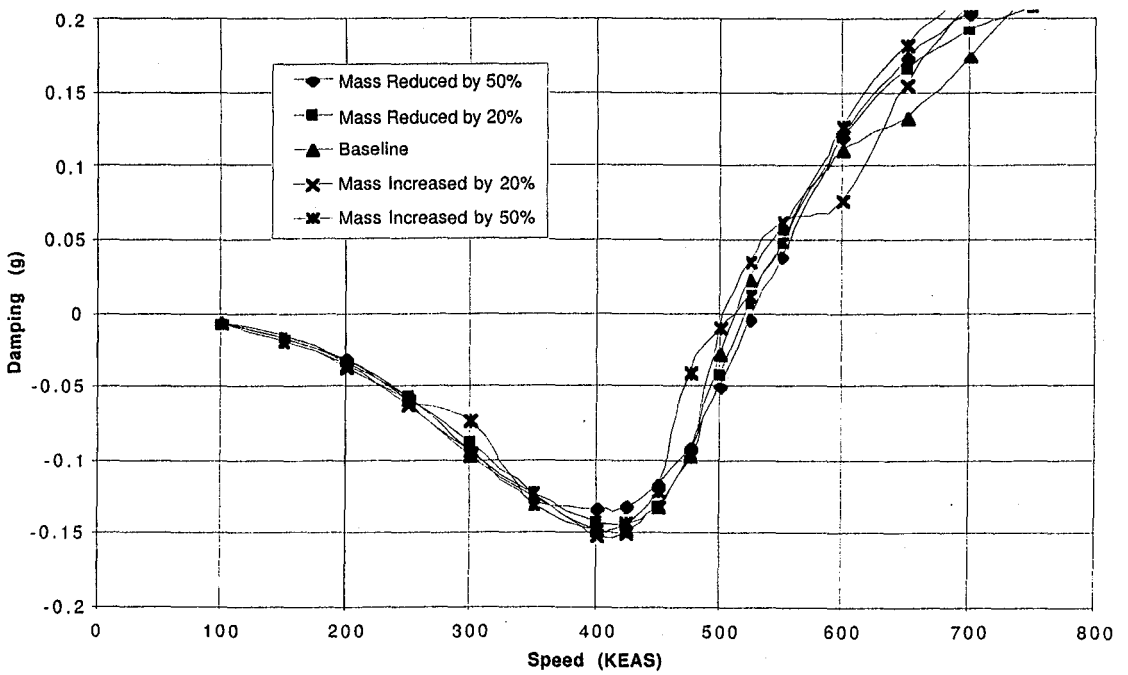

Figure 3.7-2: Comparison of V-G Curves for High Frequency Hard Flutter Modes as Engine Mass is Varied. MT-1 Mass Case at Mach 0.95. Top=Symmetric, Bottom=Antisymmetric.

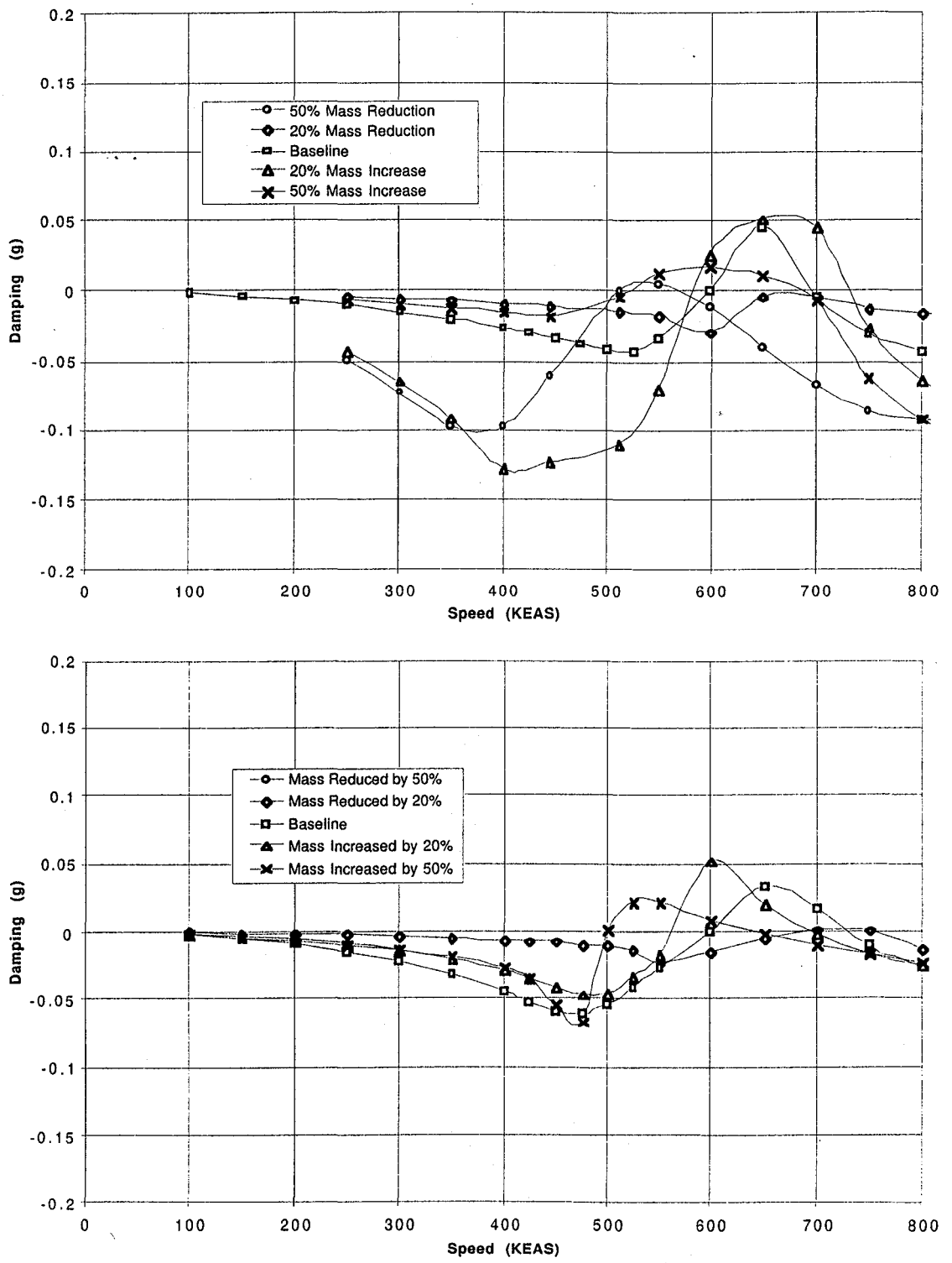

Figure 3.7-3: Comparison of V-G Curves for High Frequency Hump Flutter Modes as Engine Mass is Varied. MT-1 Mass Case at Mach 0.95. Top=Symmetric, Bottom=Antisymmetric.

3.8 Outboard Wing Skin Stiffness

While some of the variations described above showed some promise in improving the separation between the low frequency and high frequency flutter mechanisms, it was not felt that the type of separation that could be attained using these variations was adequate to ensure safe testing of the model in the TDT. In order to help improve the separation, variations were also analyzed where the skin stiffness of the outboard wing was increased in order to attempt to raise the flutter speed of the high frequency mechanisms without significantly affecting the low frequency modes.

In order to accomplish this variation, the modulus of the material making up the skin of the outboard wing panels was simply increased by 20% and 40%, resulting in two variations. The resulting vibration mode frequencies for the MT-1 mass condition are tabulated in Table 3.8-1.

The effect of varying the outboard wing skin modulus on the flutter crossings for the TCA configuration with the MT-1 mass condition is shown in Table 3.8-2, and graphically in Figure 3.8-1. This variation has a small effect on the low frequency flutter mechanisms, but stiffening the outboard wing has a strong stabilizing effect on the high frequency hard flutter modes, significantly increasing their flutter speeds.

It is recommended that the FFM be designed with an overly stiff outboard wing in order to improve test safety by raising the flutter speed of the high frequency hard flutter modes. It is not anticipated that this will compromise any of the test objectives, including ASE goals.

Mode	Symmetric			Antisymmetric		
	Baseline	+20%	+40%	Baseline	+20%	+40%
1	1.326	1.330	1.333	1.406	1.411	1.415
2	1.485	1.492	1.498	1.857	1.858	1.859
3	1.893	1.933	1.939	1.898	1.913	1.917
4	1.942	1.952	1.986	1.955	1.986	2,015
5	2.664	2.671	2.675	2.330	2.344	2,355
6	2.686	2.687	2.689	2.662	2.667	2,670
7	2.768	2.789	3.992	2.725	2.769	2,815
8	3.880	3.939	4.325	3.152	3.156	3,159
9	4.298	4.311	4.928	4.130	4.130	4.130
10	4.891	4.911	5.010	4.439	4.469	4.493

Table 3.8-1: Vibration Frequency Comparisons For Increased Outboard Wing Skin Stiffness. MT-1 Mass Condition at Mach 0.95.

		Flutter Speed		
		Baseline	+20%	+40%
Symmetric	Low Freq	505 1.664	495 1.666	489 1.668
	High Freq Hard	656 5.596	681 5.845	709 6.008
	High Freq Hump	600 5.085	632 5.143	692 5.200
Antisymm.	Low Freq	623 1.747	620 1.752	616 1.753
	High Freq Hard	514 4.092	564 4.296	626 4.557
	High Freq Hump	601 5.052	610 5.133	619 5.134

Table 3.8-2: Flutter Crossing Comparisons for Increased Outboard Wing Skin Stiffness. MT-1 Mass Condition at Mach 0.95.

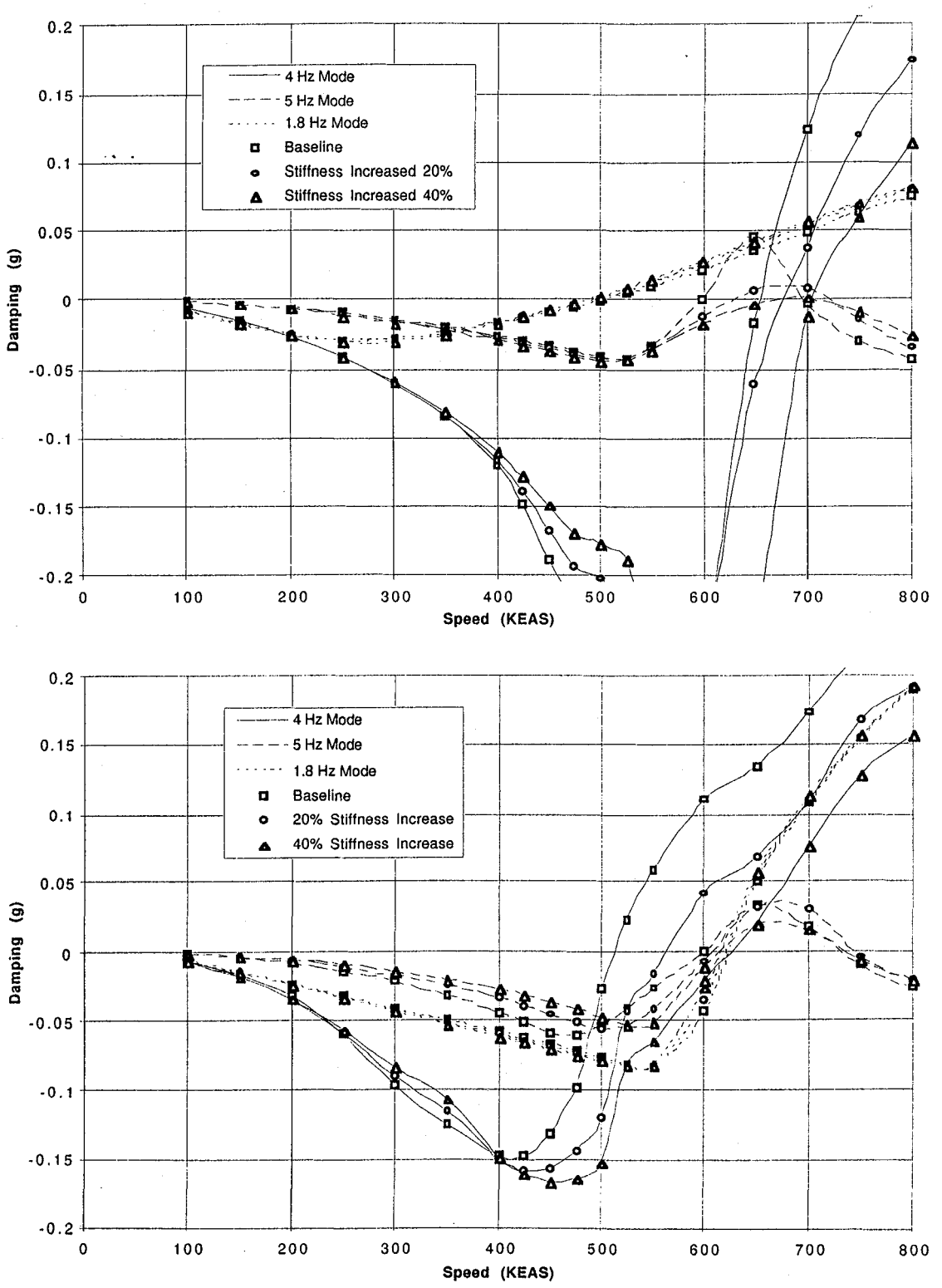

Figure 3.8-1: Comparison of V-G Curves for Flutter Modes as Outboard Wing Skin Modulus is Varied. MT-1 Mass Case at Mach 0.95. Top=Symmetric, Bottom=Antisymmetric.

3.9 Wingtip Ballast Weight

Another possible technique for improving the separation between the low frequency mechanisms and the high frequency hard flutter modes is by adding balance weights to the wingtip. Conventional flutter wisdom would suggest that by adding a mass to the front spar near the tip of the wing, the flutter speed of bending/torsion flutter mechanisms can be increased. If a wingtip ballast weight was successful in improving the separation between flutter mechanisms, this technique would be preferable to wing skin stiffening since it could potentially be "undone" by simply removing the masses. If the model was still available after all program goals were met, it might then be possible to remove the tip masses and do the extremely risky testing for the high frequency mechanisms.

In order to explore this possibility, a set of analyses were performed where tip masses of 100 lb, 200 lb, 500 lb, and 1000 lb were added to the front spar of the outboard wing. In order to reduce local mode problems, the masses were broken up to eight equal mass elements, and one was attached to each of the outboard four upper and lower surface nodes on the front spar. The resulting vibration mode frequencies are shown in Table 3.9-1. The addition of tip masses causes only slight frequency reductions.

The effects of the wingtip ballast mass on the flutter crossings of the TCA at Mach 0.95 with the MT-1 mass case are shown in Table 3.9-2. As expected, there is almost no effect on the low frequency modes. There is a significant change in flutter speed in the high frequency symmetric modes, but fairly little change in the high frequency antisymmetric modes. For the 500 lb and 1000 lb tip masses, the character of the high frequency flutter mechanisms changed significantly.

Figures 3.9-1 through 3.9-3 show the effect of wingtip masses on the V-G traces for the interesting flutter modes. In Figure 3.9-2, the change in character of the high frequency hard flutter mechanism can clearly be seen (actually it becomes a hump mode).

Since the tip mass had a minimal effect on the separation between the low frequency symmetric mechanism and the high frequency antisymmetric hard flutter mode, wingtip ballast weights are not recommended for the FFM.

Mode	Symmetric					Antisymmetric				
	Base.	100	200	500	1000	Base.	100	200	500	1000
1	1.326	1.325	1.322	1.315	1.299	1.406	1.404	1.403	1.397	1.386
2	1.485	1.482	1.478	1.469	1.447	1.857	1.857	1.855	1.822	1.745
3	1.893	1.873	1.854	1.803	1.738	1.898	1.887	1.874	1.859	1.859
4	1.942	1.942	1.942	1.941	1.941	1.955	1.948	1.942	1.935	1.932
5	2.664	2.663	2.662	2.658	2.651	2.330	2.326	2.323	2.313	2.302
6	2.686	2.686	2.685	2.685	2.684	2.662	2.661	2.659	2.654	2.643
7	2.768	2.764	2.761	2.752	2.743	2.725	2.717	2.710	2,695	2.683
8	3.880	3.872	3.865	3.845	3.819	3.152	3.151	3.150	3.147	3,141
9	4.298	4.298	4.297	4.295	4.293	4.130	4.130	4.129	4.129	4.129
10	4.891	4.888	4.886	4.880	4.870	4.439	4.435	4.431	4.420	4.404

Table 3.9-1: Vibration Frequency Comparison For Wingtip Ballast Mass Variations. MT-1 Mass Condition at Mach 0.95.

		Flutter Speed				
		Baseline	100	200	500	1000
Symmetric	Low Freq	505 1.664	503 1.665	501 1.663	496 1.663	482 1.660
	High Freq Hard	656 5.596	704 5.570	707 5.506	536 3.380	N/F
	High Freq Hump	600 5.085	641 5.041	637 5.046	737 4.992	560 3.230
Antisym.	Low Freq	623 1.747	625 1.752	626 1.753	627 1.757	628 1.764
	High Freq Hard	514 4.092	528 4.075	538 4.030	573 3.932	627 3.771
	High Freq Hump	601 5.052	624 5.043	648 5.035	728 4.994	N/F

Is this correct?

Table 3.9-2: Flutter Crossing Comparison For Wingtip Ballast Mass Variations. MT-1 Mass Condition at Mach 0.95.

[redacted]

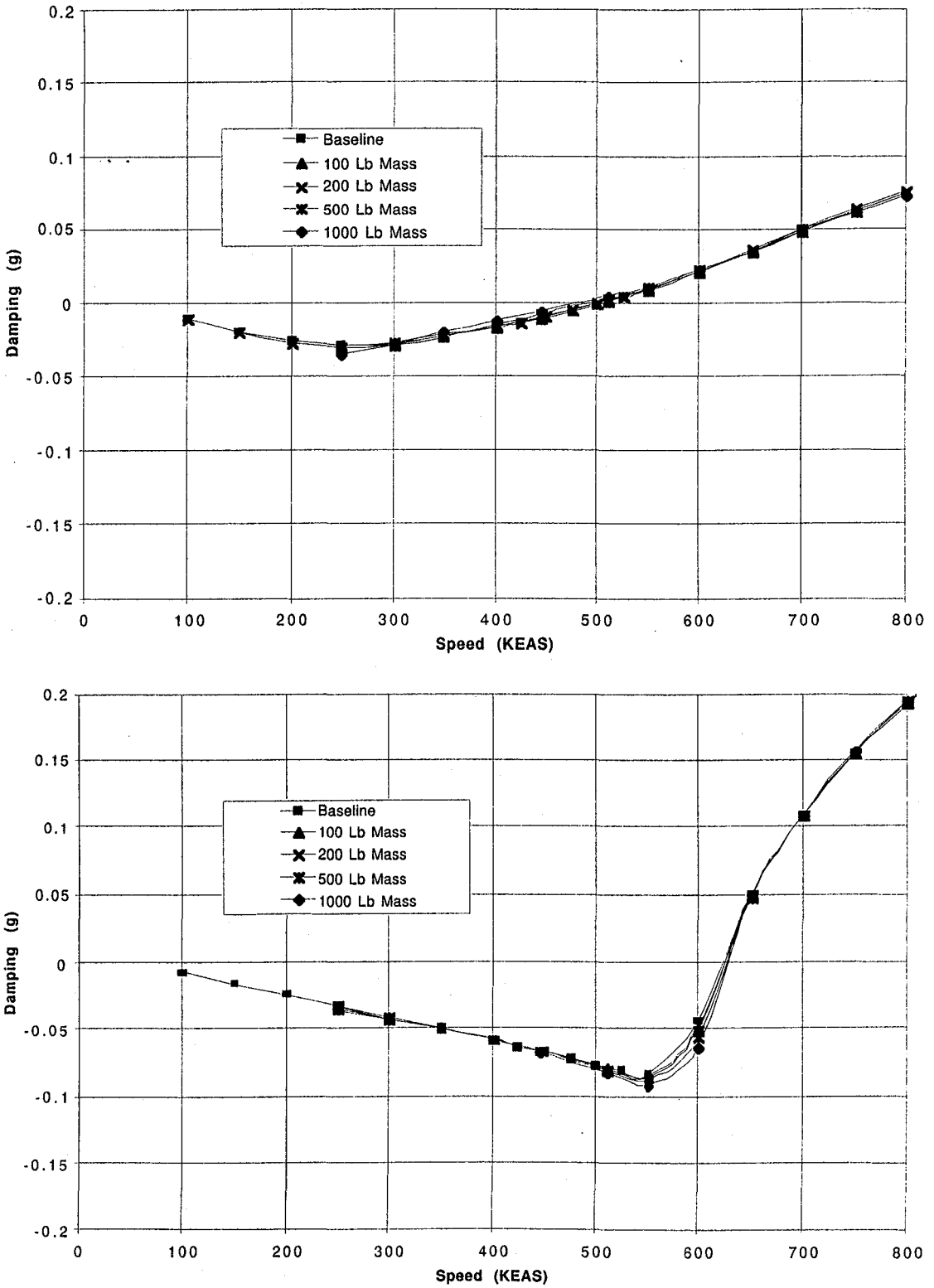

Figure 3.9-1: Comparison of V-G Curves for Low Frequency Flutter Modes as Wingtip Ballast Mass is Varied. MT-1 Mass Case at Mach 0.95. Top=Symmetric, Bottom=Antisymmetric.

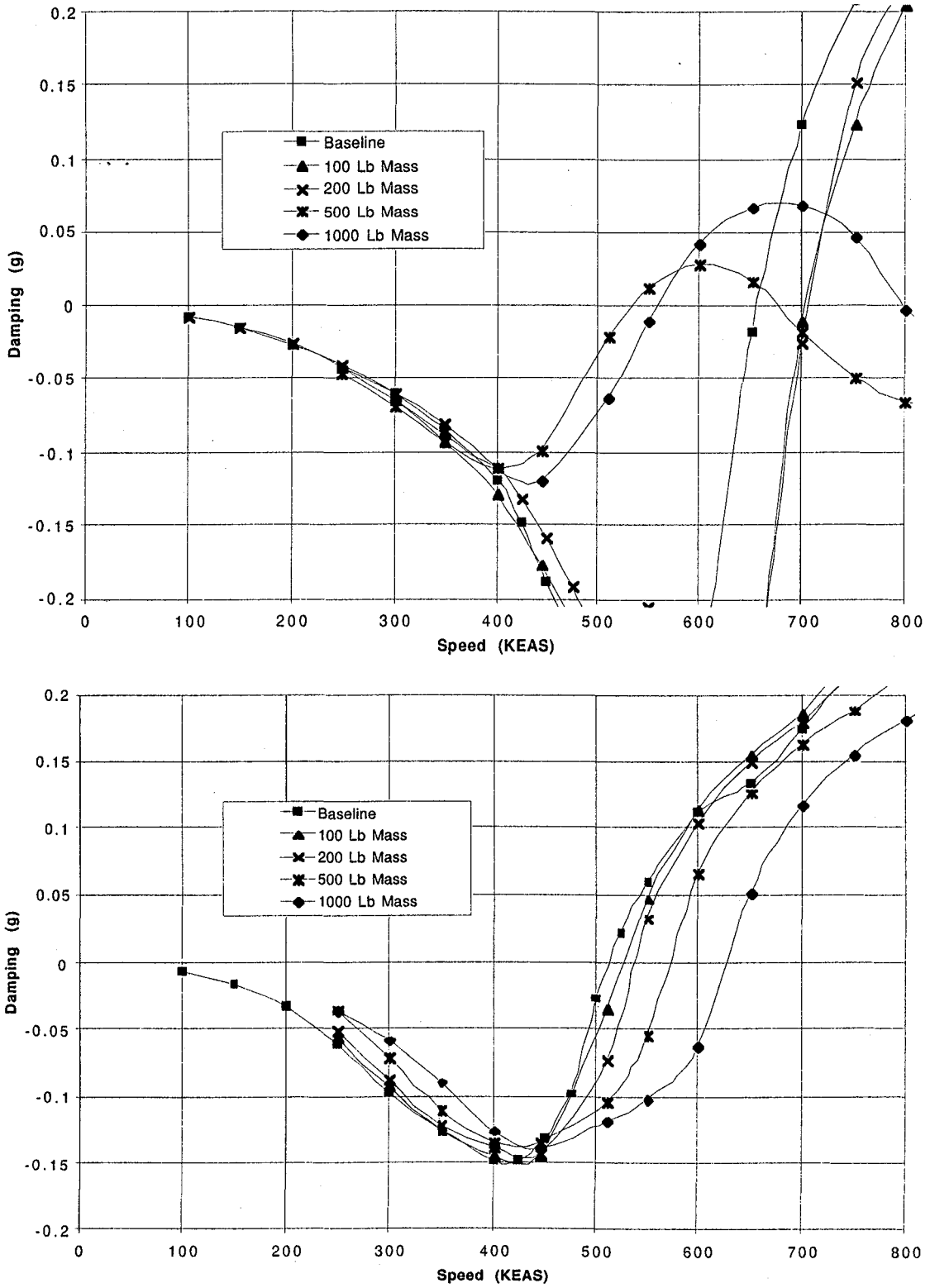

Figure 3.9-2: Comparison of V-G Curves for High Frequency Hard Flutter Modes as Wingtip Ballast Mass is Varied. MT-1 Mass Case at Mach 0.95. Top=Symmetric, Bottom=Antisymmetric.

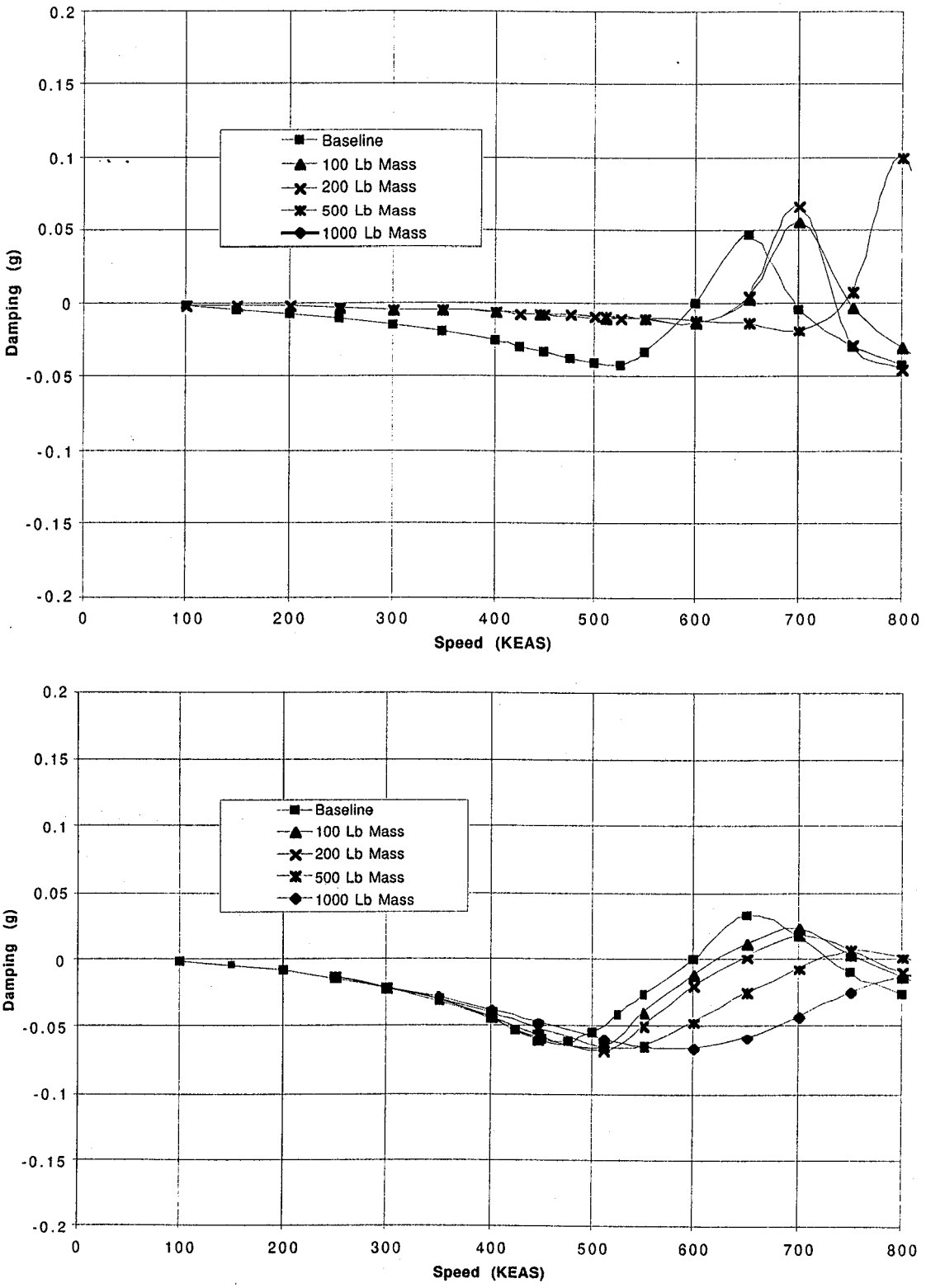

Figure 3.9-3: Comparison of V-G Curves for High Frequency HumpFlutter Modes as Wingtip Ballast Mass is Varied. MT-1 Mass Case at Mach 0.95. Top=Symmetric, Bottom=Antisymmetric.

3.10 Reduced Stiffness Scaling

While most of this document has been focused on improving the separation between the low frequency target flutter mechanisms and the potentially catastrophic high frequency hard flutter modes, there are other potential shortcomings of the current scaling point as well. One potential problem is the relatively high frequency of the flutter modes of interest when converted into model scale. Using current model scale factors, the flutter frequencies of the model in the tunnel will be roughly eleven times the flutter frequencies of the model in air. Therefore, a 1.5 Hz airplane scale flutter mechanism would result in a roughly 16.5 Hz flutter mechanism in the tunnel. This could be very risky to test due to the speed with which things happen , and the difficulty in stopping the test in a sufficiently short time when flutter is encountered.

One possible variation that could help alleviate this problem is off-design scaling, in which the model is built to be intentionally softer than a scaled-down airplane. This reduces the modal frequencies and therefore the flutter frequencies, and also reduces the dynamic pressure at which flutter occurs. The drawback is that the flutter mechanisms of interest might be modified, resulting in a questionable test.

In order to investigate the possibility of reduced stiffness scaling on the FFM, and the potential impact in terms of scaling and possible corruption of the relevant flutter mechanisms, an analysis was performed in which the airplane-scale frequencies were arbitrarily reduced by 20%. This is equivalent to a 36% reduction in model stiffness. The resulting V-G and V-F plots for the MT-1 mass condition at Mach 0.95 are shown in Figures 3.10-1 and 3.10-2. The essential mechanisms appear to be similar, and include the familiar symmetric low frequency, symmetric high frequency hard flutter, symmetric high frequency hump mode, antisymmetric low frequency, antisymmetric high frequency hard flutter, and antisymmetric high frequency hump modes. One surprise is the addition of another flutter mechism, an intermediate frequency symmetric hump mode with a fairly low flutter speed.

The flutter speeds and frequencies are tabulated in Table 3.10-1. For comparison, a column is also shown in which the flutter speeds and frequencies obtained from the reduced stiffness analysis are scaled up by 125% for direct comparison with the baseline analysis. The discrepancy between the baseline and the scaled reduced stiffness results is an indication of the "other" effects of the reduced stiffness scaling (changes in reduced frequency, etc.).

Based on these results, it appears that reduced stiffness scaling is a viable option for reducing the flutter frequencies of the FFM model, and as long as a careful analysis is performed, it is possible that the character of the target flutter mechanisms can be preserved. Of course, the model designers must be very careful not to introduce new mechanisms that jeopardize testing of the target modes. While reduced stiffness scaling appears to offer some benefits, there are still many unknowns, and it is recommended that it only be used if a strong requirement exists. It should also be emphasized that no analysis has been performed to evaluate the feasibility of building the wind tunnel model components with the required stiffness reduction, and if reduced stiffness scaling is to be employed in the FFM program, a detailed model-scale analysis must be performed to investigate these issues.

		Flutter Speed & Frequency		
		Baseline	Reduced Stiffness	Scaled Reduced Stiffness
Symmetric	Low Freq	505 1.664	365 1.327	456 1.658
	High Freq Hard	656 5.596	545 4.442	681 5.553
	High Freq Hump	600 5.085	475 4.045	594 5.057
	Mid Freq Hump	N/F	386 2.769	482 3.461
Antisymmetric	Low Freq	623 1.747	496 1.406	620 1.757
	High Freq Hard	514 4.092	400 3.233	500 4.041
	High Freq Hump	601 5.052	464 4.038	580 5.048

Table 3.10-1: Flutter Crossing Comparison for Reduced Stiffness Scaling Analysis. MT-1 Mass Condition at Mach 0.95. Difference Between Scaled Reduced Stiffness and Baseline Results is the Isolated Effect of Off-Design Scaling.

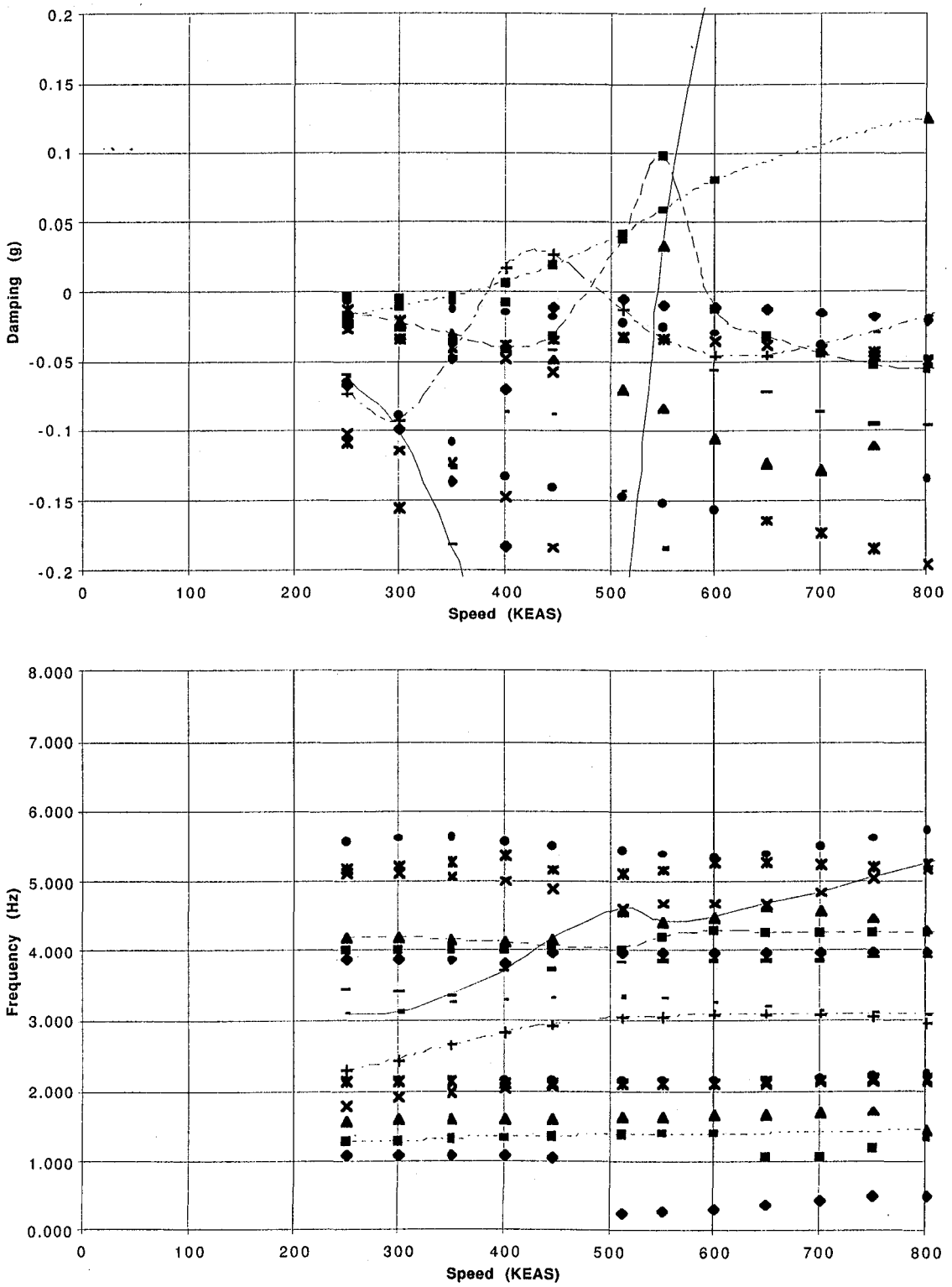

Figure 3.10-1: V-G and V-F Curves Reduced Stiffness Scaling (Frequencies Reduced by 20%). Symmetric Boundary Condition, MT-1 Mass Case at Mach 0.95.

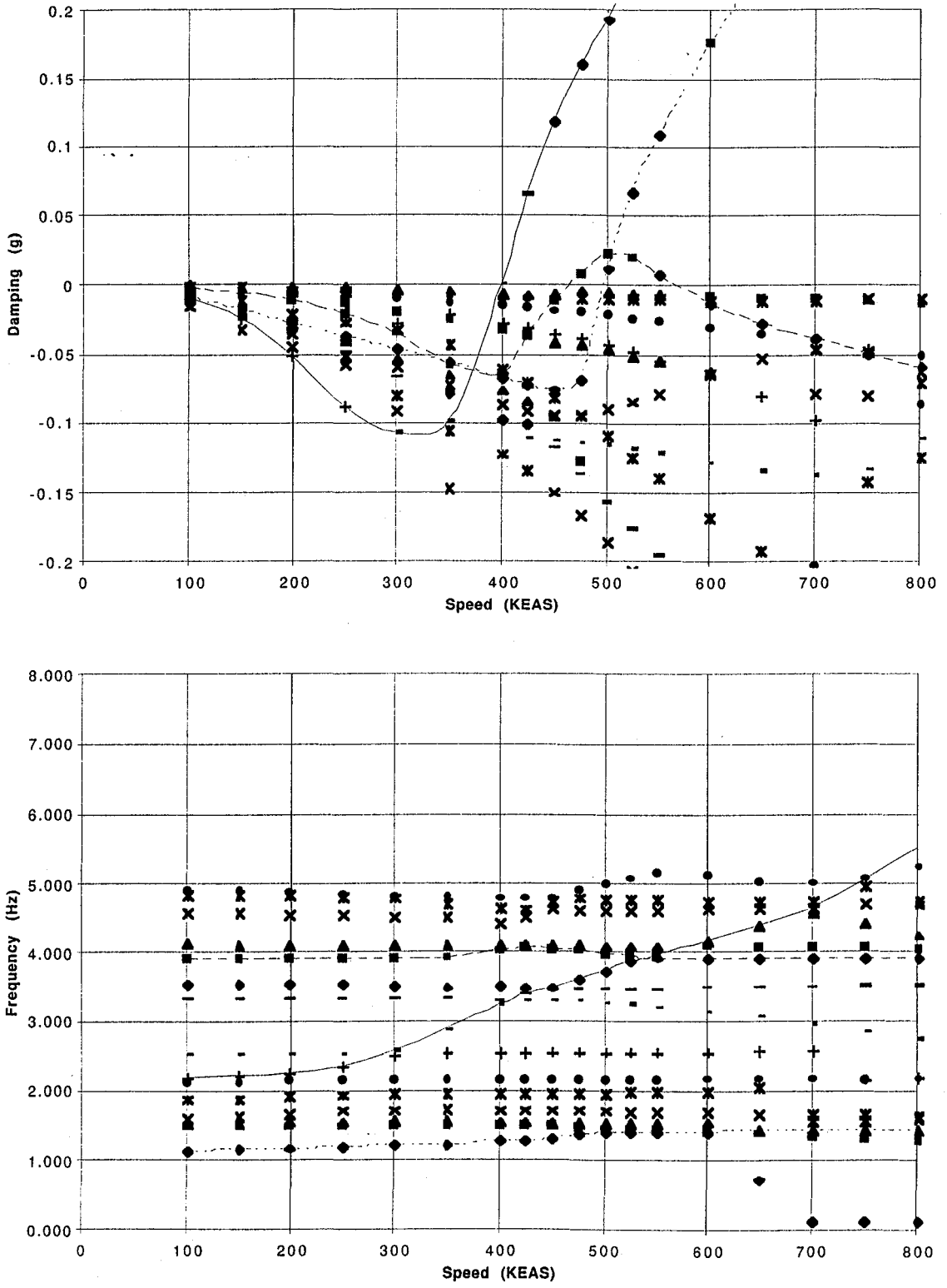

Figure 3.10-2: V-G and V-F Curves Reduced Stiffness Scaling (Frequencies Reduced by 20%). Antisymmetric Boundary Condition, MT-1 Mass Case at Mach 0.95.

4. Flutter Testing Configuration

Once the parametric sensitivity analyses discussed in Section 3 were performed, the goal was to use the information gleaned to help define an airplane-scale configuration appropriate for designing the FFM model. The primary concerns were that the design configuration should exhibit the target low frequency symmetric flutter mode, and that that mode be critical by a large margin and over a wide Mach range.

The first decision was the selection of the MT-1 mass case. This mass case was chosen because it was a heavy weight condition (therefore buildable), it had a forward C.G. (therefore more statically stable), and it s flutter characteristics were attractive. It was also determined that the design configuration should have double fuselage mass (due primarily to buildability concerns) and that the outboard wing skin panels should be stiffened by 40%. It was also determined that strength sizing would be used as a starting point. The resulting configuration was analyzed, and the resulting flutter boundaries are shown in Figure 4-1

It can clearly be seen from Figure 4-1 that the symmetric low frequency mechanism is critical over a Mach range from 0.6 to 1.0, and that the antisymmetric low frequency mechanism is critical above Mach 1.0. None of the high frequency mechanisms are critical in the range from Mach 0.6 to 1.2. This flutter boundary is considered acceptable for model scaling, and the scale factors selected are shown in Table 4-1, and were chosen such that the 3% damping crossing of the symmetric low frequency flutter mechanism at Mach 0.95 would occur at a dynamic pressure of 150 PSF in the TDT test section.

The flutter mechanism for the symmetric low frequency target mechanism is shown in Figure 4-2. A comparison with Figure 2-4 shows that the mechanism of the recommended FFM design configuration is essentially identical to the low frequency symmetric mode of the baseline flutter sized TCA airplane.

In order to evaluate the wind tunnel model performance that will result if the FFM is designed from this configuration, an analysis was performed in which the atmospheric properties of air were replaced with R-12, and the appropriate scale factors were applied to allow analysis at airplane scale. The results of this analysis were then scaled back down to model scale, and a set of Q-G and Q-F plots were constructed that represent the expected behavior of the FFM model in the TDT test section. These plots are shown in Figures 4-3 (a-e) and 4-4 (a-e).

The flutter boundaries of the scaled-down TCA are tabulated in Table 4-2, and shown in Figure 4-5 superimposed on the TDT operating envelope. Both the zero-damping crossings and the 3%-damping crossings are shown to help give an indicatioin of the steepness of the crossing. The boundaries appear to be acceptable, and this configuration is recommended as the FFM design point.

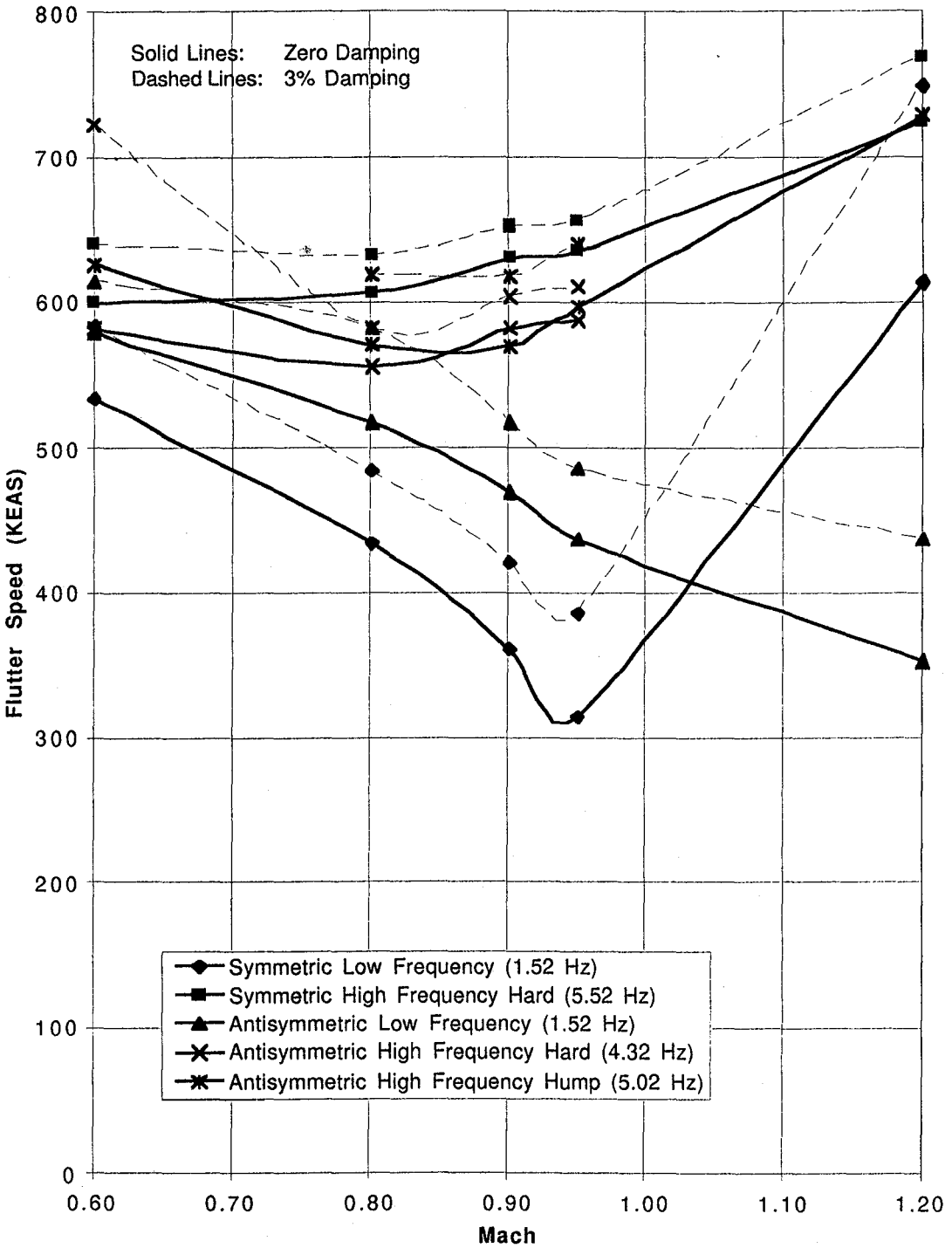

Figure 4-1: Flutter Boundaries of Recommended FFM Design Configuration in Air (Airplane Scale).

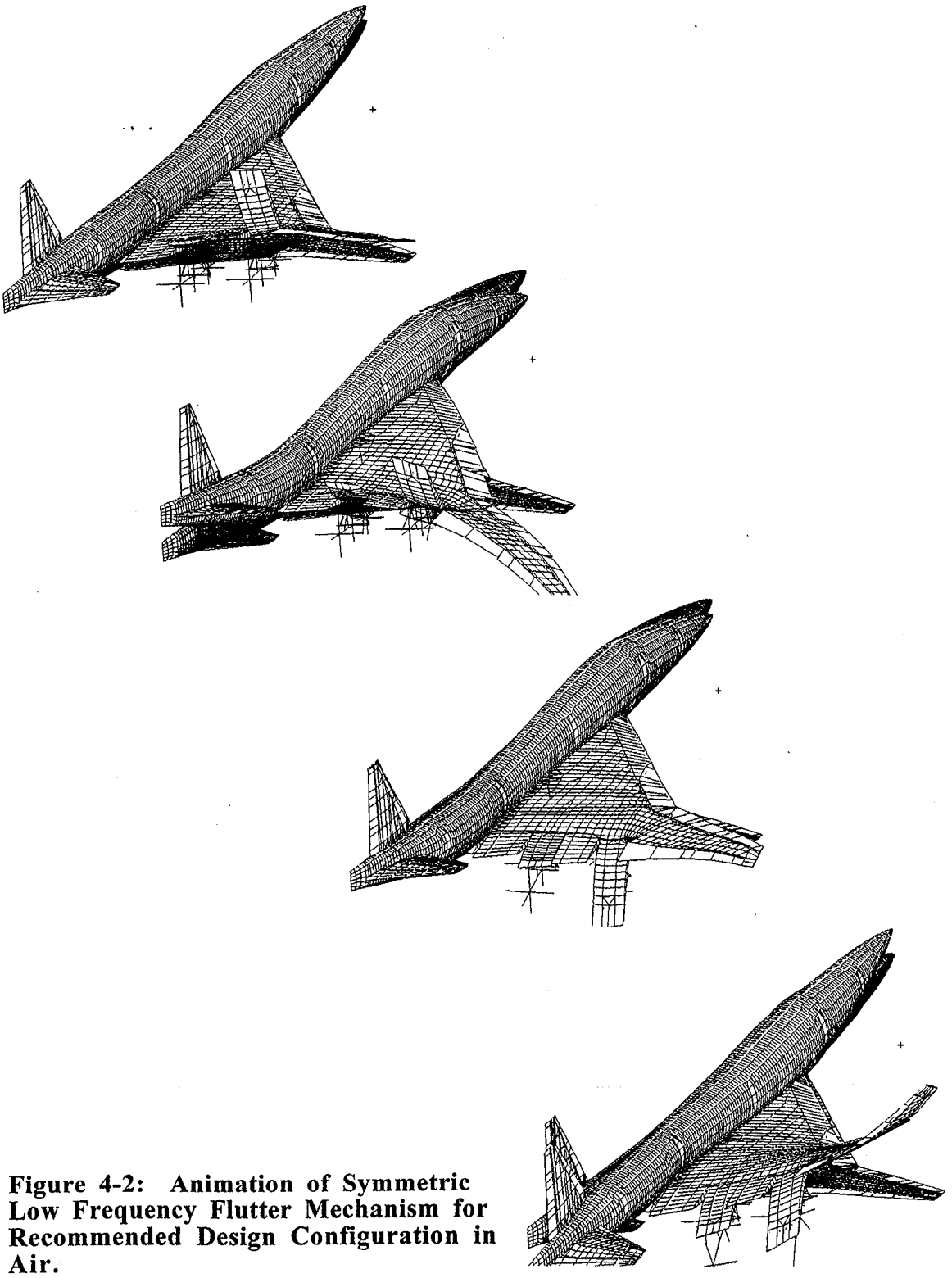

Figure 4-2: Animation of Symmetric Low Frequency Flutter Mechanism for Recommended Design Configuration in Air.

	Airplane	Model
Mach	0.95	0.95
Length	326.0	16.0
Flutter Q	540.0	150.0
Speed of Sound	1026.0	548.0
Weight (lb)	877,586.0	101.0

Parameter	Units	Model/Airplane
Mach	(l/t)/(l/t)	1.0
Length	l	0.0491
Mass	m	1.151×10^{-4}
Time	t	0.0919
Stream Density	m/l^3	0.9737
Stream Velocity	l/t	0.5341
Stream Pressure	m/lt^2	0.2778
Static Unbalance	ml	5.650×10^{-6}
Running Mass	m/l	2.346×10^{-3}
Mass Moment of Inertia	ml^2	2.773×10^{-7}
Running Inertia	ml	5.650×10^{-6}
Frequency	l/t	10.88
Stiffness:		
Bending Rigidity		1.612×10^{-6}
Torsional Rigidity		1.612×10^{-6}
Spring Constants:		
Bending Spring		1.363×10^{-2}
Torsion Spring		3.284×10^{-5}
Force	ml/t^2	6.691×10^{-4}
Torque	ml^2/t^2	3.284×10^{-5}
Acceleration	l/t^2	5.81
Flexibility Coefficients:		
Delta due to Force	t^2/m	73.35
Theta due to Force	t^2/ml	1494.51
Theta due to Moment	t^2/ml^2	30450.56

Table 4-1: Recommended FFM Scale Factors for FFM Design Configuration.

Mach	Symmetric			Antisymmetric		
	Low Frequency	High Frequency Hard	High Frequency Hump	Low Frequency	High Frequency Hard	High Frequency Hump
0.60	320/391 18.4/18.7	424/>500 62.3/?	N/F	>500	388/>500 56.8/?	N/F
0.80	189/239 17.7/18.1	390/431 60.8/60.7	N/F	301/452 17.0/18.8	341/389 55.8/55.6	352/N/F 48.3/?
0.90	129/177 17.1/17.6	402/439 60.2/60.3	N/F	221/281 16.7/17.1	347/409 55.0/54.9	366/N/F 48.2/?
0.95	98/152 16.6/17.3	416/451 59.7/59.9	N/F	186/239 16.6/16.9	374/445 54.8/54.9	394/N/F 48.1/?
1.20	430/>500 21.1/?	>500	N/F	119/183 15.8/16.5	494/>500 56.6/>	N/F

Table 4-2: Flutter Crossings of the Recommended Configuration Scaled to Model Scale. Anslysis Performed in Freon. Flutter Dynamic Pressure (PSF) and Frequency (Hz) Shown for g=0.00/g=0.03.

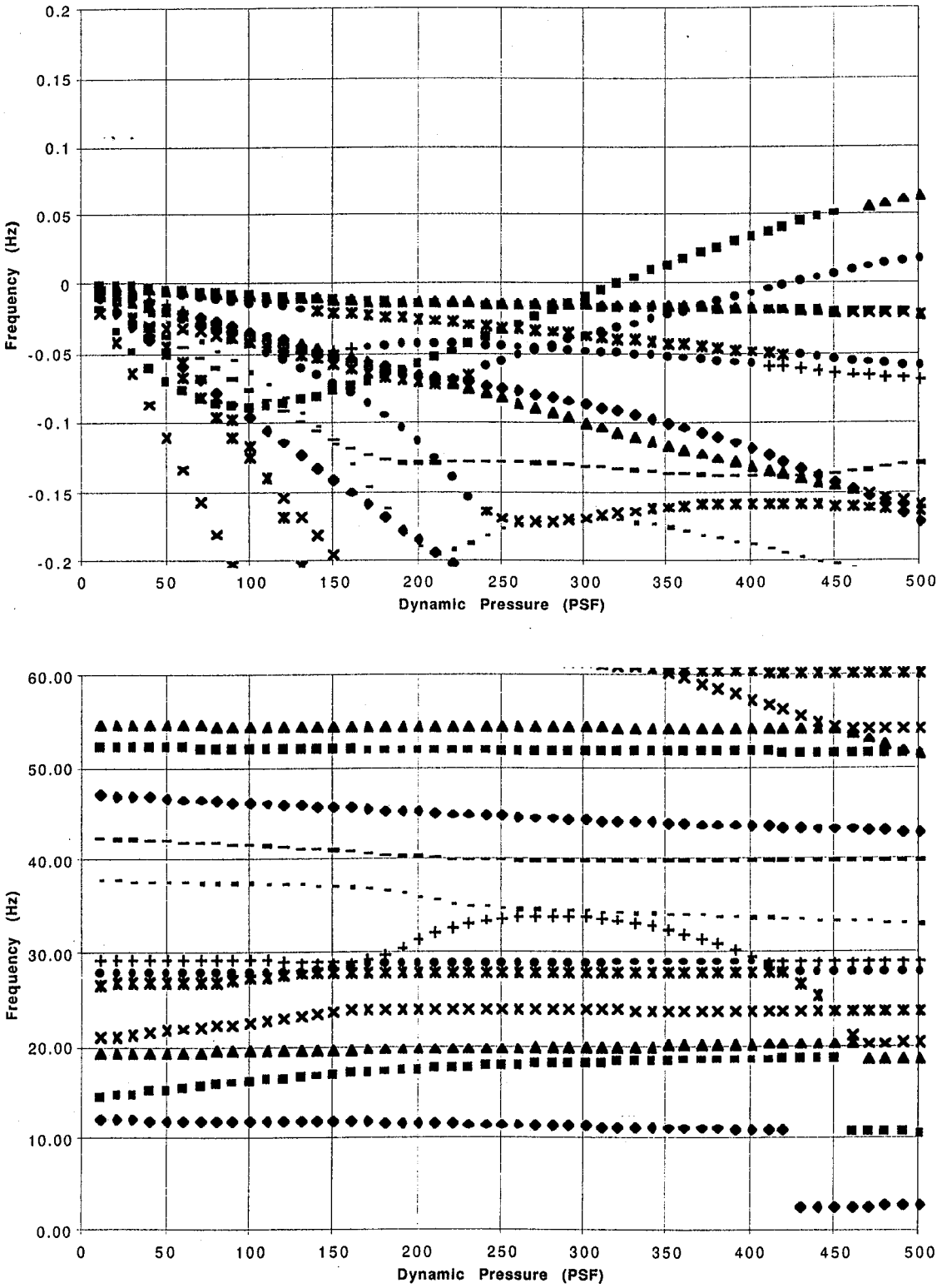

Figure 4-3(a): V-G and V-F Curves for the FFM Recommended Design Configuration In Freon (Model Scale). Symmetric, Mach 0.60.

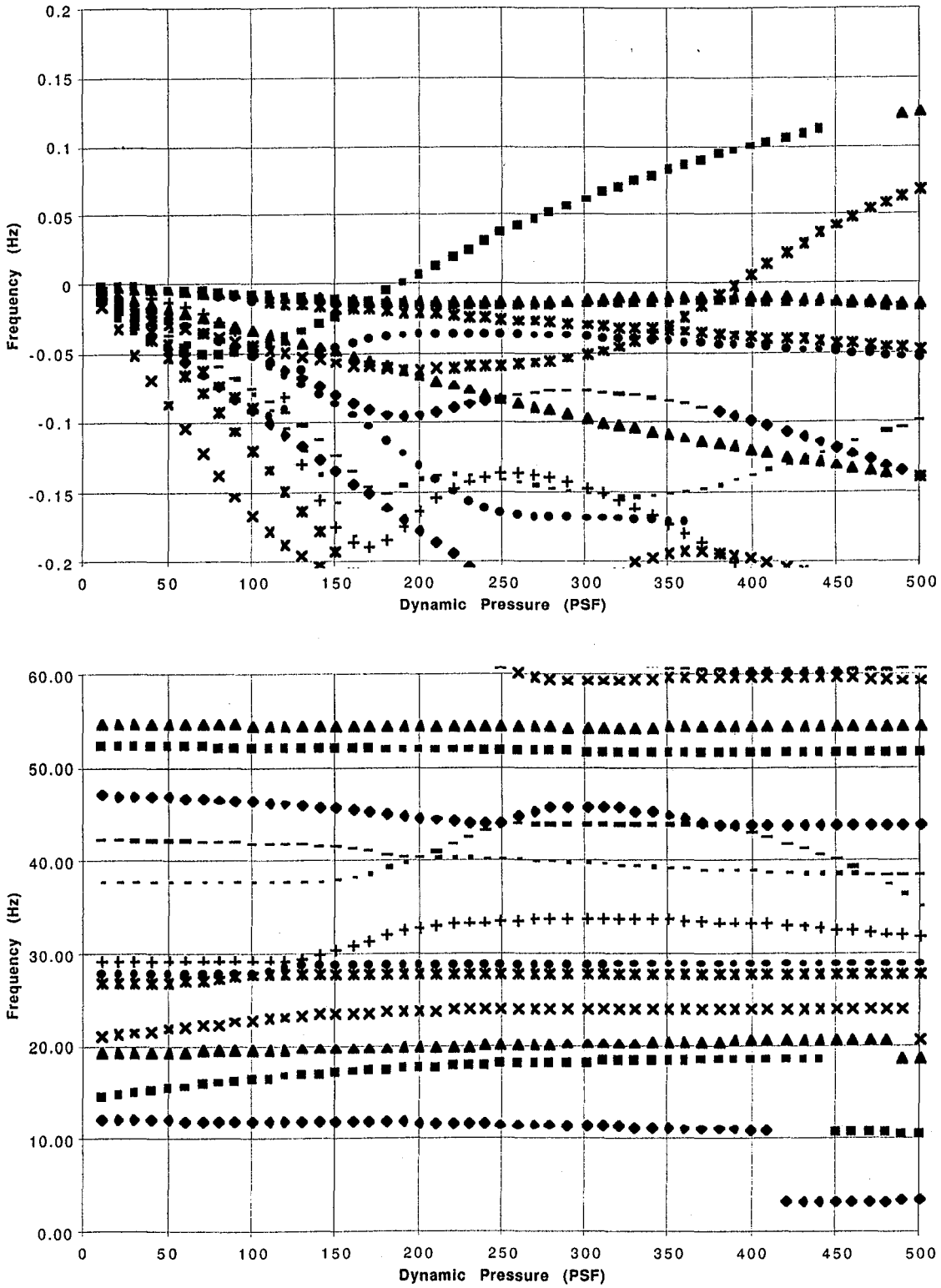

Figure 4-3(b): V-G and V-F Curves for the FFM Recommended Design Configuration In Freon (Model Scale). Symmetric, Mach 0.80.

[redacted]

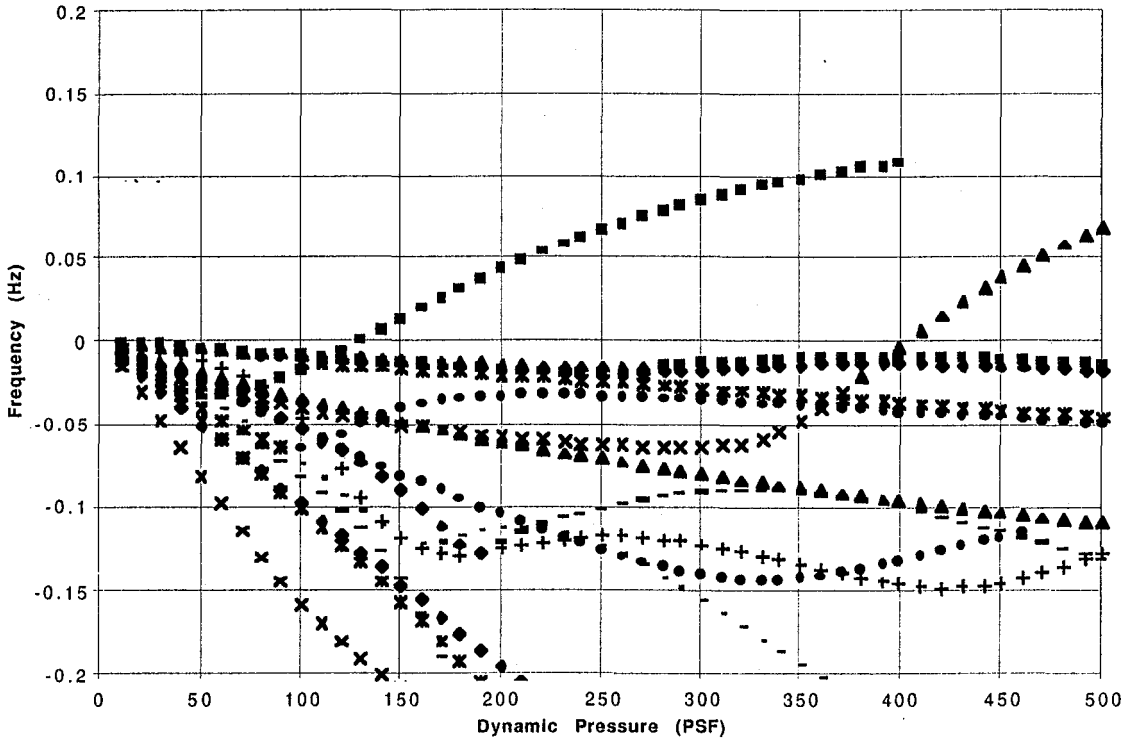

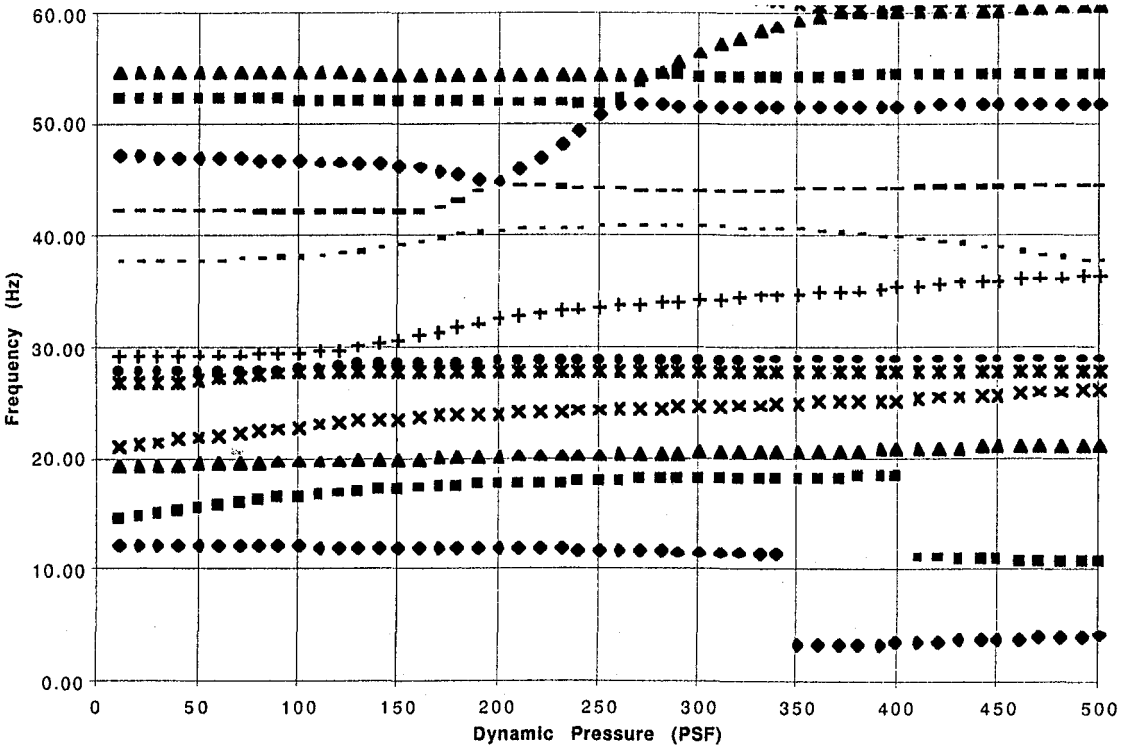

Figure 4-3(c): V-G and V-F Curves for the FFM Recommended Design Configuration In Freon (Model Scale). Symmetric, Mach 0.90.

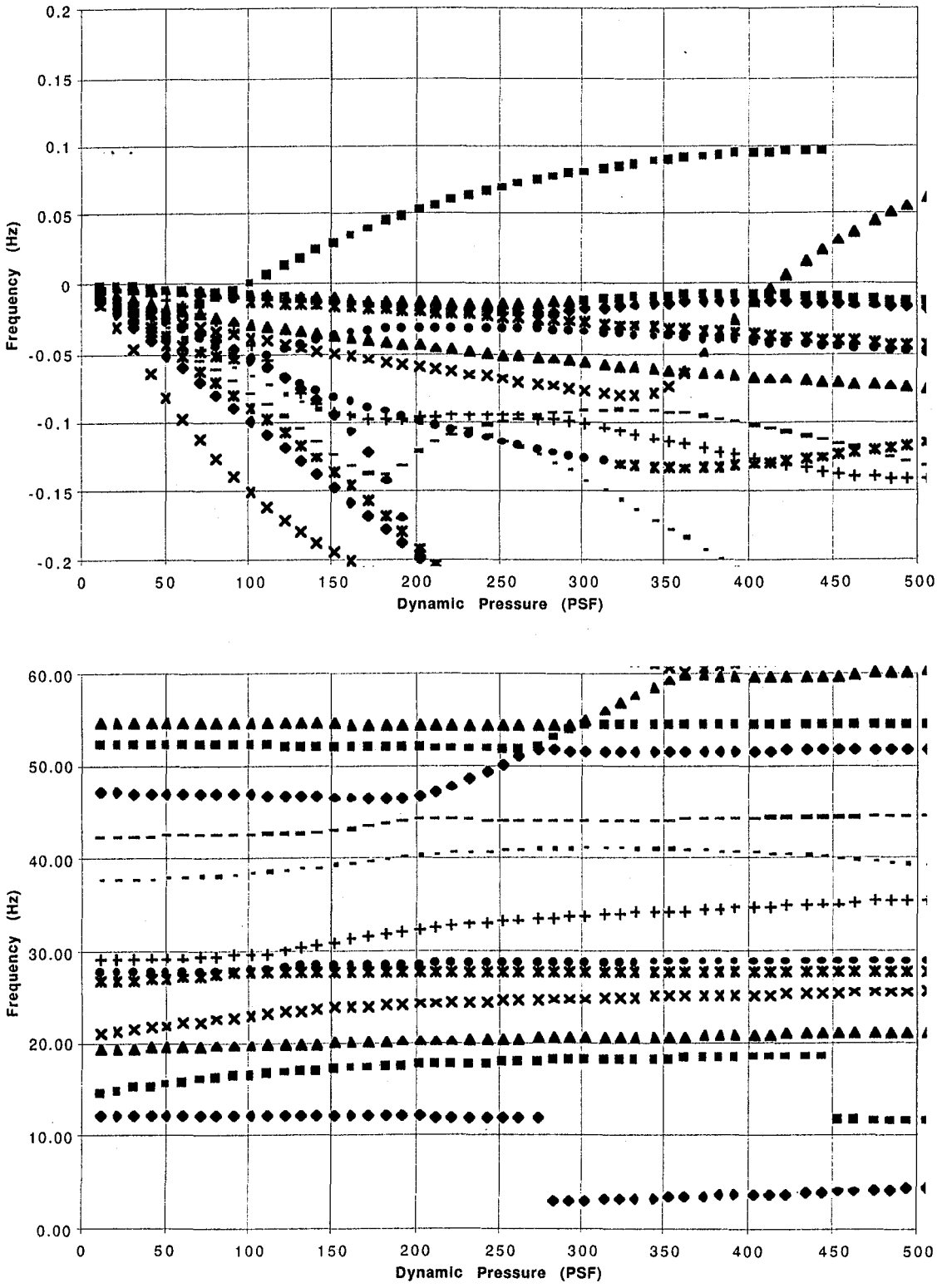

Figure 4-3(d): V-G and V-F Curves for the FFM Recommended Design Configuration In Freon (Model Scale). Symmetric, Mach 0.95.

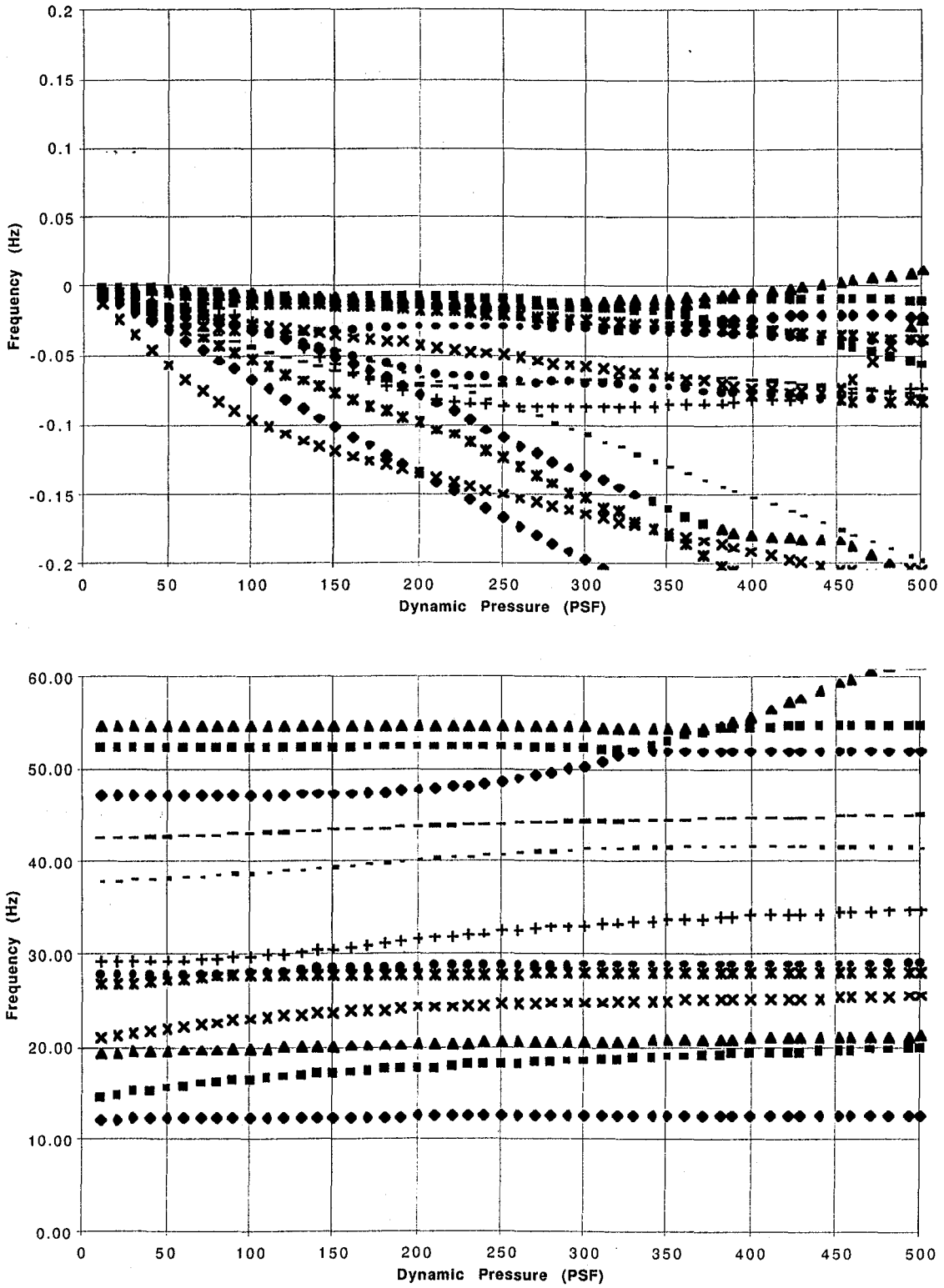

Figure 4-3(e): V-G and V-F Curves for the FFM Recommended Design Configuration In Freon (Model Scale). Symmetric, Mach 1.20.

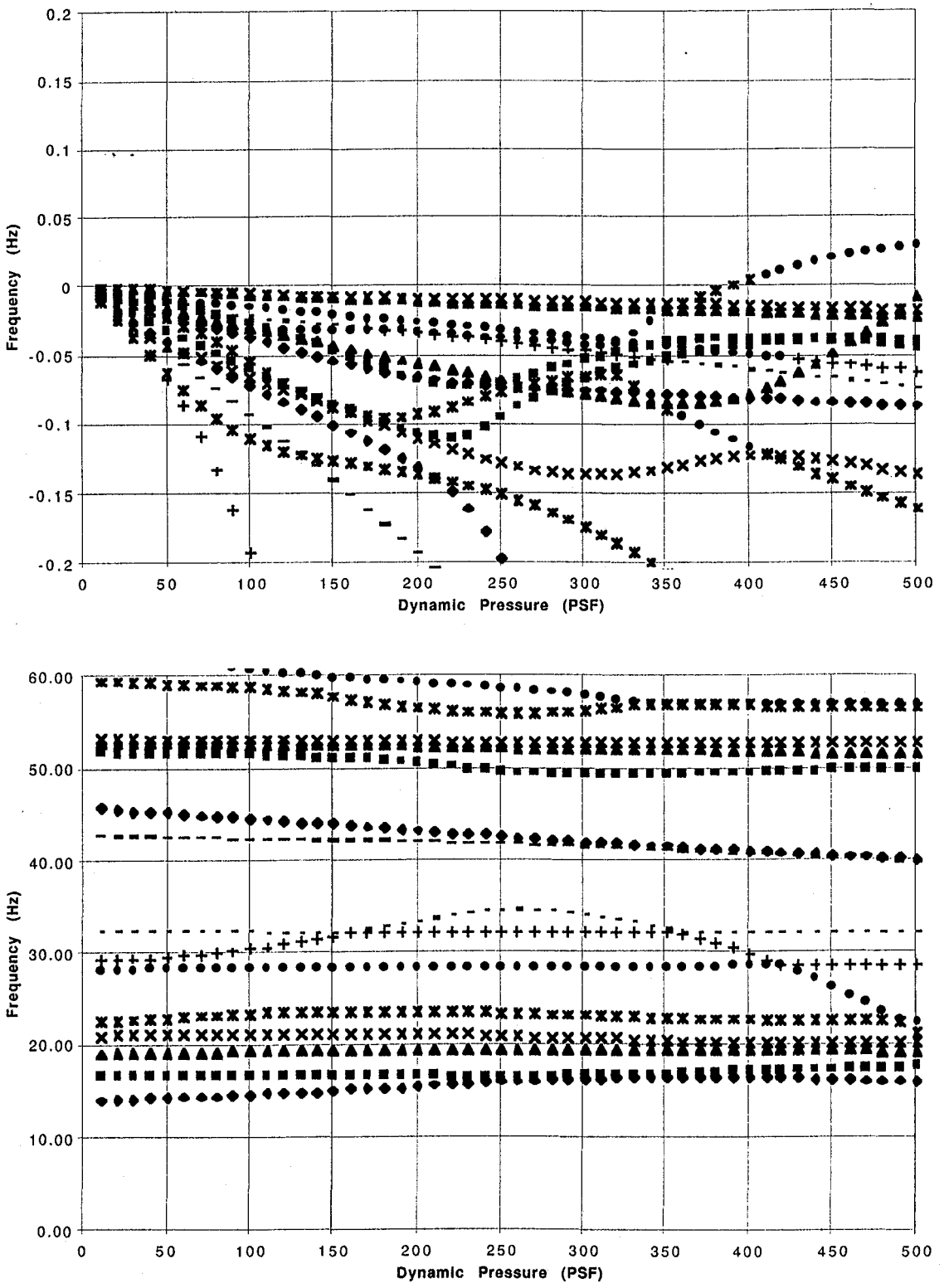

Figure 4-4(a): V-G and V-F Curves for the FFM Recommended Design Configuration In Freon (Model Scale). Antisymmetric, Mach 0.60.

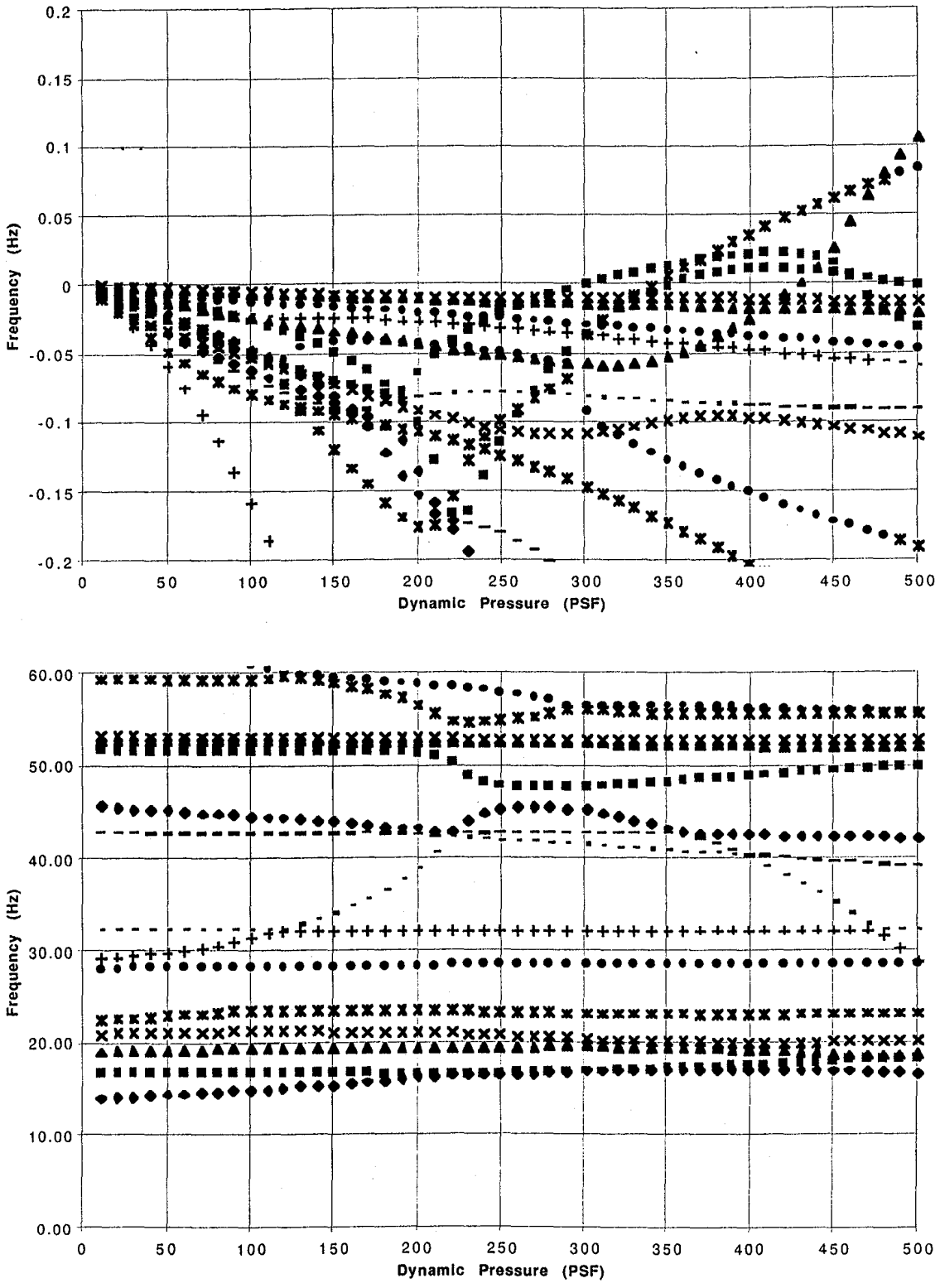

Figure 4-4(b): V-G and V-F Curves for the FFM Recommended Design Configuration In Freon (Model Scale). Antisymmetric, Mach 0.80.

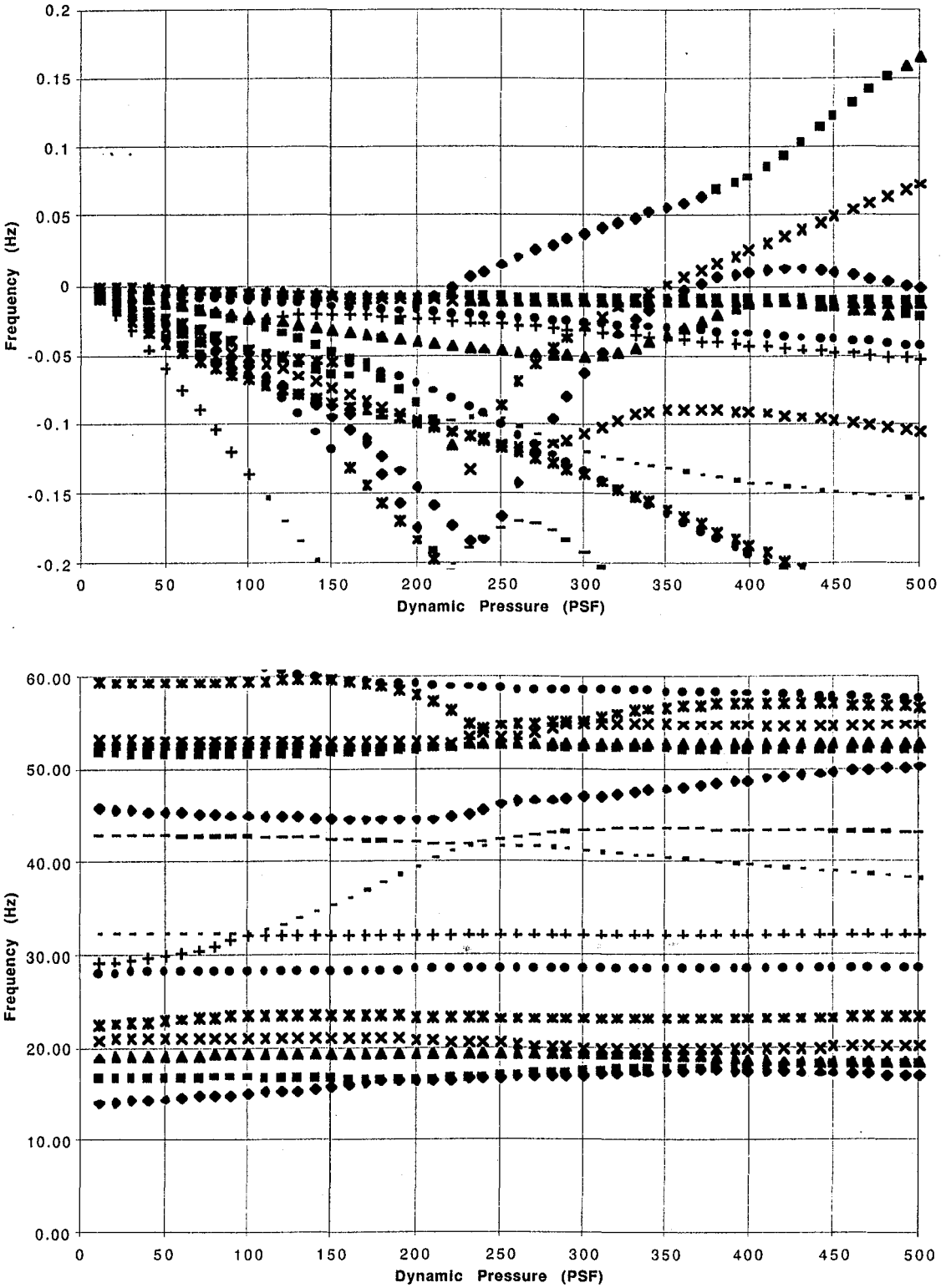

Figure 4-4(c): V-G and V-F Curves for the FFM Recommended Design Configuration In Freon (Model Scale). Antisymmetric, Mach 0.90.

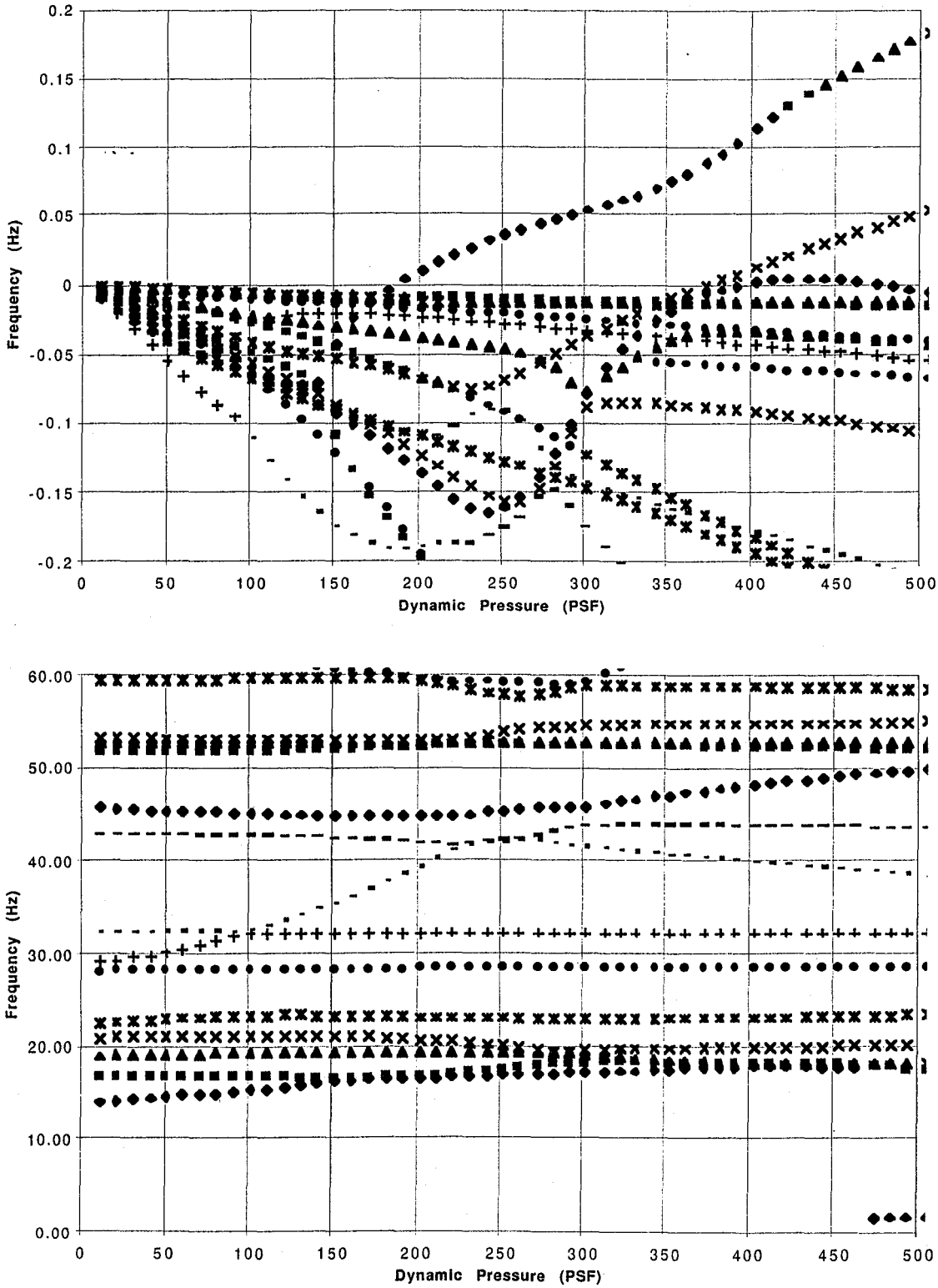

Figure 4-4(d): V-G and V-F Curves for the FFM Recommended Design Configuration In Freon (Model Scale). Antisymmetric, Mach 0.95.

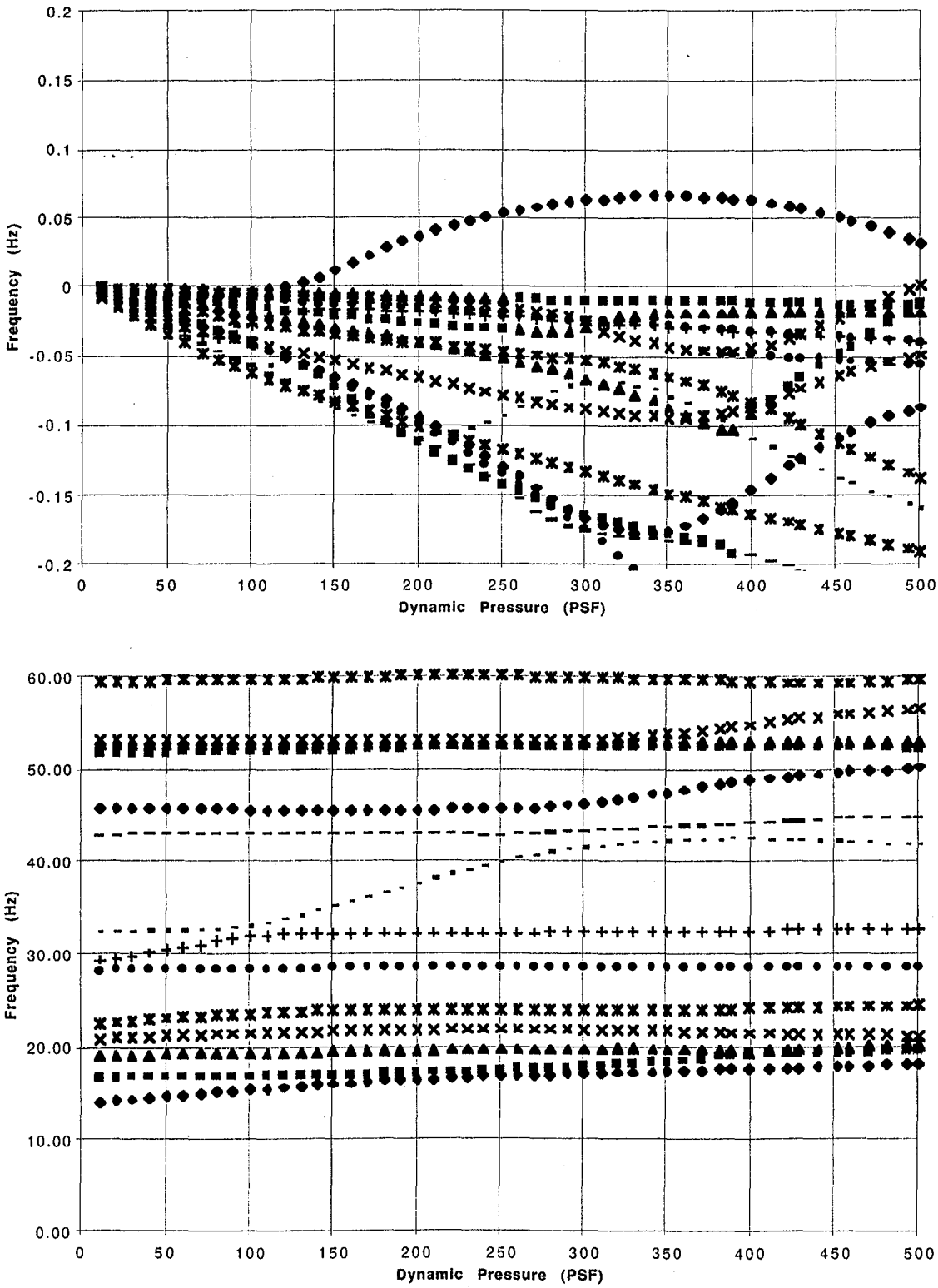

Figure 4-4(e): V-G and V-F Curves for the FFM Recommended Design Configuration In Freon (Model Scale). Antisymmetric, Mach 1.20.

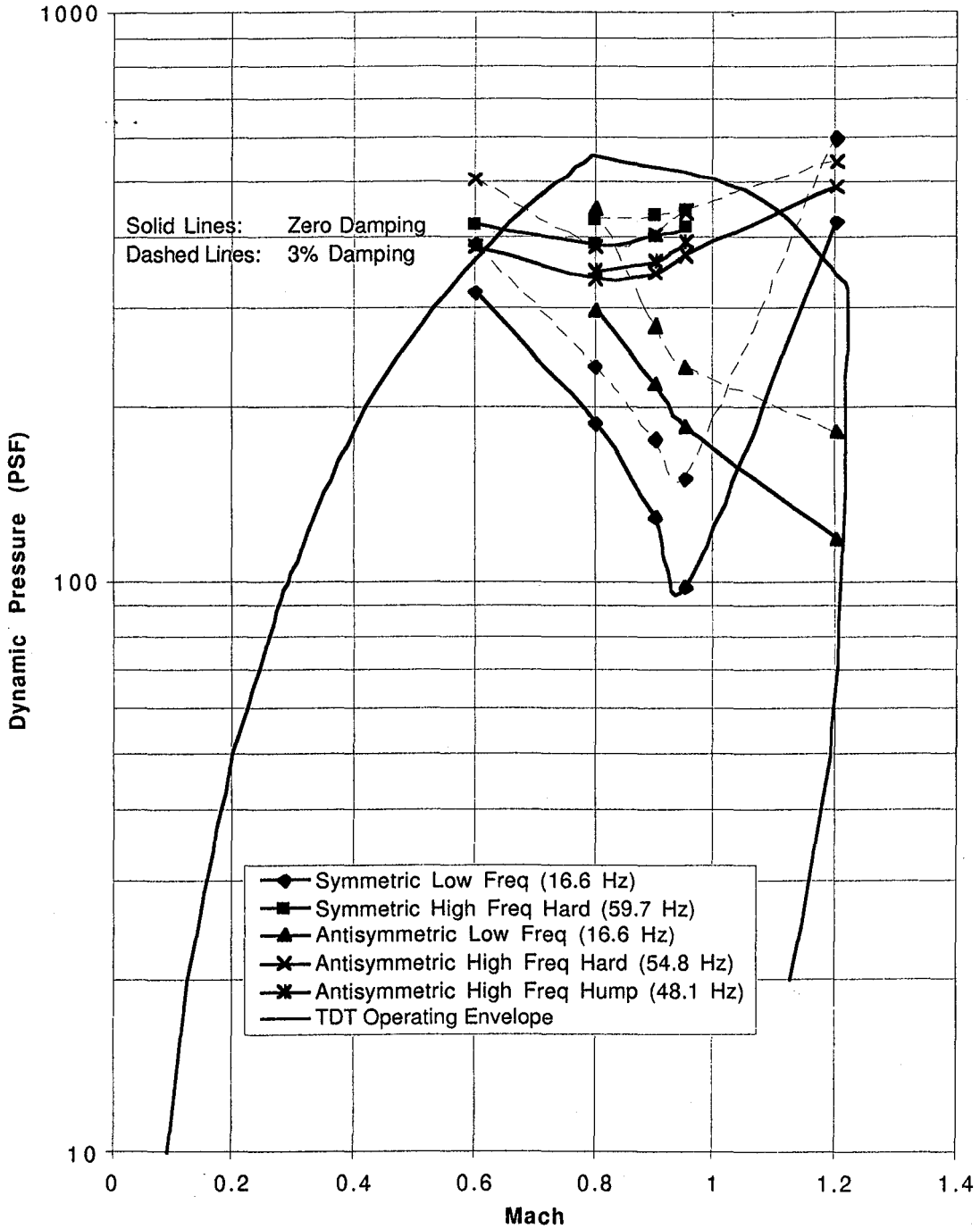

Figure 4-5: Flutter Boundaries of FFM Recommended Design Configuration In Freon (Model Scale).

5. Conclusions and Recommendations

Several conclusions can be made from the analyses described in the previous sections. The most important conclusion from the point of view of the ASE models program is that a candidate configuration and set of scale factors have been identified that appear to offer acceptable model-scale flutter characteristics in for testing in the TDT. This configuration consists of:

- Strength-Sized TCA
- Double Fuselage Mass
- 40% Stiffness Increase of Outboard Wing Skins

This configuration exhibits a model-scale flutter mechanism that represents one of the low-frequency symmetric flutter mechanisms of the TCA vehicle, with a flutter dynamic pressure of about 150 PSF and a flutter frequency of about 16-17 Hz. The flutter boundaries of the dangerous (from a testing point of view) high frequency flutter mechanisms have been raised to about 350-400 PSF, allowing a sufficient safety margin. The model weight using this configuration and scaling point is a very buildable 100 pounds.

If there is a strong requirement to reduce the flutter frequencies or increase the weight of the ASE models, a preliminary analysis indicates that off-design reduced stiffness scaling might be a viable method of achieving these goals, and will probably not significantly influence the character of the target flutter mechanisms.

Apart from the selection of the candidate design configuration, several additional conclusions can be drawn from the analyses performed. Specifically, the results indicate that it will be very valuable to perform flutter testing on parametric variations including engine aerodynamics, engine mass/CG position, and pylon stiffness. These parameters also offer some possibility of a "flutter fix" for the full-scale HSCT vehicle.

Perhaps of more interest to the ASE models program, the engine mass, stiffness, and CG position parameters offer some attractive options (at least at first glance) for "flutter stopper" mechanisms to improve test safety. If a decoupler pylon could be designed that significantly reduced the engine pitching stiffness, the flutter speed could almost instantly be increased substantially, improving model survivability. This might be more effective than using the tunnel bypass valves by themselves.

Finally, it should be emphasized that while these analyses offer some valuable insight into the FFM design, they are not a substitute for a rigorous flutter analysis of the FFM model itself. When a model-scale finite element model is available, a model-scale flutter analysis must be performed, and the adequacy of the recommended configuration must be re-evaluated.

6. Bibliography

1. Boyd, W. N., *Flutter Sensitivity Study of the HSCT TCA Configuration as a Semispan Aeroelastic Wind Tunnel Model,* HSR Aeroelasticity Deliverable Report, DTF 26-1-07, November 5, 1997.
2. Pak, C. G., *Engine Flutter Sensitivity Analysis of the Baseline HSCT Model,* HSR Aeroelasticity Deliverable Report, November, 1995.
3. Baker, M. L., *Effects of Wing/Fuselage/Tail Coupling on Flutter of the HSCT 2.4-7A Arrow Wing Configuration, and Implications to the HSR Flexible Full Span Flutter Model,* HSR Aeroelasticity Deliverable Report, December, 1995.
4. Zwillenberg, P. A., *Parametric Flutter Sensitivities for a Reference H Configuration,* HSR Aeroelasticity Deliverable Report, December 22, 1995.
5. Boyd, W. N. and Zwillenberg, P. A., *Implications of Parametric Flutter Sensitivities of a Reference H Configuration for a Full Span Flexible Wind Tunnel Model,* HSR Aeroelasticity Deliverable Report, December 22, 1995.

7. Appendix A: Baseline Flutter Analysis Results

The following plots show the V-G and V-F data for flutter analysis of the baseline flutter sized TCA model. The plots are identified using a unique three or four digid subcase identifier. The format of the subcase identifier is:

$$ID=200+1000*n_{sym}+20*n_{mach}+n_{mass}$$

where:

n_{sym}	=	0 for symmetric
	=	1 for antisymmetric
n_{mach}	=	0 for Mach 0.60
	=	1 for Mach 0.80
	=	2 for Mach 0.90
	=	3 for Mach 0.95
	=	4 for Mach 1.20
n_{mass}	=	1 for Mass Case MT-1
	=	2 for Mass Case MT-2
	=	3 for Mass Case MT-3
	=	4 for Mass Case MT-4
	=	5 for Mass Case MF-1
	=	6 for Mass Case MF-2
	=	7 for Mass Case MF-3
	=	8 for Mass Case MF-4
	=	9 for Mass Case MO-1
	=	10 for Mass Case MO-2
	=	11 for Mass Case MO-3
	=	12 for Mass Case MO-4
	=	13 for Mass Case ML-1
	=	14 for Mass Case ML-2
	=	15 for Mass Case ML-3
	=	16 for Mass Case ML-4
	=	17 for Mass Case MCTW
	=	18 for Mass Case MCI
	=	19 for Mass Case MCM
	=	20 for Mass Case MCF